2013

Backscatter And Attenuation Properties Of Mammalian Brain Tissues

Pushpani Vihara Wijekularatne
University of Mississippi

BACKSCATTER AND ATTENUATION PROPERTIES OF MAMMALIAN BRAIN TISSUES

A Thesis
Presented in partial fulfillment of requirements
for the degree of Master of Science
in the Department of Physics and Astronomy
The University of Mississippi

by

PUSHPANI VIHARA WIJEKULARATNE

May 2013

ABSTRACT

Traumatic Brain Injury (TBI) is a common category of brain injuries, which contributes to a substantial number of deaths and permanent disability all over the world. Ultrasound technology plays a major role in tissue characterization due to its low cost and portability that could be used to bridge a wide gap in the TBI diagnostic process. This research addresses the ultrasonic properties of mammalian brain tissues focusing on backscatter and attenuation. Orientation dependence and spatial averaging of data were analyzed using the same method resulting from insertion of tissue sample between a transducer and a reference reflector. Apparent backscatter transfer function (ABTF) at 1 to 10 MHz, attenuation coefficient and backscatter coefficient (BSC) at 1 to 5 MHz frequency ranges were measured on ovine brain tissue samples. The resulting ABTF was a monotonically decreasing function of frequency and the attenuation coefficient and BSC generally were increasing functions of frequency, results consistent with other soft tissues such as liver, blood and heart.

DEDICATION

I lovingly dedicate this thesis to my parents and husband, who supported me for everything.

LIST OF ABBREVIATIONS AND SYMBOLS

TBI Traumatic Brain Injury

MRI Magnetic Resonance Imaging

CT Computerized Tomography

ABTF Apparent backscatter transfer function

BSC Backscatter coefficient

SL Signal loss

P Pressure

r Position vector

t Time

∇ Gradient operator

∇^2 Laplacian operator

ρ Density

β Compressibility

$\tilde{\rho}$ Density 'fluctuation' term

$\tilde{\beta}$ Compressibility 'fluctuation' term

$\overline{\rho}$ Spatial mean value of the density

$\overline{\beta}$ Spatial mean value of compressibility

σ_S Total scattering cross-section

S Total power scattered

I Incident wave intensity

$\sigma_d(\phi_s, \theta_s)$ Differential cross-section

$d\Omega$ Solid angle

$\sigma_{bs} = \sigma_d(0, \pi)$ Differential cross-section for backscatter

σ_a Absorption cross-section

σ_t Attenuation cross-section

μ_s Scattering coefficient

μ_{bs} Backscattering coefficient

$|S(\omega)|^2$ Apparent backscatter transfer function

$|F_{tissue}(\omega)|^2$ Fourier power spectrum for the brain tissue in a given position or an orientation

$|F_{steel\ plate}(\omega)|^2$ Fourier power spectrum for the reference steel plate

α Attenuation coefficient

Z Impedance

T Transmission coefficient

v Speed of sound through a medium

d Sample thickness

A_1 Amplitude of the first reflected signals from the polished steel plate through water path

A_2 Amplitude of the first reflected signals from the polished steel plate through the sample

Γ Amplitude reflection coefficient of steel plate reflector

R Focal length of the transducer

ω Radial frequency

c Speed of sound through tissue sample

ACKNOWLEDGEMENTS

I would like to express my deepest appreciation to my research advisor, Prof. Joel Mobley for giving me the opportunity to work on this exciting project. Without his guidance and persistent support, this dissertation would not have been possible. His intellectual and personal guidance has influenced me to think and work as a scientist in my career.

Also sincerely thank goes to the members of my defense committee, Dr. Cecille Labuda and Dr. Charles Church for taking the time to review this work. I would like to thank to the past and present members of Prof. Mobley's group for the utmost support given to maintain high quality research.

My heartiest gratitude goes to my parents, and to my loving husband Nuwan, for the encouragement given me especially during unbearable times in my life. Also I want to thank all of my friends at The University of Mississippi, especially Sumudu Tennakoon for the positive influence and assistance given to me throughout these years.

Finally I want to thank each and every individual of The Department of Physics and Astronomy at The University of Mississippi for the tremendous support, guidance and the encouragement given to me.

CONTENTS

Abstract …….....ii

Dedication…….....iii

List of abbreviations and symbols……..iv

Acknowledgements……vi

List of tables……ix

List of figures……...x

1. Introduction……..1

1.1 Significance of the study……..1

1.2 Brain Anatom……..……4

1.3 Review of related Literature……8

1.4 Theoretical framework of the study……...12

2. Methods……..22

2.1 Experimental set up……...22

2.2 Dynamic range……..26

2.3 Sample preparation…….……..30

2.3.1 Spatial averaging on mammalian brain tissues……...30

2.3.2 Orientation dependence of backscatter and attenuation data on mammalian brain tissues……...34

2.4 Data acquisition……....40

2.5 Analysis……47

3. Results……54

3.1 Spatially averaged backscatter and attenuation data of ovine brain tissues……54

3.1.1 Apparent backscatter transfer function…….....54

3.1.2 Attenuation coefficient……..60

3.1.3 Backscatter coefficient……..68

3.2 Orientation dependence of backscatter and attenuation data of ovine brain tissues……....76

3.2.1 Apparent backscatter transfer function……...76

3.2.2 Attenuation coefficient……...79

3.2.3 Backscatter coefficient……...84

4. Discussion……..91

5. Conclusions……99

6. References……100

7. List of Appendices ……..103

8. Vita……118

LIST OF TABLES

Table 1.3.1: Attenuation coefficient of some biological samples and water……..11

LIST OF FIGURES

1. Figure 1.1.1: Frequencies 20 Hz – 20 kHz is the most familiar region for human hearing. Sound waves of frequencies above the threshold of human hearing (20 kHz) are known as the ultrasound. Frequencies falling below 20 Hz are considered as infrasonic…….2

2. Figure 1.1.2: A diagram represents the possible backscattered signals in the presence of a space-filling lesion in brain. The diagram indicates the space filling lesion there is a signature of asymmetry in the signals…….....3

3. Figure 1.2.1: Three major parts of the mammalian brain: the brain stem, the cerebellum and the cerebrum……..5

4. Figure 1.2.2: A picture of a ovine brain. It shows the three major parts of a mammalian brain. The brain stem, the cerebellum and the cerebrum. Cerebrum is the largest area of the brain and has two hemispheres and each hemisphere has four lobes…….6

5. Figure 1.2.3: Comparison of main three parts human brain with ovine brain. Ovine brain has all the same parts as of a human brain but small in size……...……...7

6. Figure 1.4.4.1: Illustration of the transmission wave through water-tissue-water media…….17

7. Figure 2.1.1: Illustration of the data acquisition system ……..23

8. Figure 2.1.2: Top view of the water tank with the reference, tissue sample and the transducer placed in it…….....24

9. Figure 2.1.3: A photograph of the apparatus set-up ……..…….....25

10. Figure 2.2.1: The dynamic range measurements on the steel plate reflections for the full range of frequencies …….....27

11. Figure 2.2.2: The dynamic range measurements on the steel plate reflections for the best range of frequencies…….....28

12. Figure 2.2.3: The dynamic range measurements with a sample in place …….....29

13. Figure 2.3.1.1: A photograph of the tissue sample, which is 1.4cm in height and about 2.4cm in diameter …..…….....30

14. Figure 2.3.1.2: Tissue sample with the holder …….....30

15. Figure 2.3.1.3: Rails used to change the distance in two perpendicular directions…….....31

Figure 2.3.1.4: Side view of the water tank with the reflector, tissue sample and the transducer placed in it. Two directions of the movement of the tissue sample are depicted ……..32

17. Figure 2.3.1.5: Top view of the water tank with reflector, tissue sample and the transducer placed in it …….....33

18. Figure 2.3.2.1: One hemisphere of the ovine brain …….....34

19. Figure 2.3.2.2: The cylindrically-shaped tissue sample, which is 11.5 mm in diameter and about 30 mm in height …….....35

20. Figure 2.3.2.3: A photograph of the sample holder with the tissue sample attached…….36

21. Figure 2.3.2.4: A photograph of the rotating stage.....…….....37

22. Figure 2.3.2.5: Top view of the water tank with the reference, tissue sample and the transducer placed in it. The direction of the movement of the tissue sample is depicted……..38

23. Figure 2.3.2.6: Side view of the water tank with the reference, tissue sample and the transducer placed in it. The direction of the movement of the tissue sample is depicted……..39

24. Figure 2.4.1.1: Steel plate reflections through water path only. The small waveforms

after the first reflected signal are due to the reverberations……..……41

25. Figure 2.4.1.2: Enlarged first reflected signal…….42

26. Figure 2.4.1.3: Backscatter data can be easily identified with the steel plate reflections as the reference……..……42

27. Figure 2.4.1.4: Enlarged backscatter data. We are interested in the backscatter data between the signals from two boundaries……...43

28. Figure 2.4.2.1: A side view of the diagram for spatial averaging of the backscatter and attenuation data in two perpendicular directions.……..…….……44

29. Figure 2.4.3.1: The diagram represents the orientation dependence of the tissue sample with the use of rotating stage……..……..…….45

30. Figure 2.4.3.2: Illustration of top view of the plane of tissue sample when collecting data on 30-degree increments……46

31. Figure 2.5.1:Applying the gate to the backscatter data between the two boundaries.A Hanning window was used as the gate for this study……...…...……..47

32. Figure 2.5.2: Close representation of the selected backscatter data using the Hanning window……..……..……...48

33. Figure 2.5.3: Applying the hanning window as a sliding window on to a selected backscatter data……..…....……..49

34. Figure 2.5.4: Applying the hanning window on to a reflected signal…….51

35. Figure 2.5.5: Comparison of first reflection signals through water path only and tissue…...52

36. Figure 3.1.1.1: ABTF on 15 positions of *x* direction-Sample 1……...……..55

37. Figure 3.1.1.2: ABTF on 15 positions of *y* direction-Sample 1……..56

38. Figure 3.1.1.3: Averaged values of ABTF on two perpendicular directions *x*

and *y* -Sample 1.....57

39. Figure 3.1.1.4: Spatially averaged ABTF with standard deviation-sample 1..……...58

40. Figure 3.1.1.5: Spatially averaged ABTF-all 4 samples…….59

41. Figure 3.1.1.6: ABTF averaged over 4 samples with standard deviation……...60

42. Figure 3.1.2.1: Attenuation coefficient on 15 positions of *x* direction-Sample 1……...61

43. Figure 3.1.2.2: Attenuation coefficient on 15 positions of *y* direction-Sample 1……...62

44. Figure 3.1.2.3: Best frequency range - attenuation coefficient (on *x* direction- Sample 1)…63

45. Figure 3.1.2.4: Best frequency range - attenuation coefficient (on *y* direction- Sample 1)…63

46. Figure 3.1.2.5: Attenuation coefficient averaged over *x* and *y* directions- Sample 1…….64

47. Figure 3.1.2.6: Attenuation coefficient with standard deviation- Sample 1 ……..65

48. Figure 3.1.2.7: Attenuation coefficient averaged over 2 perpendicular directions

-All 4 samples……..……..66

49. Figure 3.1.2.8: Attenuation coefficient averaged over 4 samples with standard deviation…67

50. Figure 3.1.3.1: Backscatter coefficient on 15 positions of *x* direction- Sample1……...69

51. Figure 3.1.3.2: Backscatter coefficient on 15 positions of *y* direction- Sample 1……..70

52. Figure 3.1.3.3: Averaged values of BSC on two perpendicular directions-Sample 1……71

53. Figure 3.1.3.4: BSC with standard deviation – *x* direction……..……...72

54. Figure 3.1.3.5: BSC with standard deviation – *y* direction…….72

55. Figure 3.1.3.6: BSC with standard deviation – Sample 1……...73

56. Figure 3.1.3.7: Backscatter coefficient averaged over 2 perpendicular directions

- All 4 samples…….……..74

57. Figure 3.1.3.8: Backscatter coefficient averaged over 4 samples with standard deviation…75

58. Figure 3.2.1.1: ABTF on 13 orientations - Brain tissue sample 2……..77

59. Figure 3.2.1.2: ABTF averaged over angles with standard deviation–Sample 2……77

60. Figure 3.2.1.3: ABTF averaged over angels-All 5 samples……78

61. Figure 3.2.1.4: ABTF averaged over 4 samples with standard deviation…….....79

62. Figure 3.2.2.1: Attenuation coefficient on 13 orientations - Sample 2……...80

63. Figure 3.2.2.2: Best frequency range for the attenuation coefficient……..81

64. Figure 3.2.2.3: Attenuation coefficient averaged over angles –Sample 2……..82

65. Figure 3.2.2.4: Attenuation coefficient averaged over angels-All 5 samples…….....83

66. Figure 3.2.2.5: Attenuation coefficient averaged over 5 samples with standard deviation…84

67. Figure 3.2.3.1: BSC on 13 orientations - Sample 2……85

68. Figure 3.2.3.2: BSC on 0^o to 150^o - Sample 2……86

69. Figure 3.2.3.3: BSC on 180^o to 360^o - Sample 2……86

70. Figure 3.2.3.4: BSC with standard deviation – Sample 2……..87

71. Figure 3.2.3.5: BSC with standard deviation at1-5 MHz – Sample 2……88

72. Figure 3.2.3.6: BSC averaged over angels-All 5 samples……..89

73. Figure 3.2.3.7: BSC averaged over 4 samples with standard deviation…….90

74. Figure 4.1: Reflected signal with different gate sizes…….....92

75. Figure 4.2: ABTF with different gate sizes……....93

76. Figure 4.3: The diagram represents the spatial averaging of data while performing the orientation dependence measurements……...…….94

77. Figure 7.1: Position of the Hanning window after the front reflection from sample……113

78. Figure 7.2: Backscatter data with Hanning window...…….....…….....113

1. INTRODUCTION

1.1 Significance of the study

The disruption of the normal function of brain cells is broadly referred to by the term 'brain injury' which contributes to a substantial number of health problems all over the world. Traumatic brain injury (TBI) is a common category of brain injuries that is a leading cause of death and permanent disability worldwide especially in young adults and children. Many TBI's result from vehicle accidents and other incidents such as falls and violence and go undiagnosed. When a person suffers a TBI there are no first responder tools capable of directly detecting the damage with the technology presently available. The general process for evaluating a potential head injury is to go for MRI (magnetic resonance imaging) or X-ray CT (computerized tomography) scans as soon as possible to evaluate the location of brain injury for treatments or rehabilitation options [1, 2]. Though these modalities are available they are very expensive and available only in medical centers. This is where ultrasonics applications have the potential to play a major role. Due to its low cost and portability, ultrasound technology could be used to bridge a wide gap in the TBI diagnostic process.

Sound waves of frequencies above the threshold of human hearing (20 kHz) are known collectively as ultrasound, which has a wide range of applications in medical and industrial fields. Figure 1.1.1 shows the frequency spectrum of acoustic waves and phenomena and applications associated with different regions. We are interested in the ultrasonic range that is useful in biomedical applications. The medical specialties, obstetrics and gynecology, cardiology and, urology applications all rely on the diagnostic power of ultrasonic imaging

technology. In addition to its ability to provide rapid, high-quality images, it is non-ionizing and has a long record of safety.

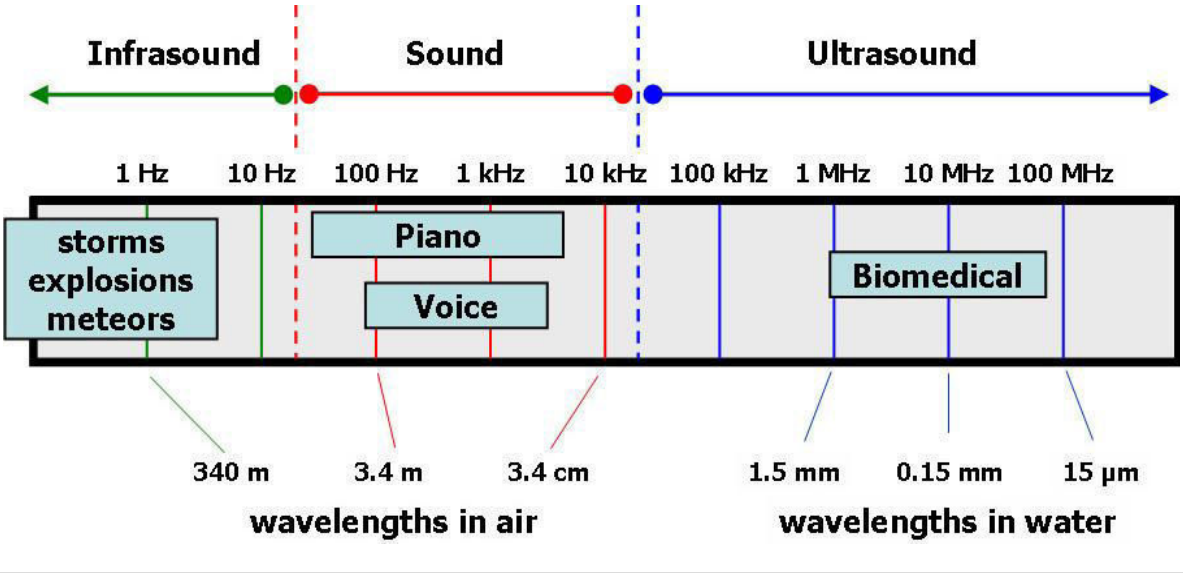

Figure 1.1.1: Frequencies 20 Hz – 20 kHz is the most familiar region for human hearing. Sound waves of frequencies above the threshold of human hearing (20 kHz) are known as the ultrasound. Frequencies falling below 20 Hz are considered as infrasonic.

Tissue characterization by ultrasound is a promising approach to detect and quantify the pathologic changes in the body non-invasively. In this project ultrasound is used to study the properties of mammalian brain tissues, in particular, backscatter and attenuation, which are intrinsic ultrasonic properties that can be used to characterize many tissues. The most important parameters in this work are those ultrasonic properties of mammalian brain tissues that could be useful to identify a possible pathological condition in the human brain. The structure of the human brain exhibits left- right symmetry which could be exploited for diagnostic purposes by applying ultrasound on opposite sides of the head and comparing the measurements of ultrasonic scattering properties for asymmetry of the signal when a space-filling lesion is present due to a TBI as shown in Figure 1.1.2.

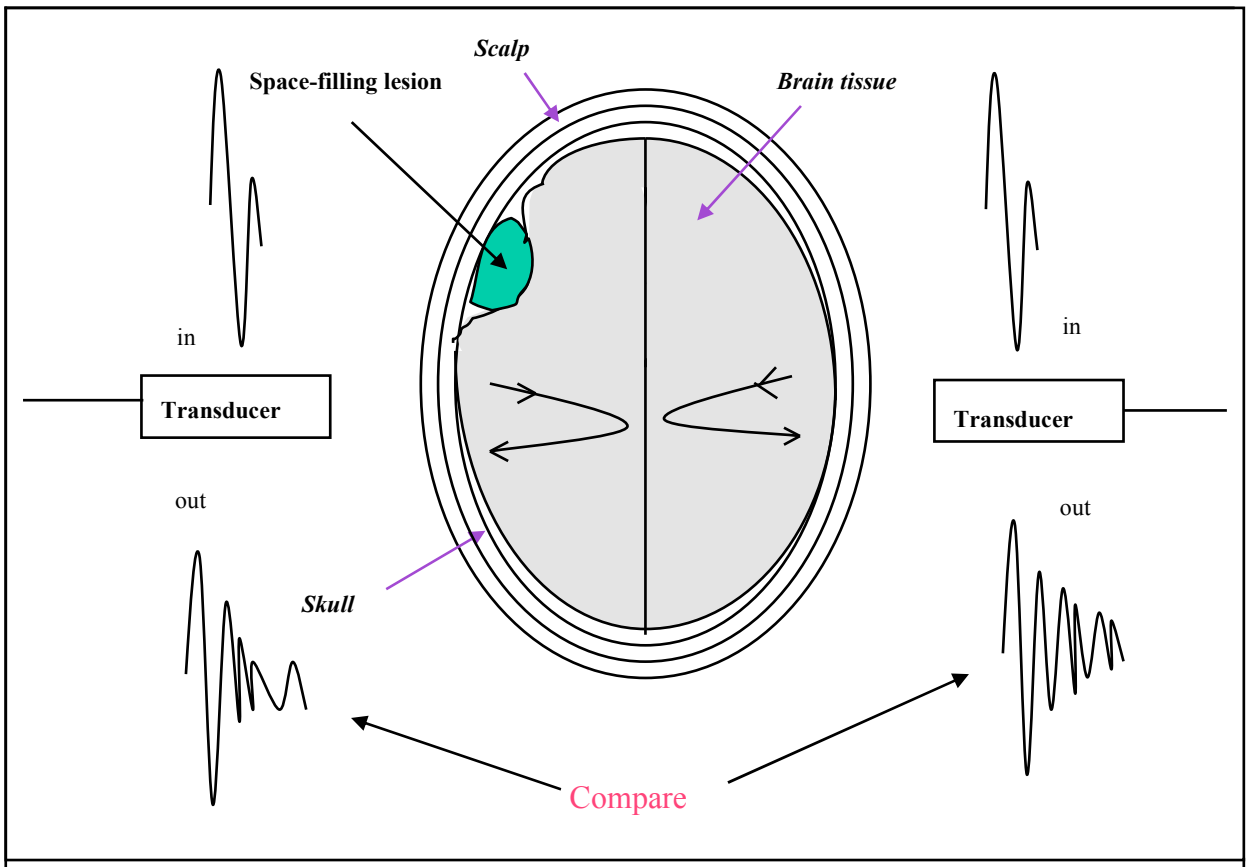

Figure 1.1.2: A diagram represents the possible backscattered signals in the presence of a space-filling lesion in brain. The diagram indicates the signature of a space filling lesion as an asymmetry the backscatter signals.

Figure 1.1.2 depicts a strategy for detecting TBI's with a space-filling lesion. Ultrasound is launched into opposite sides of the head with two transducers and the returning backscatter signals compared for any type of asymmetry due to a space –filling lesion. This strategy rests on the assumption that backscatter from normal cranium from both sides of the brain will display a certain degree of similarity [3]. This work is focused on measuring ultrasonic properties of brain tissue, and considering its applicability in identifying the presence of abnormalities with in the brain. Even with the difficulty of passing the ultrasound through cranium, this approach may provide an effective means to determine the presence of a space-filling TBI that is relatively inexpensive, safe and portable.

1.2 Brain Anatomy

For the measurements in this study ovine brains were used, which are similar in structure to human brain. An ovine brain contains all the same parts as the human brain, but is smaller in size. Mammalian brain is mainly composed of three parts, the brain stem, the cerebellum and the cerebrum as shown in Figure 1.2.1. The posterior part of the brain is the brain stem where the spinal cord enters the brain, through which the nerves in the body are connected to the brain. The brain stem consists of the midbrain, the pons and the medulla. The cerebellum or the "little brain" is located just above the brain stem. It is composed of two lateral cerebellar hemispheres and the vermis, which is a narrow worm shaped structure that connects the two hemispheres. The cerebellum contains many concentric folds called folia, which allow for a large amount of surface area. It is involved in functions that control the muscles and in the maintenance of equilibrium [4]. The cerebrum is the largest part of the brain. In humans the cerebrum covers about 85% of the brain, and this is where higher order thinking is synthesized. It is made of two hemispheres, and each hemisphere can be divided into four lobes. The frontal lobe is the front section of the cerebrum which is responsible for personality, speech, planning and problem solving. The parietal lobe is the top area of the cerebrum, and it deals with recognition and movement. The occipital lobe is the back section and is associated with vision. The temporal lobes are on the side and are involved with memory, language and speech functions. Each lobe is composed of an outer layer (grey matter) and an inner layer (white matter), which is more homogeneous. Physically one can feel the difference between those two tissues, as grey matter is softer than white matter. Figure 1.2.2 shows a picture of an ovine brain used in this study. As previously mentioned, the ovine brain structure is similar to the human brain structure. Concerning the difference in mass, the brain of a human adult has mass about 1400 g where that

of ovine brain is about 100 g [5]. Due to the difficulty in obtaining human brain samples and the low cost and high availability of ovine brains, the latter are used in this work. Figure 1.2.3 provides a size comparison of human and ovine brains.

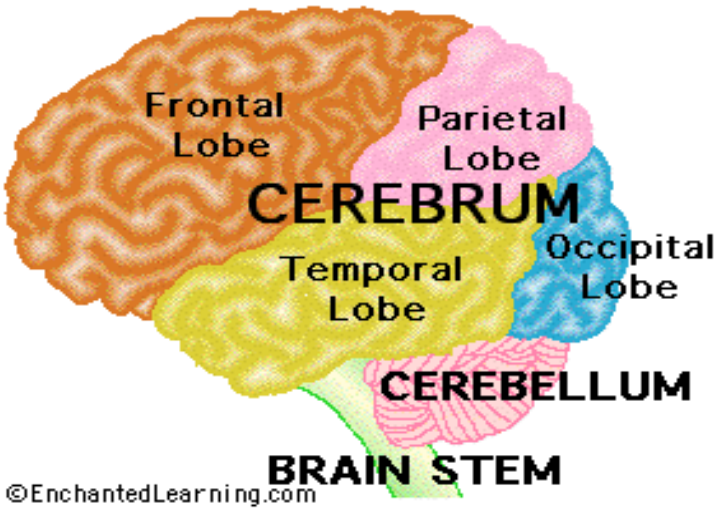

Figure 1.2.1: Three major parts of the mammalian brain: the brain stem, the cerebellum and the cerebrum.(Picture from http://www. enchantedlearning.com/subjects/anatomy/brain/structure.shtml)

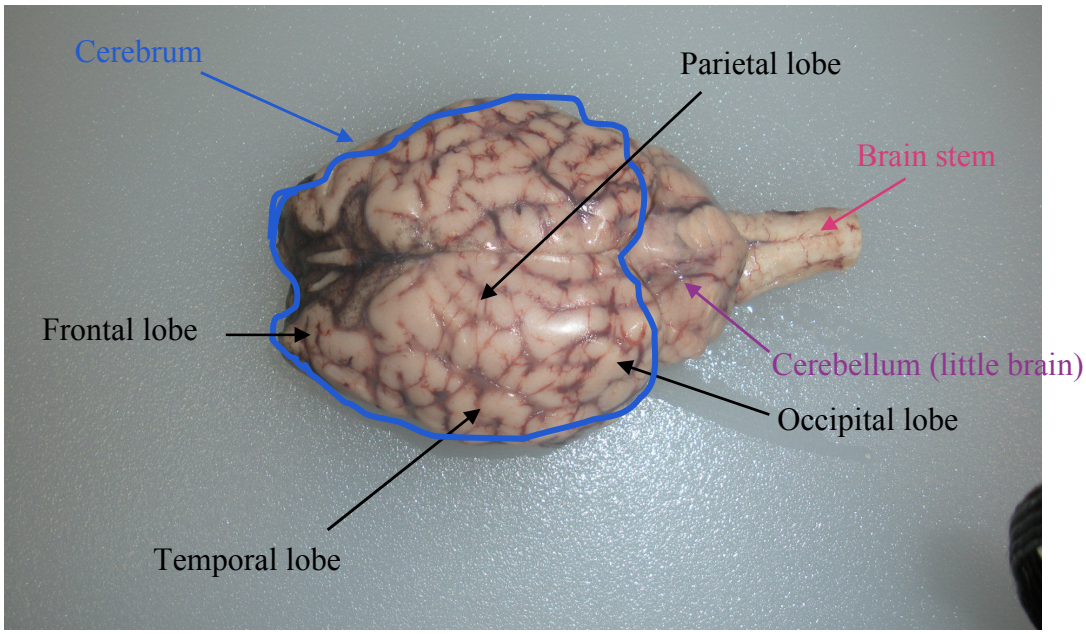

Figure 1.2.2: A picture of an ovine brain. It shows the three major parts of a mammalian brain: The brain stem, the cerebellum and the cerebrum. The cerebrum is the largest area of the brain and has two hemispheres and each hemisphere consists of four lobes.

Figure 1.2.2 is a picture of an ovine brain that was used in this work. These brains were obtained from the Carolina Biological Supply Company (Burlington, North Carolina, USA). Each brain was dissected, and the two hemispheres from the cerebrum, the largest area of the brain, were used for our study. Due to the small size of the ovine brain it was not possible to completely isolate the white matter from the grey matter and thus our measurements involved regions of mixed white and grey matter. In earlier work [3], the ultrasonic properties of white matter from ovine brains (ultrasonic backscatter and attenuation coefficient spectra) were presented for two orientations, 0^0 and 90^0 relative to the sagittal plane of the head and the results were consistent with the attenuation coefficient with other soft tissues such as cardiac and liver tissues. The ultrasonic attenuation coefficient and propagation speed in human brain tissues were reported in [6]. In that work, the attenuation coefficient vs frequency was measured for white,

grey and mixed matter and it was found that the grey or mixed matter has the lower attenuation and speed of sound than white matter. In addition the observed attenuation coefficient was found to be a frequency dependent negative function of temperature and the minimum propagation speed was found as a function of temperature.

As mentioned earlier the goal of this thesis is to contribute to a better understanding of the ultrasonic properties of mammalian brain tissue in the detection of brain injury, and our approach is to examine the backscatter and attenuation properties of ovine brain tissue as a function of frequency.

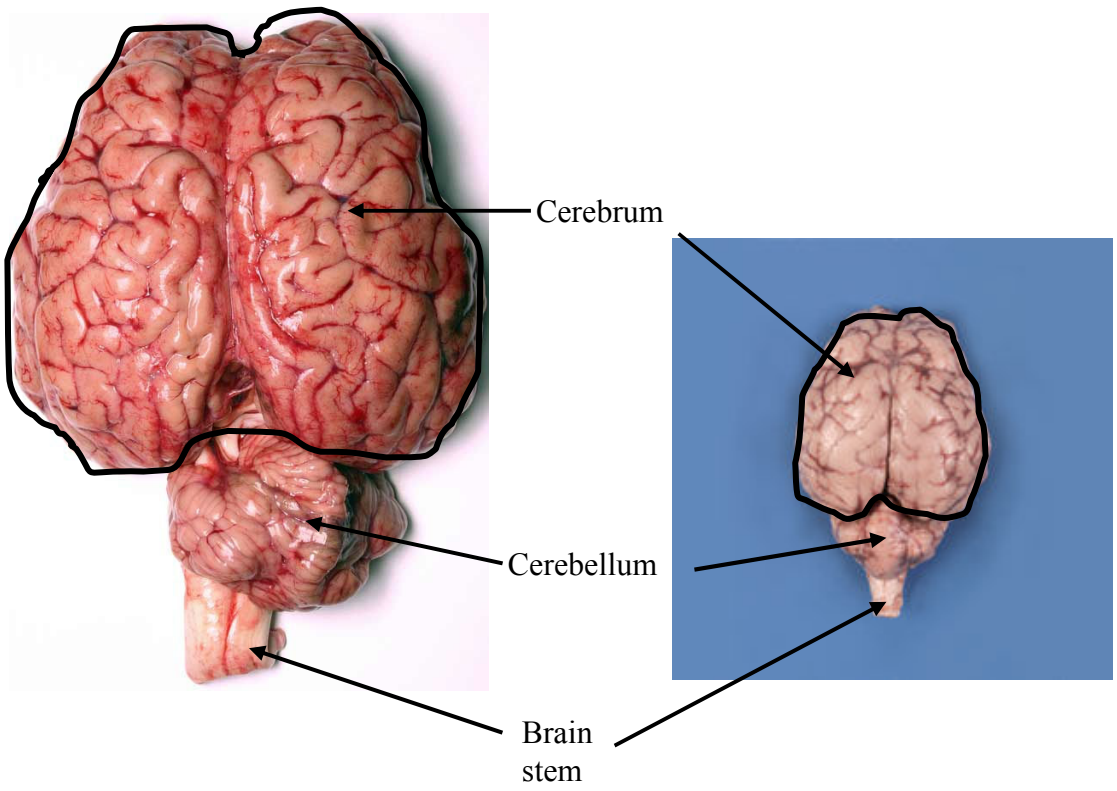

Figure 1.2.3: Comparison of main three parts human brain with ovine brain. Ovine brain has all the same parts as of a human brain but small in size. (Pictures from http://www. topnews.in/health/how-human-brain-recognizes-and-retains-patterns-images-29109,http:// www. carolina.com/product/perfect+solution+sheep+specimens.do)

1.3 Review of related Literature

Research on ultrasound and medical imaging date back to the 1940's.The first paper on medical ultrasonics was published in 1942 by Doctor Karl Theodore Dussik of Austria. Professor Ian Donald was a Scottish physician who explored the applications of ultrasound in medicine in 1950s [7, 8].

Much useful information is available from a number of past research programs concerning the ultrasonic scattering and attenuation properties of biological tissues from the brain, heart, liver and kidney [3, 6, 9, 10]. Earlier work concerned the importance of those properties in the detection of brain injury [3]. The ultrasonic scattering and attenuation properties of white matter from preserved ovine brains were examined during this study in which an anisotropy in the attenuation coefficient and backscatter was observed. During this work the transmitting transducer was used for the detection of backscatter signals and a co-axially aligned second transducer was used to capture the through transmitted signals to determine the attenuation. In our study, the same transducer was used to transmit and to capture all of the acquired signals as shown in Figure 2.3.1.

The backscatter coefficient of a tissue describes the scattering efficiency at 180^{o} as a function of frequency. Throughout this study, the backscatter coefficient was determined using the equation

$$\eta(\omega) = |S(\omega)|^2 A(\omega) B(\omega) \Gamma \qquad (1.3.1)$$

where $\eta(\omega)$ is the backscatter coefficient, $|S(\omega)|^2$ is the apparent backscatter transfer function(ABTF) and the term $A(\omega)B(\omega)\Gamma$ compensates for diffraction effects, sample attenuation, and the boundary transmissions and reflections. The ABTF is determined by

comparing the scattered signal from the brain tissue sample with the reflected signal from the steel plate that used as the reference.

Measurements of the ultrasonic attenuation coefficient and propagation speed in human brain tissues as functions of frequency, temperature, tissue type, age at death, formalin fixation and tissue aging after death *in vitro* in 22 samples from six anatomic sites in five normal human brains were reported in [6]. During this study they measured those two properties. The attenuation coefficient was measured at 1.0, 2.2, 3.0, 5.0 MHz and the propagation speed was measured at 1.0, 3.0 and 5.0 MHz. For their study, white matter (corna radiata, medulla, pons), gray matter (Island of Riel, cerebellum) and mixed matter (basal ganglia) were considered separately. The magnitudes of the reference signal and the through sample signal were compared to determine the attenuation coefficient in a manner similar to the method used in our study.

In this study they found that the white matter attenuation is 1.5 times the attenuation of gray matter and that the mixed matter has an intermediate value. During our study we focused on mixed matter of the ovine tissues and our results are in approximate agreement with this earlier work. Using the mean values, they found a slope of attenuation of 1.08 dB/cm-MHz. at 1.0, 3.0, 5.0 MHz. An important result from this study is that the attenuation coefficient values for an infant are lower than those of an adult. They have observed this using a three-day-old infant, and this difference may be due to the softness of the baby tissues and also because it is not yet as developed as an adult brain. In this work they also found that the propagation speed shows a dispersion of 1.2 $ms^{-1}MHz^{-1}$ for fresh tissues, and that of fixed tissues is 1.0 $ms^{-1}MHz^{-1}$ over the range of 1-5 MHz.

The ultrasonic attenuation coefficient, the velocity of sound propagation and the differential scattering coefficient measurements were reported on liver, spleen and brain white

matter on freshly excised normal human tissues [9]. Though it is important to use the same tissue sample for all measurements, in this study they used two different tissue samples in two different shapes for attenuation and backscattering data. For the attenuation data they used slab shaped tissue samples with parallel surfaces of 40 cm^2 and a thickness of the range 1.5-2.5 cm. During this study five different measurements were made on each tissue sample and four transducers of frequencies 1.0, 2.0, 4.0 and 6.0 MHz were used that covered the frequency range 0.5-7.0 MHz. Beyond 3.0 MHz the results show a rapid increase in the attenuation coefficient for the brain white matter than for the other two tissue types. The backscatter data were acquired using cylindrically shaped tissue samples with a radius of 1.5 cm and a length of 6.0 cm. During this study three different measurements were made on each tissue sample and three transducers of frequencies 1.0, 2.0 and 4.0 MHz were used that covered the frequency range 0.5- 4.3 MHz. For our measurements we used cylindrically-shaped tissue samples for both attenuation and backscatter data with one transducer of frequency 5.0 MHz that covered the frequency range 1-10 MHz.

Ultrasonic backscattering properties were reported on bovine heart, liver, kidney, spleen, pancreas and rat myocardium over the frequency range of 2-7 MHz [10]. In this study they observed the highest backscatter from liver and the lowest from the spleen. They also found a higher backscatter from bovine myocardium than for rat myocardium. For the backscattering measurements they found the maximum backscattering coefficient from the liver and the minimum from the spleen in the frequency range 2-7 MHz. They used cube shaped samples that were mounted on plastic square holders with stainless-steel pins around the rim.

Attenuation coefficients vary widely from medium to medium. Biological materials and water are the most commonly used media in biomedical ultrasound. Table 1.3.1 shows the slope of attenuation of some biological materials and water at the frequency of 1 MHz [11].

Material	α (dB/ cm - MHz)
Blood	0.2
Bone, cortical	6.9
Bone, trabecular	9.94
Brain	0.6
Breast	0.75
Cardiac	0.52
Connective tissue	1.57
Dentin	80
Enamel	120
Fat	0.48
Liver	0.5
Marrow	0.5
Muscle	1.09
Tendon	4.7
Soft tissue (average)	0.54
Water	0.0022

Table 1.3.1: Attenuation coefficient of some biological samples and water.

1.4 Theoretical framework of the study

Although ultrasound was used in industrial applications much earlier, the history of ultrasound as a diagnostic tool goes back to the late 1940s. When considering wave propagation and scattering, a medium in which a wave travels can be categorized as either random or deterministic. The biological tissues can be categorized as complex inhomogeneous materials. So it is interesting to know interactions of a wave in such media and to formulate and express those interactions mathematically [12]. The focus of this thesis is to examine the attenuation and backscatter properties in mammalian brain tissues. This section briefly reviews some of the basic concepts of scattering and attenuation properties.

1.4.1 Scattering

This is a general physical process where some forms of radiation, such as sound or moving particles, deviate from their straight line path due to interactions with non-uniformities in the medium through which they pass. The inhomogeneous wave equation is used to describe the interaction in such a medium and is given by equation 1.4.1.1, [13]

$$\nabla^2 p - \frac{1}{\bar{c}^2}\frac{\partial^2 p}{\partial t^2} = \frac{1}{\bar{c}^2}\tilde{\beta}\frac{\partial^2 p}{\partial t^2} + \nabla\cdot\left[\tilde{\rho}\nabla p\right] \qquad 1.4.1.1$$

where p is pressure and now it denotes a function of the three-dimensional position vector $\boldsymbol{r}$, t is the time,∇ is the gradient operator , ∇^2 is the 'Laplacian operator', $\tilde{\rho}$ is the density 'fluctuation' term and $\tilde{\beta}$ is the compressibility 'fluctuation' term, $\bar{c} \equiv 1/\sqrt{\bar{\rho}\bar{\beta}}$ with $\bar{\rho}$ and $\bar{\beta}$ denoting the spatial mean values of the density and compressibility. The fluctuation parameters $\tilde{\rho}$ and $\tilde{\beta}$ represent the properties of an inhomogeneous medium where the scattering occurs; if those terms vanish, then the wave equation becomes homogeneous.

Let's consider the inhomogeneous medium with no absorption and small fluctuations in density ρ_1 and compressibility β_1. If ρ_0 and β_0 are the constant values inside an inhomogeneous volume V, ρ_1 and β_1 are zero outside V. Then,

inside V

$$\rho(r) = \rho_0 + \rho_1(r); \qquad \beta(r) = \beta_0 + \beta_1(r) \tag{1.4.1.2}$$

outside V

$$\rho(r) = \rho_0; \qquad \beta(r) = \beta_0 \tag{1.4.1.3}$$

At the boundary of V, with the normal vector $\boldsymbol{n}$ perpendicular to the surface of V

$$\frac{\partial \rho(r)}{\partial n} = \frac{\partial \beta(r)}{\partial n} = 0 \tag{1.4.1.4}$$

The density ($\tilde{\rho}$) and compressibility ($\tilde{\beta}$) fluctuation terms can be defined as follows:

$$\tilde{\rho} \equiv \frac{\rho_0 - \overline{\rho}}{\rho_0} \tag{1.4.1.5}$$

$$\tilde{\beta} \equiv \frac{\beta_0 - \overline{\beta}}{\overline{\beta}} \tag{1.4.1.6}$$

where $\overline{\rho}$ and $\overline{\beta}$ denote the spatial mean values of the density and compressibility.

Let's define the parameters

$$\tilde{\rho}(r) = \frac{\rho_1(r) - \rho_0}{\rho_0}; \qquad \tilde{\beta}(r) = \frac{\beta_1(r) - \beta_0}{\beta_0} \tag{1.4.1.7}$$

Now the wave equation can be written as [13]

$$\nabla^2 P(r,t) - \frac{1}{c^2}\frac{\partial^2 P(r,t)}{\partial t^2} = \frac{1}{c^2}\frac{\partial^2 P(r,t)}{\partial t^2} \cdot \tilde{\beta}(t) + div[\tilde{\rho}(r) \cdot grad \cdot P(r,t)] \tag{1.4.1.8}$$

where $c = (\rho_0 \beta_0)^{-1/2}$

The solution of the above equation can be obtained using the methods of Green's functions, which is a good way to solve inhomogeneous differential equations with specific

initial conditions or boundary conditions. The solution is, [13]

$$P(r,t) = P_i(r,t) + \int_{-\infty}^{\infty} dt_0 \int_V \left\{ \frac{1}{c^2} \frac{\partial^2 P(r_0,t_0)}{\partial t^2} \cdot \tilde{\beta}(t_0) + div\left[\tilde{\rho}(r_0) \cdot grad \cdot P(r_0,t_0)\right] \right\} G(r_0,r;t_0,t) d^3 r_0$$

where $G(r_0,r;t_0,t) = \dfrac{\delta(t - t_0 - |r_0 - r|/c)}{4\pi|r_0 - r|}$ 1.4.1.9

The solution of the equation 1.4.1.9 is solved by making approximations that are going to be valid only for specific geometries. One of the important approximations useful here is the Born approximation. For a homogeneous medium the equation 1.4.1.9 is approximated by replacing $P(r,t)$ with the incident wave $P_i(r,t)$ that travels through the volume V. The Born approximation is valid only if $\tilde{\rho}(r)$ and $\tilde{\beta}(r)$ are small and the scattering is weak. When this is not true, equation 1.4.1.9 can be solved by an iterative technique with subsequent approximations. So now $P(r,t)$ can be replaced by, [13]

$$P(r,t) = P_i(r,t) + P_s(r,t) \quad 1.4.1.10$$

where $P_i(r,t)$ is the incident wave and $P_s(r,t)$ is the scattered wave.

So now the scattered wave can be solved by using the Born approximation which yields, [13]

$$P_s(r,t) = \int_{-\infty}^{\infty} dt_0 \int_V \left\{ \frac{1}{c^2} \frac{\partial^2 P_i(r_0,t_0)}{\partial t^2} \cdot \tilde{\beta}(t_0) + div\left[\tilde{\rho}(r_0) \cdot grad \cdot P_i(r_0,t_0)\right] \right\} G(r_0,r;t_0,t) d^3 r_0$$

1.4.1.11

1.4.2 Scattering Cross-Section

The effective area that describes the radiation scattered by a particle can be defined by the scattering cross-section. The total power scattered, S is proportional to the incident wave intensity I on a scatterer.

$$S \propto I \quad 1.4.2.1$$

The proportionality constant is the total scattering cross-section, σ_s

$$\sigma_s = \frac{Power\ scattered\,(S)}{Incident\ \text{int}ensity\,(I)} \rightarrow \frac{energy/time}{(energy/time)/area} = area \qquad 1.4.2.2$$

It is clear from the equation 1.4.2.2 σ_s has dimensions of area.

A differential cross-section $\sigma_d(\phi_s,\theta_s)$ can be defined in terms of the total power scattered $dS(\phi_S,\theta_S)$ and the solid angle $d\Omega$ in angular direction (ϕ_s,θ_s) and is given by the equation,

$$\sigma_d(\phi_s,\theta_s) = \lim_{d\Omega \to 0} \frac{dS(\phi_s,\theta_s)}{Id\Omega} = \lim_{d\Omega \to 0} \frac{d\sigma_s}{d\Omega} \qquad 1.4.2.3$$

Backscatter is the differential cross-section for $\theta = \pi$,

$$\sigma_{bs} = \sigma_d(0,\pi) \qquad 1.4.2.4$$

The absorption cross-section (σ_a) and the extinction cross-section (σ_t) encompasses the total of scattering and absorption are given by equations 1.4.2.5 and 1.4.2.6,

$$\sigma_a = \frac{Power\ absorbed}{Unit\ incident\ \ flux(I)} \qquad 1.4.2.5$$

$$\sigma_t = \sigma_s + \sigma_a \qquad 1.4.2.6$$

For certain media scattering is incoherent and the power scattered will be proportional to the volume of such a medium. So for media that scatter incoherently the scattering coefficient μ_s is defined as a measure of scattering, which gives the scattering cross section per unit volume, which has the units of m^{-1}. The differential scattering coefficient μ_d, absorption coefficient μ_a, attenuation coefficient μ_t and backscattering coefficient μ_{bs} can be defined in a similar way as μ_s. The backscatter coefficient is the main parameter of interest in the work reported here.

1.4.3 Backscatter

Backscatter is the reflection of signals or particles back in the direction they came from. The apparent backscatter transfer function (ABTF) is determined by comparing the scattered

signal from the brain tissue sample with the reflected signal from the steel plate that is used as a reference. The apparent backscatter transfer function is given by, [3]

$$\left|S(\omega)\right|^2 = \frac{\left|F_{tissue}(\omega)\right|^2}{\left|F_{steel\ \ plate}(\omega)\right|^2} \qquad 1.4.3.1$$

where $\left|S(\omega)\right|^2$ is the apparent backscatter transfer function, $|F_{tissue}(\omega)|^2$ is proportional to the Fourier power spectrum for the brain tissue in a given position or an orientation, $\left|F_{steel\ \ plate}(\omega)\right|^2$ is proportional to the Fourier power spectrum for the reference steel plate.

1.4.4 Attenuation

Attenuation is the loss of energy of any kind of flux in the forward direction through a medium. We are interested in biological tissues as the medium and ultrasound as the energy flux. The total loss of sound due to the tissue is influenced by scattering, absorption, refraction and reflection. The attenuation coefficient (α) is an important parameter that can be used to quantify how the intensity of a beam is reduced as it passes through a specific medium; it is measured by the units of dB/cm/MHz.

The incoming wave from the transducer, will be partially transmitted across boundary 1 which is water-tissue. It loses energy to attenuation (scattering and absorption losses) as it crosses the sample, and then it is partially transmitted across boundary 2 which is tissue-water. It then reflects back from the Steel plate and repeats the transmission process in the other direction. This is illustrated on Figure 1.4.4.1.

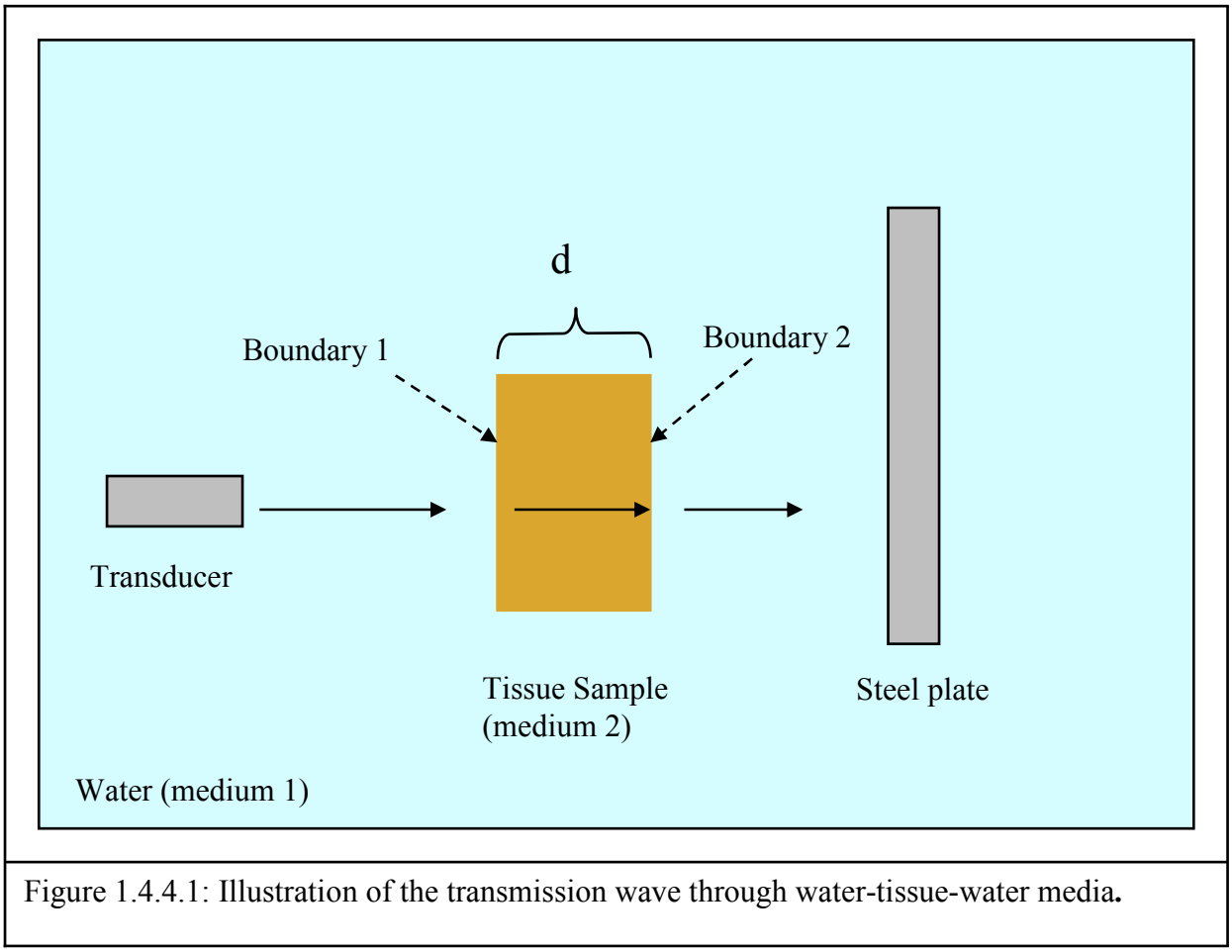

Figure 1.4.4.1: Illustration of the transmission wave through water-tissue-water media.

The amplitude (a_1) of the transmission wave through water(medium 1)-tissue(medium 2)-water(medium 1) can be written as,

$$a_1 = t_{12}\, e^{-\alpha d}\, t_{21} \qquad 1.4.4.1$$

where, t_{12} is the transmission coefficient at boundary 1 between water and tissue, α is the attenuation coefficient, d is the sample thickness and t_{21} is the transmission coefficient at boundary 2 between tissue and water. So the amplitude of the wave that returns to the transducer is given by,

$$a_2 = \left(t_{12}\, e^{-\alpha d}\, t_{21}\right)^2 \qquad 1.4.4.2$$

When the transducer and the steel plate present in the water tank, there is only the reflected

signal through the water path, and the Fourier tranform of the water-path-only signal can be written as,

$$F_1 = F_{wp}(\omega) \qquad 1.4.4.3$$

When the tissue sample presents in between the transducer and the steel plate the Fourier transform is given by,

$$\left|F_2\right| = \left|F_{wp}(\omega)\right|(t_{12}\,t_{21})^2\, e^{-2\alpha d} \qquad 1.4.4.4$$

where $F_{wp}(\omega), t_{12}, t_{21}, \alpha$ and d have the same meanings as above.

Then the signal loss (SL) is calculated by,

$$SL = \frac{F_2}{F_1} = (t_{12}\,t_{21})^2\, e^{-2\alpha d} \qquad 1.4.4.5$$

SL can be written using the amplitudes of the first reflected signals from the polished steel plate through water path (A_1) and the sample (A_2).

$$SL = \frac{A_2}{A_1} \qquad 1.4.4.6$$

Now from equations 1.4.4.5 and 1.4.4.6,

$$SL = \frac{A_2}{A_1} = (t_{12}t_{21})^2 e^{-2\alpha d} \qquad 1.4.4.7$$

Now taking ln on both sides of the equation 1.4.4.7,

$$\ln\left(\frac{A_2}{A_1}\right) = \ln\left((t_{12}\,t_{21})^2\, e^{-2\alpha d}\right)$$

$$\ln\left(\frac{A_2}{A_1}\right) = 2\ln t_{12}\,t_{21} - 2\alpha d$$

$$2\alpha d = 2\ln t_{12}\,t_{21} - \ln\left(\frac{A_2}{A_1}\right)$$

$$\alpha = \frac{\ln t_{12}\,t_{21}}{d} - \frac{\ln\left(\frac{A_2}{A_1}\right)}{2d} \qquad 1.4.4.8$$

The equation 1.4.4.8 gives the units of α in nepers/length**.** Since we are interested on the units of dB/length for the α**,** logarithm to the base 10 was used for the calculations.So the equation 1.4.4.8 becomes,

$$\alpha = \frac{20 \log_{10} t_{12} t_{21}}{d} - \frac{20 \log_{10}\left(\frac{A_2}{A_1}\right)}{2d} \qquad 1.4.4.9$$

t_{12} and t_{21} can be replaced using the impedance and density values of each medium,

$$t_{12} = \frac{2\rho_1 Z_2}{\rho_2 (Z_1 + Z_2)} \qquad 1.4.4.10$$

$$t_{21} = \frac{2\rho_2 Z_1}{\rho_1 (Z_1 + Z_2)} \qquad 1.4.4.11$$

where ρ_1 is the density of medium 1 which is water, ρ_2 is the density of medium 2 which is tissue, Z_1 is the impedance of medium 1 and the Z_2 is the impedance of medium 2.

Now the term $t_{12}t_{21}$, the coefficient of transmission (T) becomes,

$$t_{12}t_{21} = \frac{4Z_1 Z_2}{(Z_1 + Z_2)^2} = T \qquad 1.4.4.12$$

Now equation 1.4.4.9 becomes,

$$\alpha = \frac{20 \log_{10}\left(\frac{4 Z_1 Z_2}{(Z_1 + Z_2)^2}\right)}{d} - \frac{20 \log_{10}\left(\frac{A_2}{A_1}\right)}{2d} \qquad 1.4.4.13$$

The acoustic impedance Z is defined as the product of the density and the velocity, [14]

$$Z = \rho v \qquad 1.4.4.14$$

where ρ is the density of medium and v is the speed of sound through that medium.

Therefore,

$$Z_1 = \rho_1 v_1 \text{ and } Z_2 = \rho_2 v_2 \qquad 1.4.4.15$$

where ρ_1 is the density of water, ρ_2 is the density of tissue, v_1 is the speed of sound through water, v_2 is the speed of sound through tissue and Z_1, Z_2 are the acoustic impedances of water and tissue respectively.

So the equation 1.4.4.13 becomes,

$$\alpha = \frac{20 \log_{10}\left(\frac{4\rho_1 v_1 \rho_2 v_2}{(\rho_1 v_1 + \rho_2 v_2)^2}\right)}{d} - \frac{20 \log_{10}\left(\frac{A_2}{A_1}\right)}{2d} \qquad 1.4.4.16$$

where α, ρ_1, ρ_2, v_1, v_2, A_1, A_2 and d have the meanings as mentioned above.

1.4.5 Backscatter Coefficient (μ_{bs})

As mentioned in section 1.4.2 for a medium that scatters incoherently, the backscattering coefficient μ_{bs} is defined as a measure of backscattering, which gives the scattering cross section per unit volume. The backscatter coefficient can be expressed in terms of the apparent backscatter transfer function ($|S(\omega)|^2$), the attenuation coefficient (α) and some correction factors, [15]

$$\mu_{bs}(f) = \frac{\Gamma^2}{4T^4} R^2 F(\alpha,\tau) \frac{1}{V(f)} \left\langle |S(\omega)|^2 \right\rangle \qquad 1.4.5.1$$

where μ_{bs}(f) is the frequency-dependent backscatter coefficient, Γ is the amplitude reflection coefficient of steel plate reflector, T is the transmission coefficient between water and the tissue, R is the focal length of the transducer, $V(f)$ is the frequency-dependent beam volume and $F(\alpha,\tau)$ is an attenuation correction factor that is given in equation 1.4.5.2

$$F(\alpha,\tau) = e^{4\alpha(f)x} e^{\alpha(f)c\tau} \frac{2\alpha c\tau}{e^{\alpha c\tau} - e^{-\alpha c\tau}} \qquad 1.4.5.2$$

where α is the frequency dependent attenuation coefficient, c is speed of sound through tissue sample, x is the position of the window relative to the front wall of the sample and τ is the gate duration of Hanning window.

1.4.6 Models

Tissues are complex inhomogeneous materials. Although they have a regular deterministic structure, it has been found empirically that their scattering properties can be modeled as a random medium. It is useful to consider simple theoretical models to measure the acoustic properties of such media. The discrete scattering model and the inhomogeneous continuum model are two such models that deal with complex media [13]. The first model consists of a homogeneous substrate with embedded the scatterers at random positions, and the latter is useful for a medium from which the average incoherent scattering arises from fluctuations in density and compressibility.

For our study we modeled ovine brain tissue samples as a random collection of particles, which exhibit incoherent scattering when spatially averaged. By spatial averaging we are able to average away the randomness.

2 METHODS

2.1 Experimental set up

The data were acquired using the system shown in Figure 2.1.1. The pulser / receiver (Olympus Model 5800) generates a high voltage electric pulse which will be converted into ultrasound at the transducer. The transducer has a center frequency of 5 MHz and a focal length of 2". The transducer was operated in pulse-echo mode. The sample was placed between the transducer and the steel plate reflector in a water tank as shown in Figure 2.1.2. The water acts as the ultrasonic couplant that facilitates the transmission of sound energy between the transducer and the test sample. The steel plate reflector acts as an ultrasonic mirror and is used as a reference reflector in this technique. An oscilloscope (LeCroy Waverunner 432) was used to capture the receiving signals and a special script was used to download those data to a computer that can be saved for further analysis. The data was collected at a sample rate of 1 Gs/s. After saving the data all the mathematical operations were done using MATLAB (R2011a).

Figure 2.1.2 shows a picture of the water tank setup used to perform orientation dependent data acquisition with a cylindrically shaped tissue sample. Here the sample was mounted to a rotating stage as shown in Figure 2.3.2.5 in order to collect data on different orientations from 0^0 to 360^0. For the spatial averaging acquisition the rotating stage was replaced by rails as shown in Figure 2.3.1.3 that can be used to move the sample in two perpendicular directions. Figure 2.1.3 shows a photograph of the data acquisition setup.

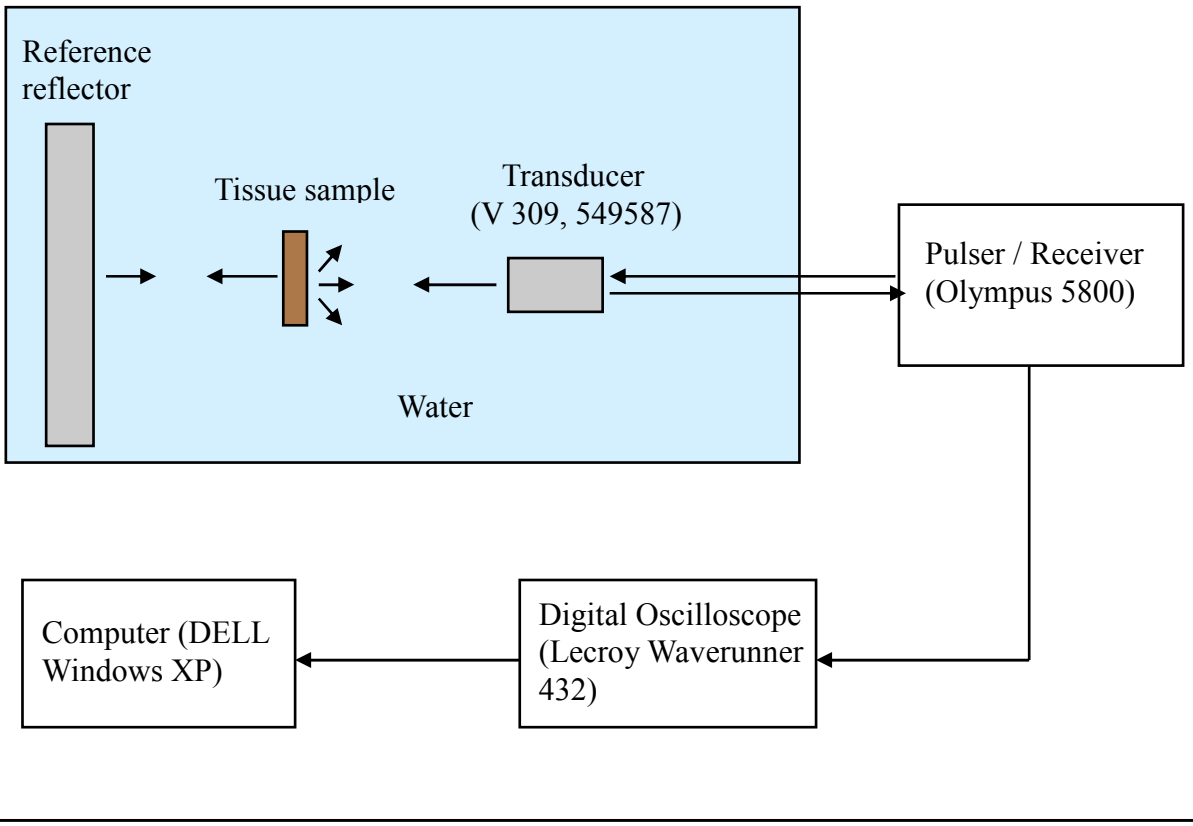

Figure 2.1.1: Illustration of the data acquisition system

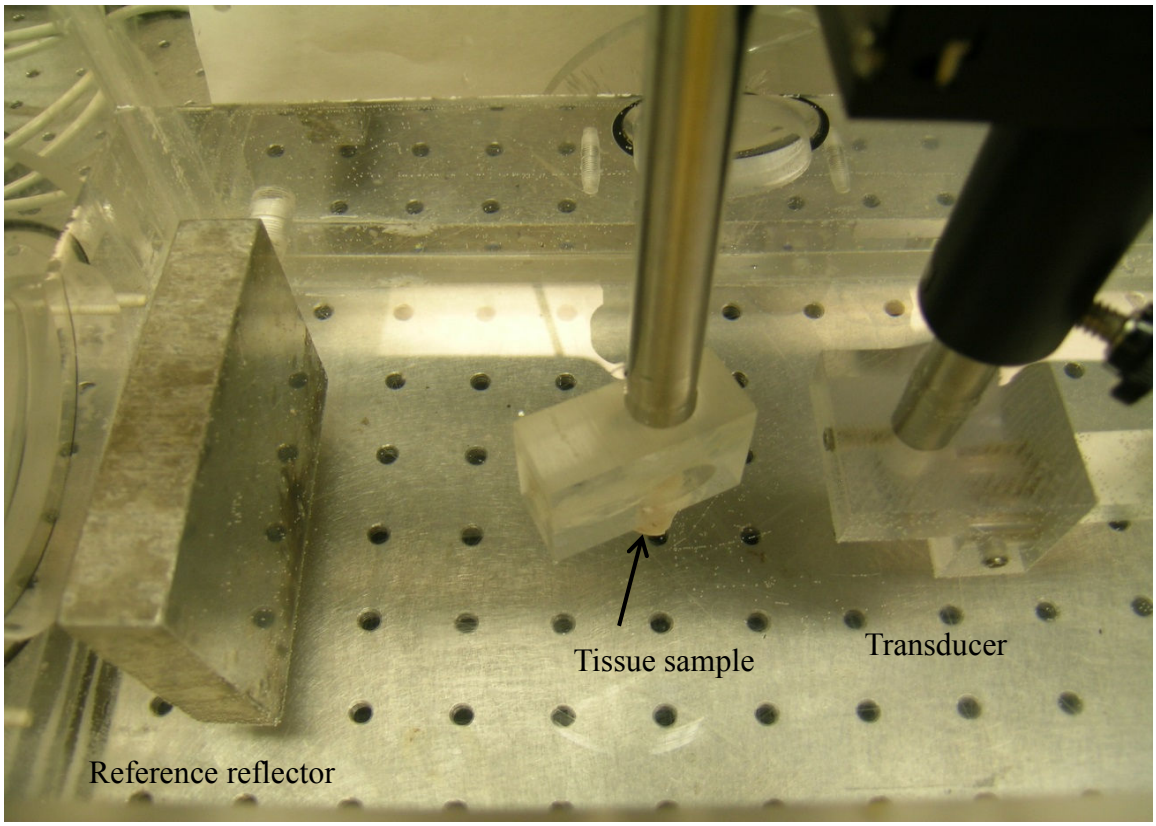

Figure 2.1.2: Top view of the water tank showing the reference, tissue sample and the transducer.

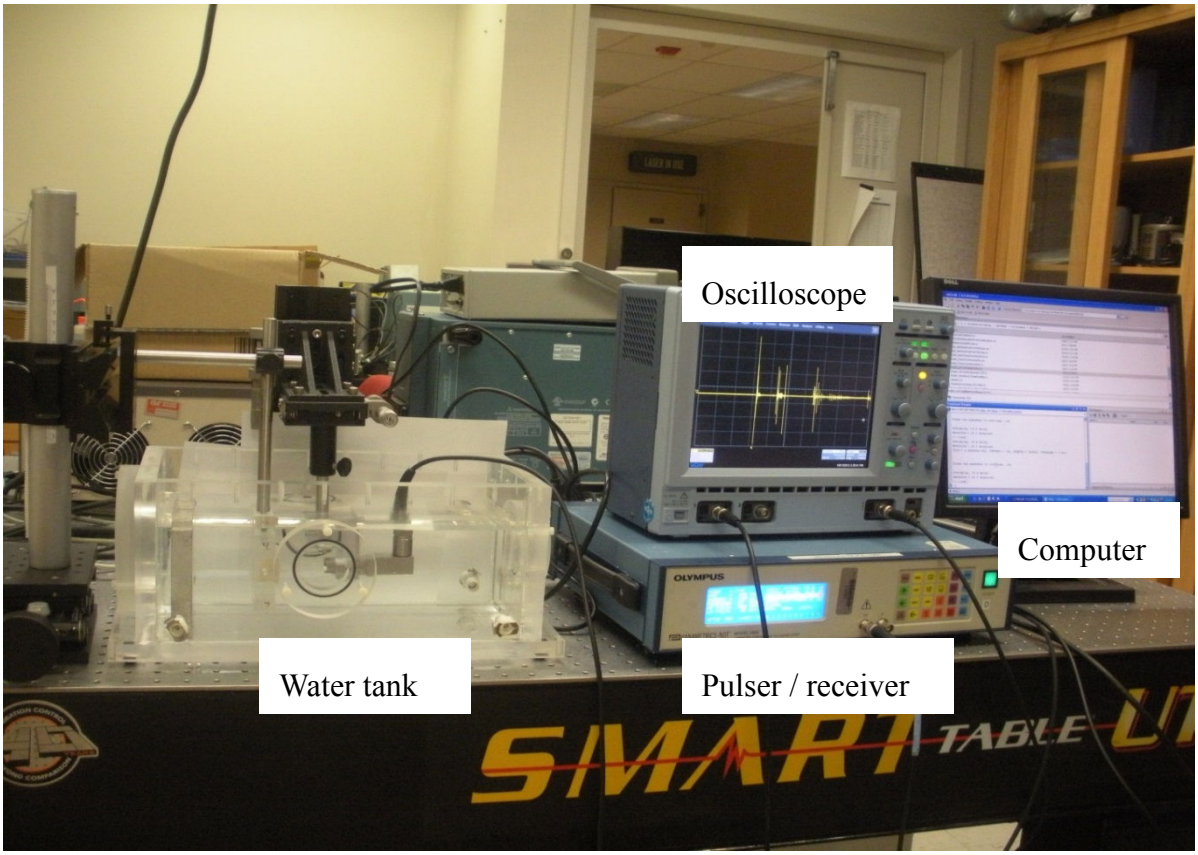

Figure 2.1.3: A photograph of the apparatus set-up.

2.2 Dynamic range

The initial step in the measurement process is to establish the dynamic range of our system which gives the largest and the smallest signals that we can measure accurately and defines the range over which our system responds linearly. The process is as follows. First reflected signals from the steel plate, were acquired starting with 60 dB gain setting and stepping down in 10 dB steps to 0 dB which is the full amplification range of the pulser/receiver. The same procedure was done for the backscatter data of the sheep brain tissues after inserting the sample in between the transducer and the steel plate, without changing the alignment of the transducer and the steel plate.

Figure 2.2.1 represents the dynamic range for the 1st reflected signal from the steel plate. From the plot it is clear that the frequency range 1-10 MHz shows a smooth pattern for 0 dB to 40 dB. However the 50 dB and 60 dB signals do not follow the trend because those two reflected signals saturated the amplifier, which is clear from the clipping of the waveforms as seen on the scope. Frequencies above 10 MHz represent noise. Therefore 1-10 MHz gives the best range of linearity for our measurement system. The range from 1-10 MHz was used for the measurements.

Figure 2.2.2 shows the dynamic range spectra for the measurement system from 1 to 10 MHz. It is clear from the diagram that the difference between two adjacent signals is 10 dB for the lower five curves, and it maintains that same difference throughout the measurement band with amplifier gain settings from 0 to 40 dB. The smooth featureless spectra also indicate that the alignment of the ultrasonic system is good. Figure 2.2.3 shows the dynamic range measurements with a brain tissue sample in place.

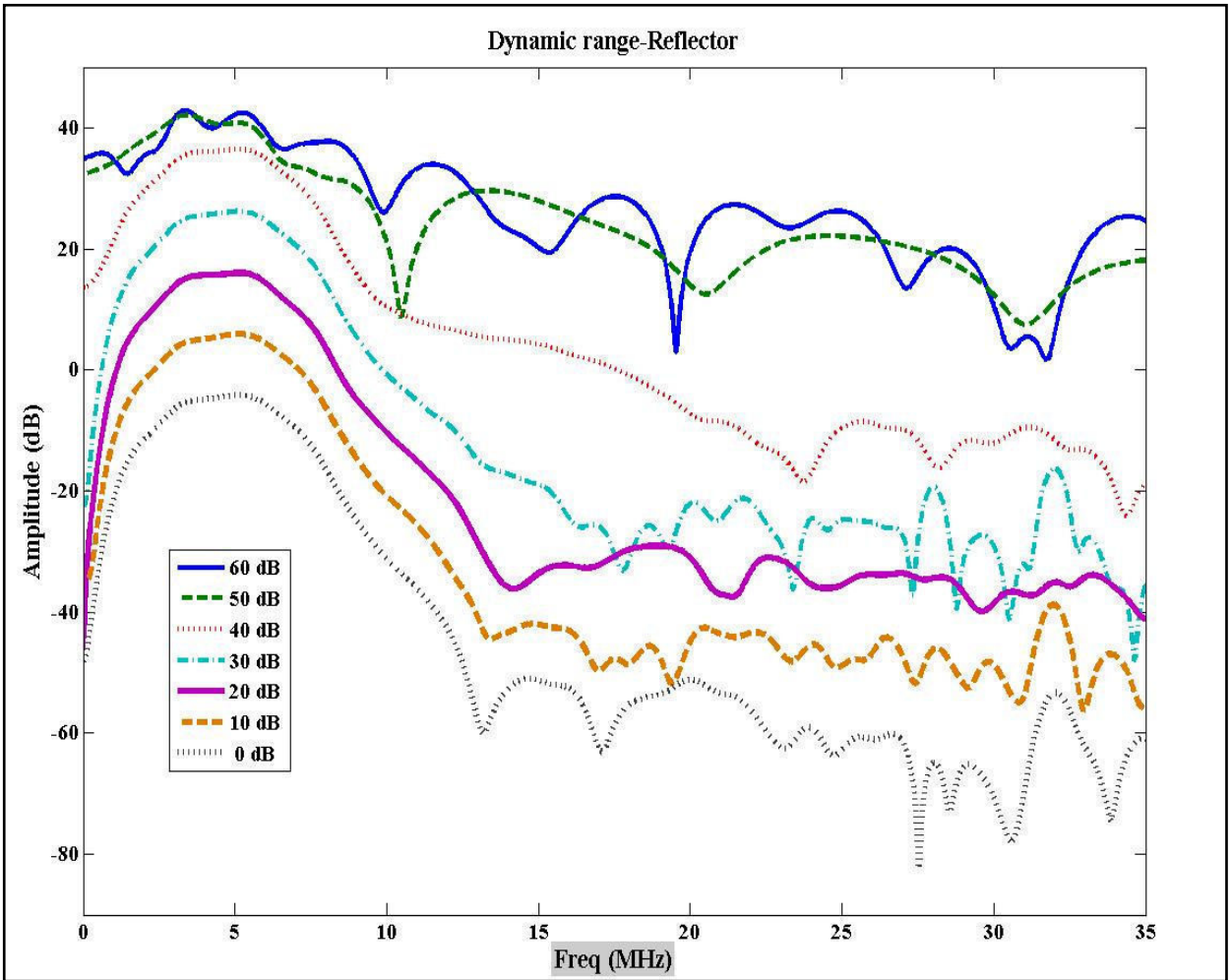

Figure 2.2.1: The dynamic range measurements on the steel plate reflections for the full range of frequencies.

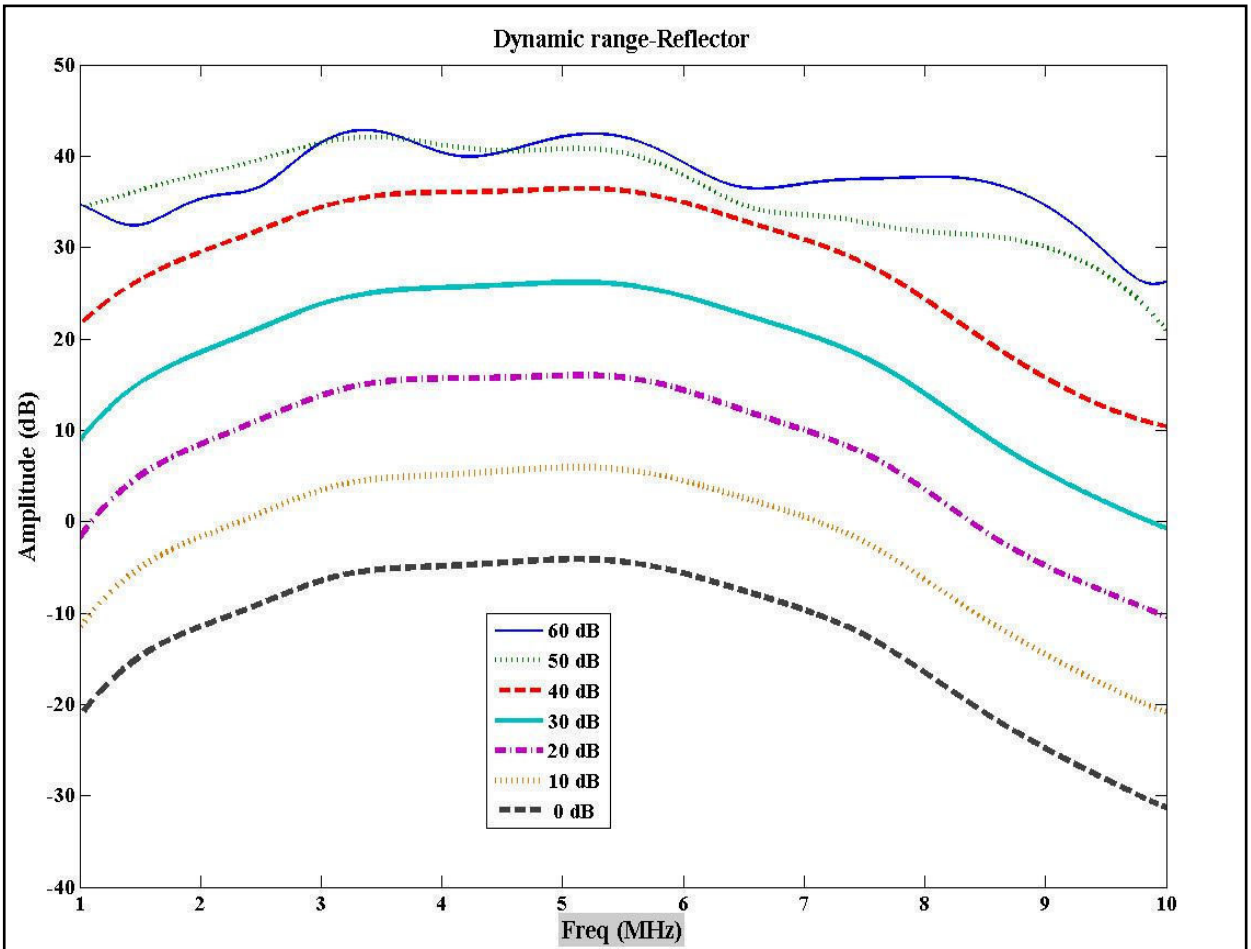

Figure 2.2.2: The dynamic range measurements on the steel plate reflections for the best range of frequencies.

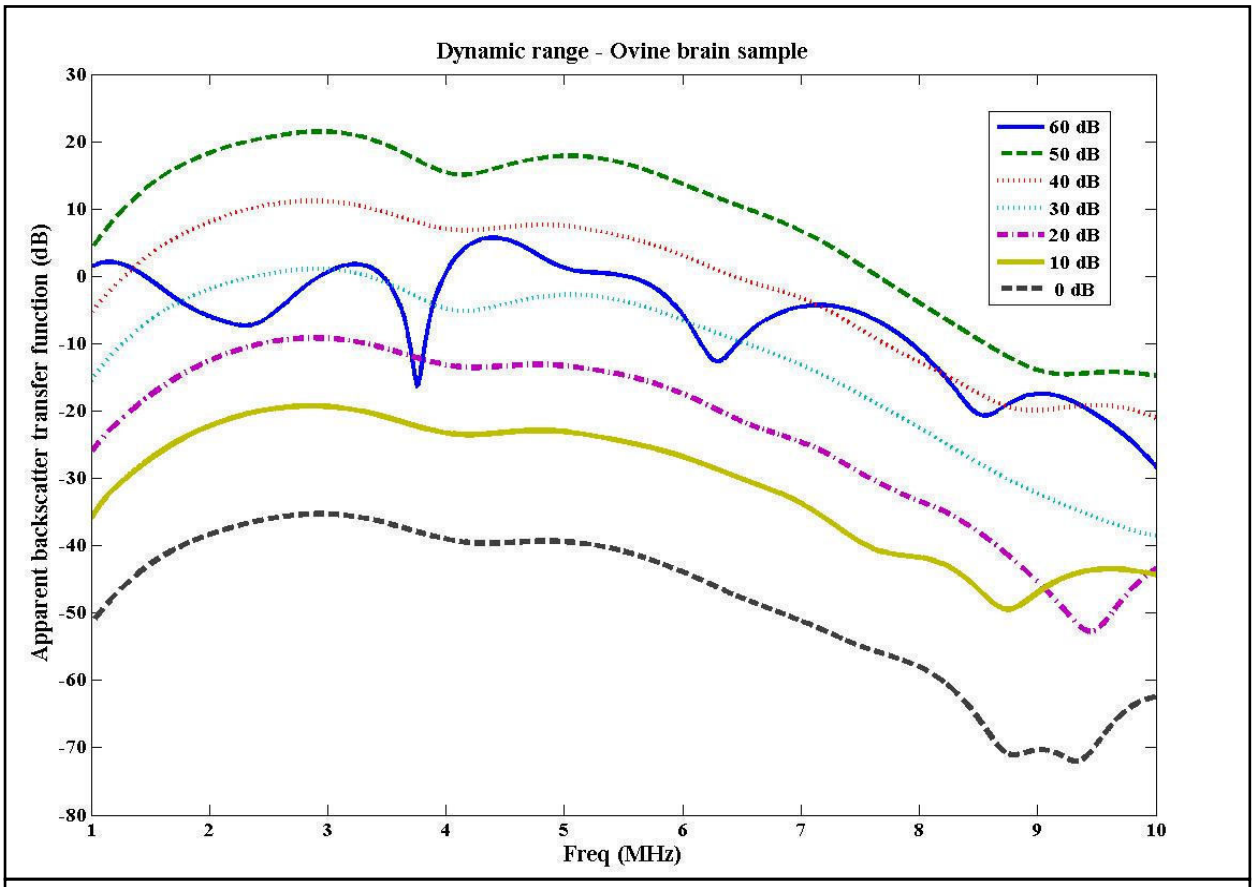

Figure 2.2.3: The dynamic range measurements with a sample in place.

2.3 Sample preparation

2.3.1 Spatial averaging on mammalian brain tissues

In this study the ovine brain tissues used as the samples were obtained from the Carolina Biological Supply Company. The ovine brain was separated into the two hemispheres, and a sharp knife was used to obtain small cylindrically shaped tissue samples that are made from parts from the temporal and parietal lobes as shown in Figure 2.3.1.1. Then the sample was inserted into the sample holder as shown in Figure 2.3.1.2. After attaching the sample to the sample holder, it was mounted to a post which connected via a cross clamped second post to two rails that have the ability to change distances in two perpendicular directions as shown in Figure 2.3.1.3. Four samples were examined in this work. They were cut into slices about 2.4 cm in diameter and between 1-2 cm in thickness. The thickness is a very important parameter in this study because measurements were taken through the length of the tissue sample, and the attenuation measurements depend on this. Care was taken to cut the surfaces smoothly to avoid effects due to surface roughness.

Figure 2.3.1.1: A photograph of the tissue sample, which is 1.4cm in height and about 2.4cm in diameter.

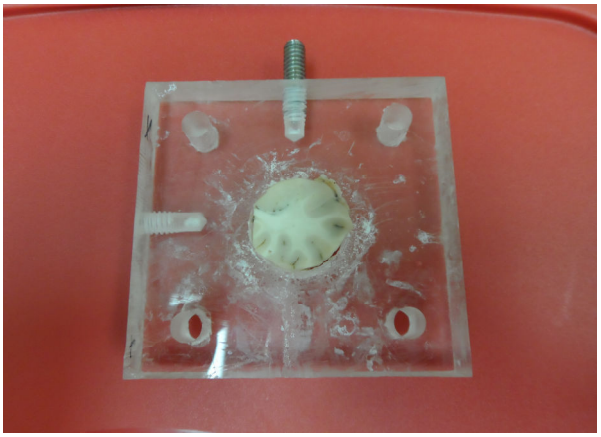

Figure 2.3.1.2: Tissue sample with the holder.

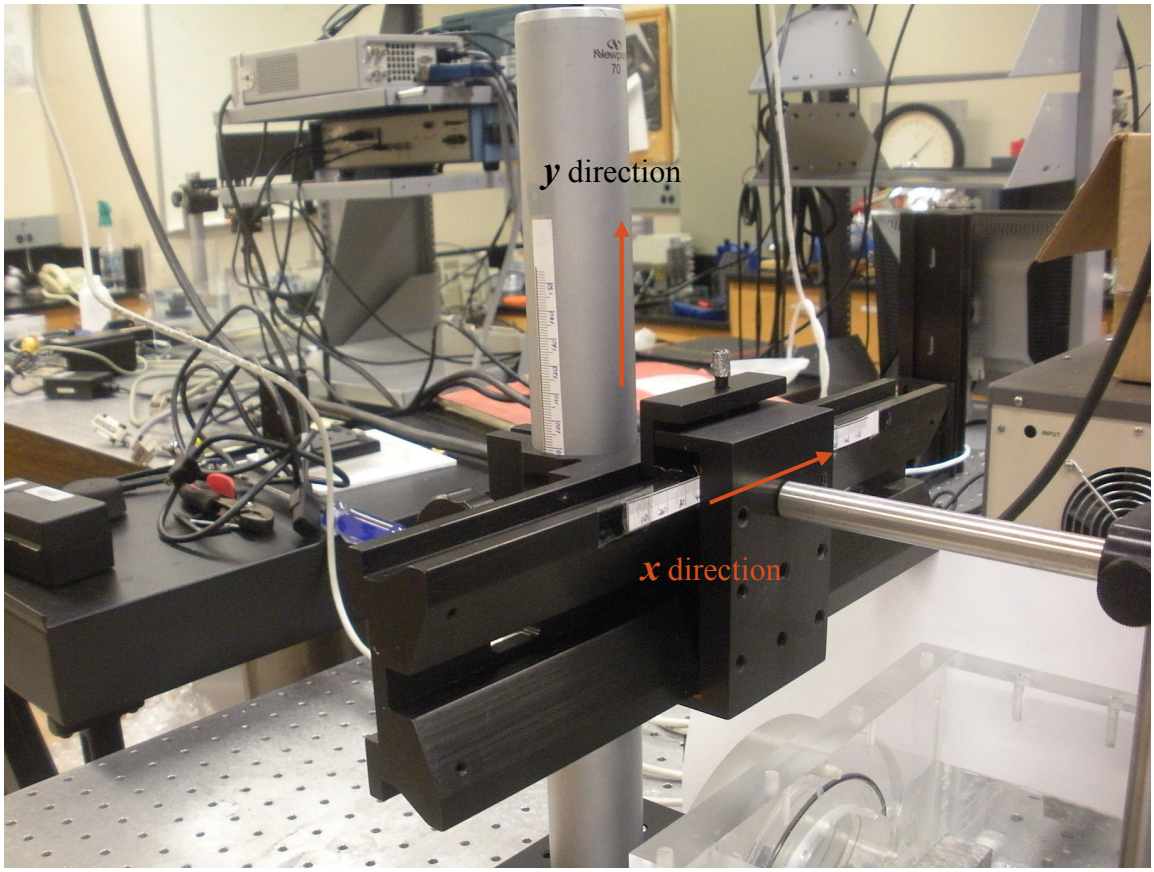

Figure 2.3.1.3: Rails used to change the distance in two perpendicular directions.

Figures 2.3.1.4 and 2.3.1.5 show the side view and the top view of the water tank respectively. The two perpendicular directions are depicted on Figure 2.3.1.4 with labels, which indicate the movements of the tissue sample while performing the experiment. Backscatter and attenuation data were collected on 15 sites spaced 1 mm apart in the tissue sample in the two directions. Special care was taken to remove the air bubbles from the system and to have good samples with out any deformations.

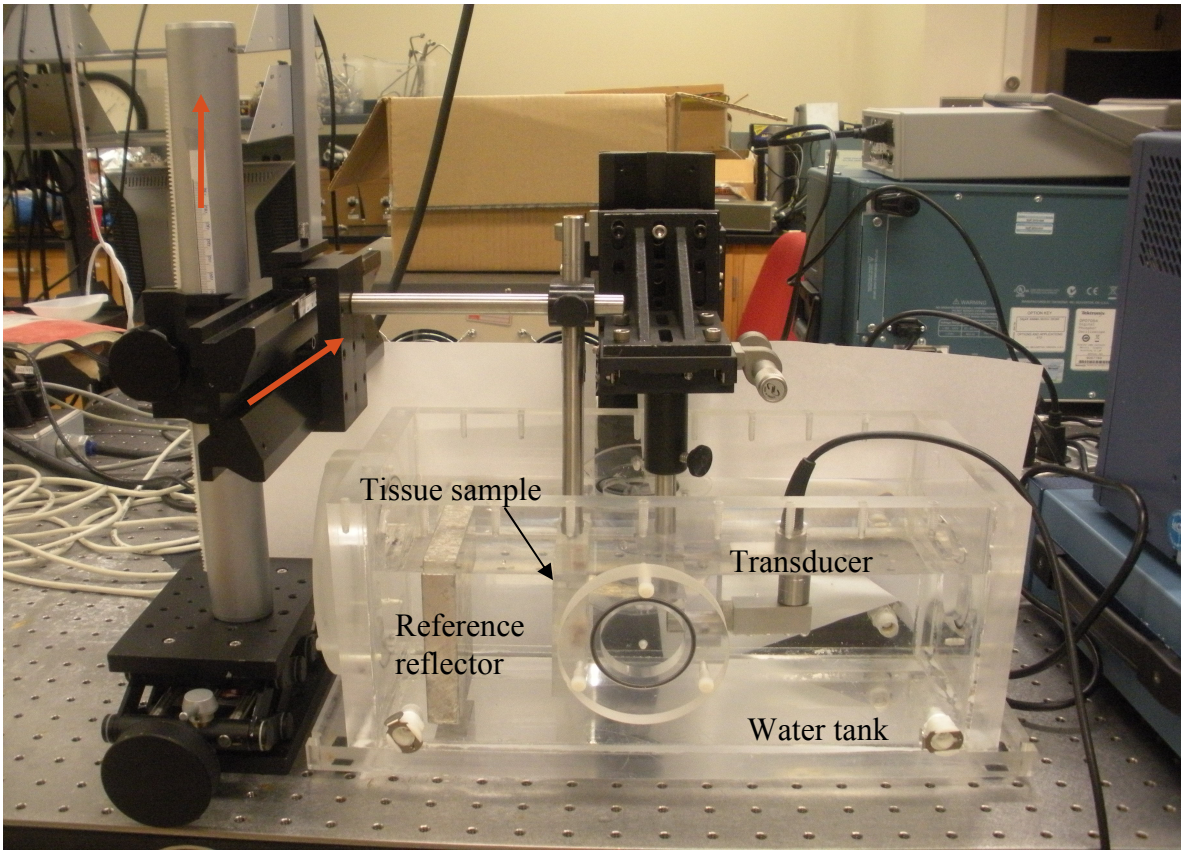

Figure 2.3.1.4: Side view of the water tank with the reflector, tissue sample and the transducer placed in it. Two directions of the movement of the tissue sample are depicted.

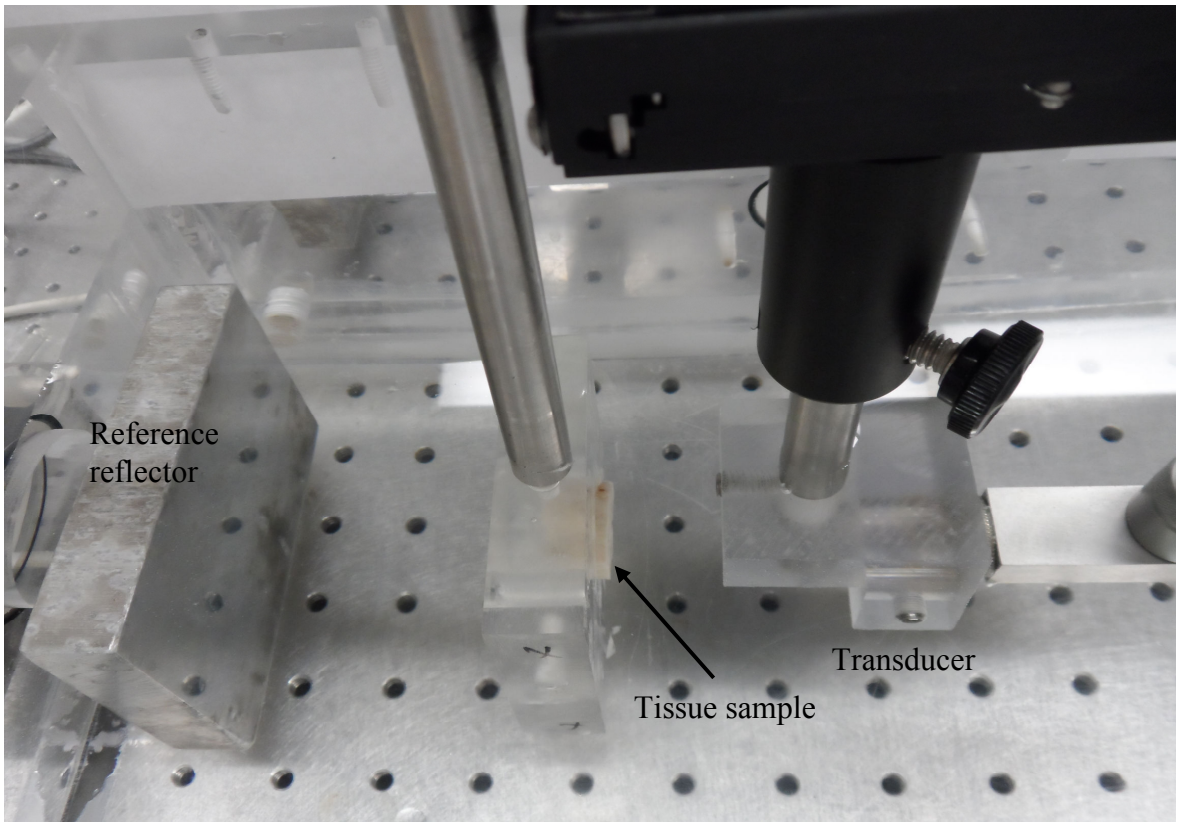

Figure 2.3.1.5: Top view of the water tank with reflector, tissue sample and the transducer placed in it.

2.3.2 Orientation dependence of backscatter and attenuation data on mammalian brain tissues – Cylindrically shaped tissue samples

The ovine brain was separated into its two hemispheres using a knife as in Figure 2.3.2.1, and a cork borer was used to obtain cylindrically shaped tissue samples between 2 and 3 cm in height from parts of the temporal and parietal lobes. The five samples examined in this study each had a diameter of 11.5 mm. After getting a smooth cylindrically shaped sample as in Figure 2.3.2.2, it was mounted to the sample holder using super glue as an adhesive as shown in Figure 2.3.2.3.Then a rotating stage as in Figure 2.3.2.4 was used to mount the sample rig in order to change the orientation of the sample while collecting data.

Figure 2.3.2.1 shows the cross section of one hemisphere of the ovine brain sample and the area that we examined. The examined tissues were mainly from the parietal lobe and the temporal lobe, with a mixture of both white and gray matter. Samples with creases and folds on tissues were discarded because those are not appropriate for good collection of data.

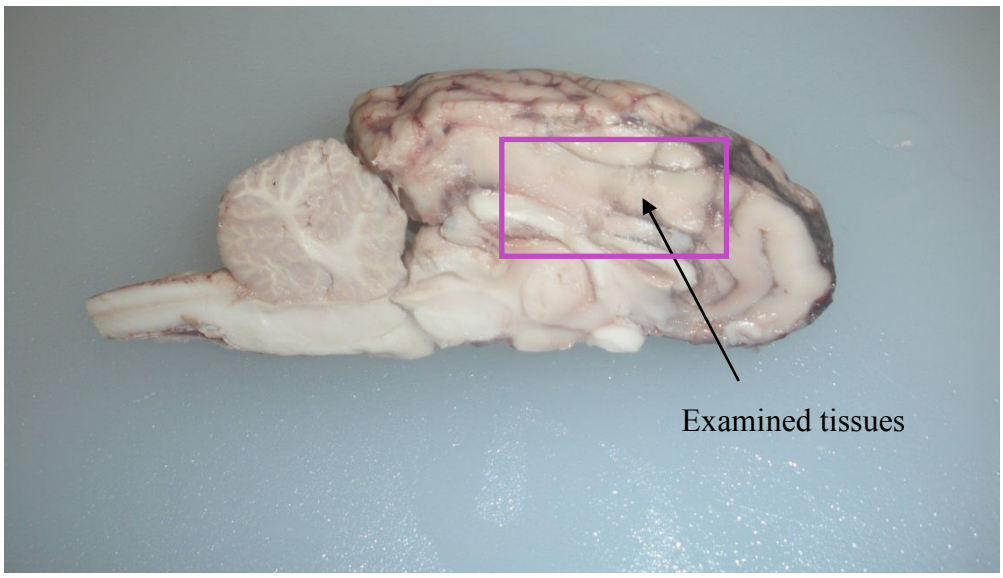

Figure 2.3.2.1: One hemisphere of the ovine brain.

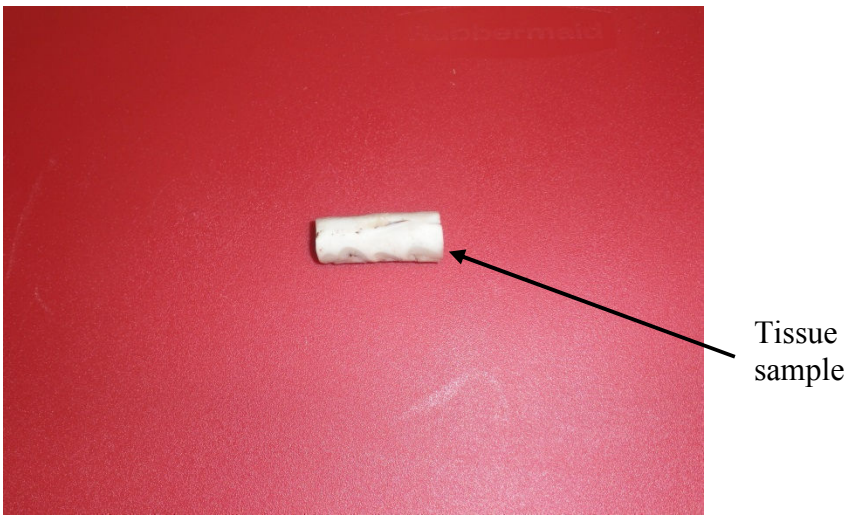

Figure 2.3.2.2: The cylindrically shaped tissue sample, which is 11.5 mm in diameter and about 30 mm in height.

Figure 2.3.2.2 shows one tissue sample that we used in this study, which was 11.5 mm in diameter and 30 mm in height. Care was taken to get smooth flat surfaces on the top and bottom of the cylindrically shaped samples.

Figure 2.3.2.3 shows the plastic sample holder that was used to mount the tissue sample. When gluing the tissue sample onto the holder care must be taken to keep the axis of the cylindrical tissue sample perpendicular to the ultrasonic beam, otherwise the ultrasonic beam will not propagate through the same plane of the tissue sample in all orientations.

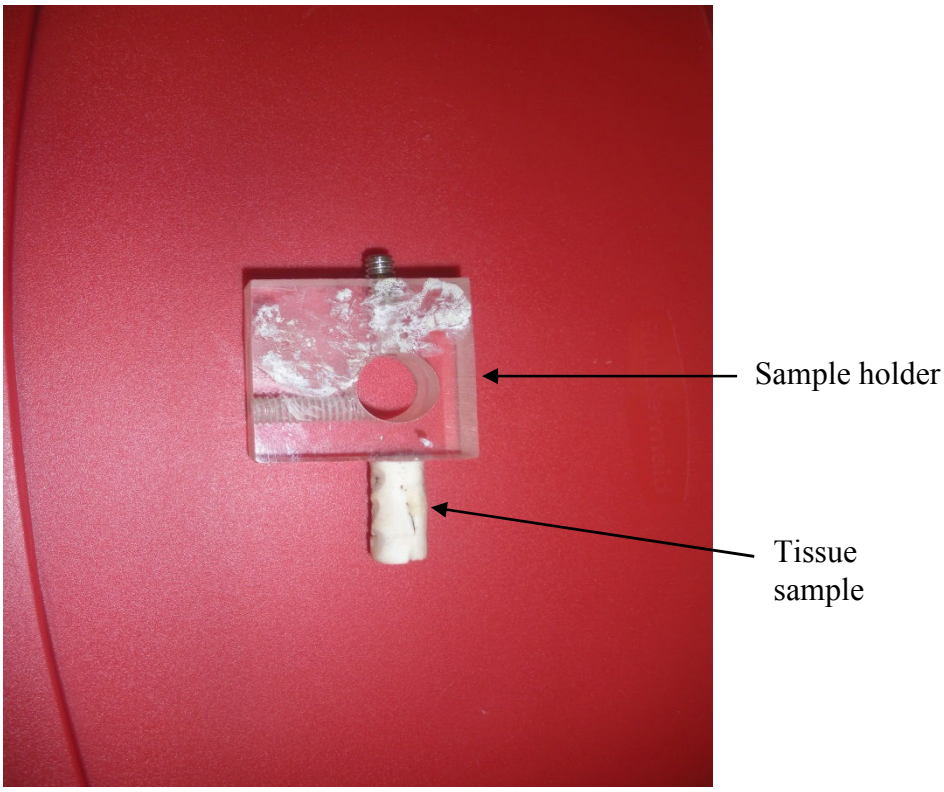

Figure 2.3.2.3: A photograph of the sample holder with the tissue sample attached.

A picture of the rotating stage is shown in Figure 2.3.2.4, which was used to change the orientation of the tissue sample from zero degrees to 360 degrees by 30-degree increments. It has the ability to rotate the sample in both directions.

Figures 2.3.2.5 and 2.3.2.6 are photographs of top and side views of the water tank, respectively, with a tissue sample in between the steel plate and the transducer. Before taking the data, the water was checked for air bubbles and if present, they were removed from the system. Prior to and during the collection of data, care was taken to avoid any deformations on the tissue samples. All the measurements were taken just after the dissection of tissue samples.

Figure 2.3.2.4: A photograph of the rotating stage.

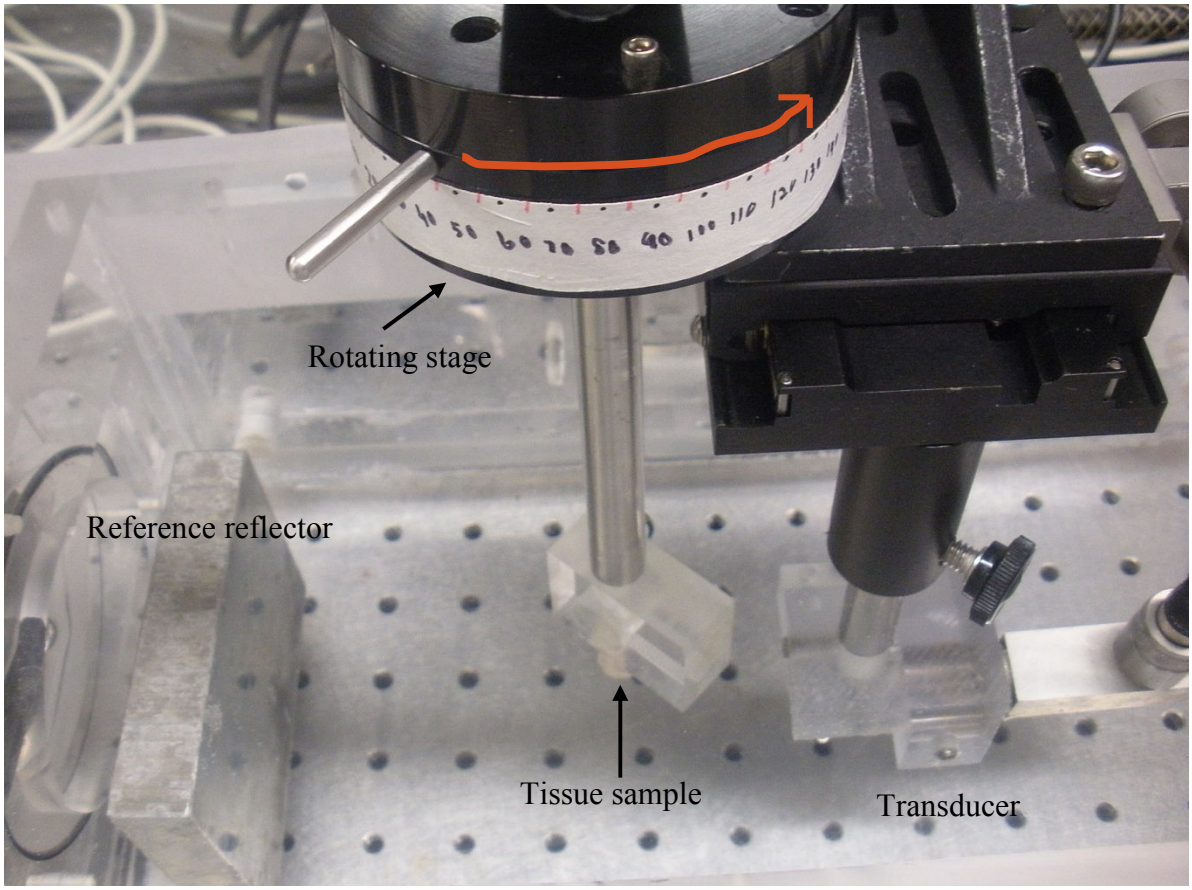

Figure 2.3.2.5: Top view of the water tank with the reference, tissue sample and the transducer placed in it. The direction of the movement of the tissue sample is depicted.

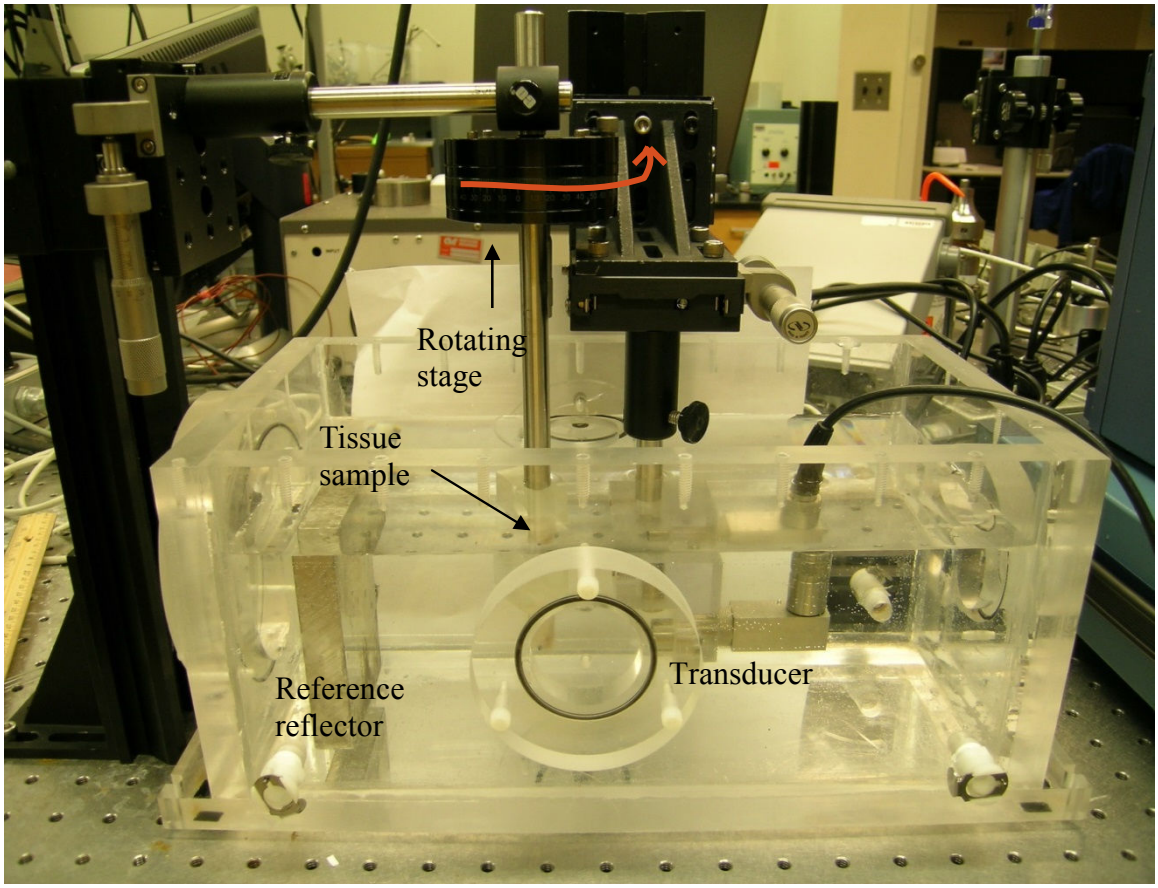

Figure 2.3.2.6: Side view of the water tank with the reference, tissue sample and the transducer placed in it. The direction of the movement of the tissue sample is depicted.

2.4 Data acquisition

2.4.1 Identifying the backscatter data

The procedure is similar to that described in [15] which dealt with measurements of the attenuation coefficient and backscatter coefficient for microsphere suspensions that can be used as a potential calibration tool. First a pulse echo signal was acquired from a polished steel plate with only a water path between the transducer and the plate as shown in Figure 2.4.1.1. The first reflection from the plate provides the reference data that will be used later to compensate for system-dependent effects. Then the tissue sample was inserted between the transducer and the steel plate, within the focal zone of the transducer, while keeping the transducer and the steel plate at their fixed positions in order to maintain the alignment during measurements. From the signals collected with the tissue in place, we can identify the backscatter data with respect to the steel plate reflections as shown in Figure 2.4.1.3. Figure 2.4.1.2 shows the first reflected signal through the water path only. The smoothness of the signal indicates the alignment of our system is good. This is important for determining the attenuation coefficient as well as the backscatter coefficient. (Equations 1.4.4.16 and 1.4.5.1)

Figure 2.4.1.3 shows the signal with the tissue in place, and the backscatter data can be easily identified. Figure 2.4.1.4 shows the enlarged backscatter data with reflections from two boundaries. The signals within the two tissue-water reflections are the backscatter data we used for the study.

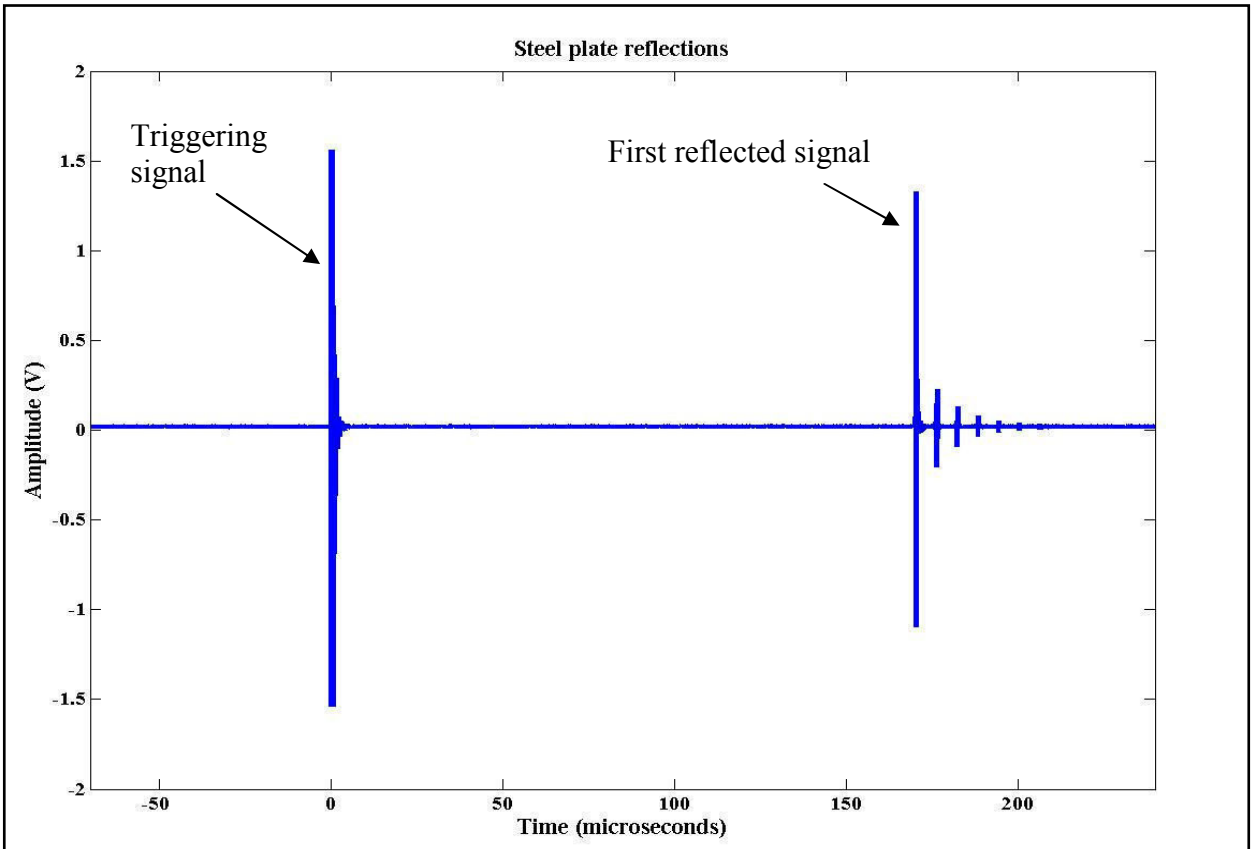

Figure 2.4.1.1: Steel plate reflections through water path only. The small waveforms after the first reflected signal are due to the reverberations.

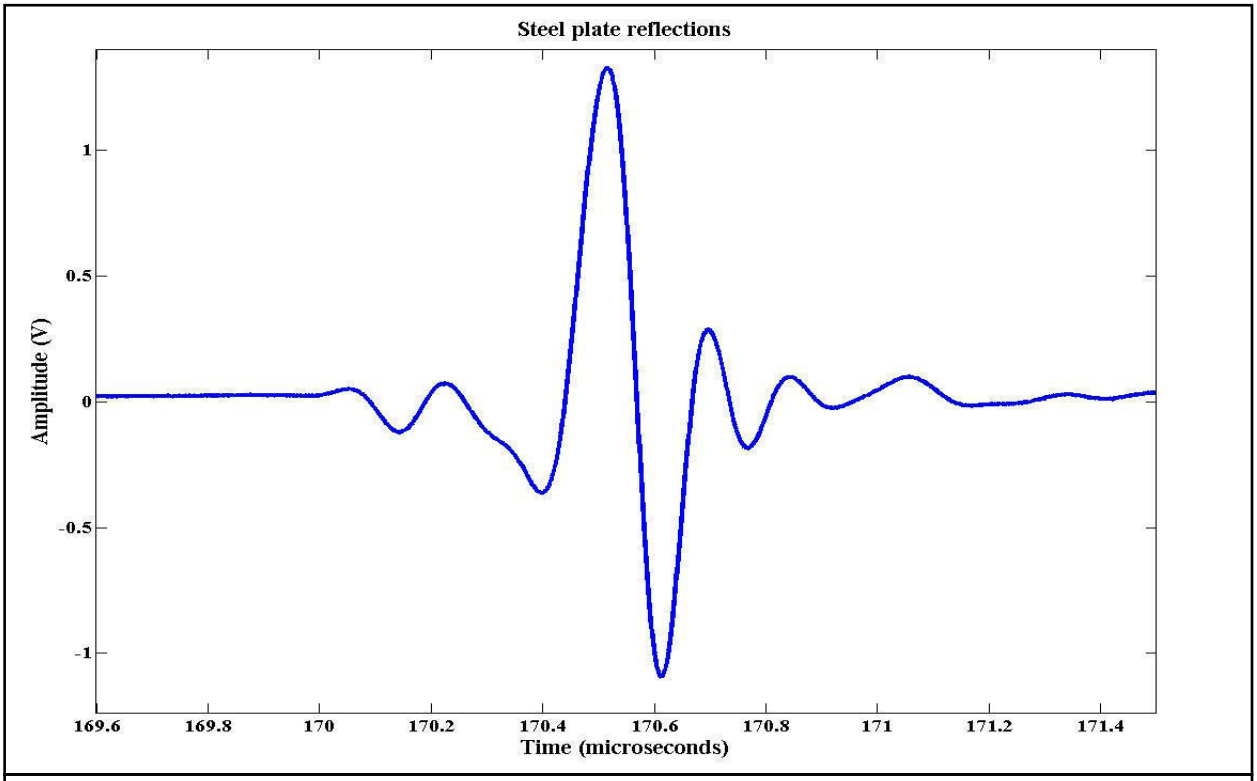

Figure 2.4.1.2: Enlarged first reflected signal.

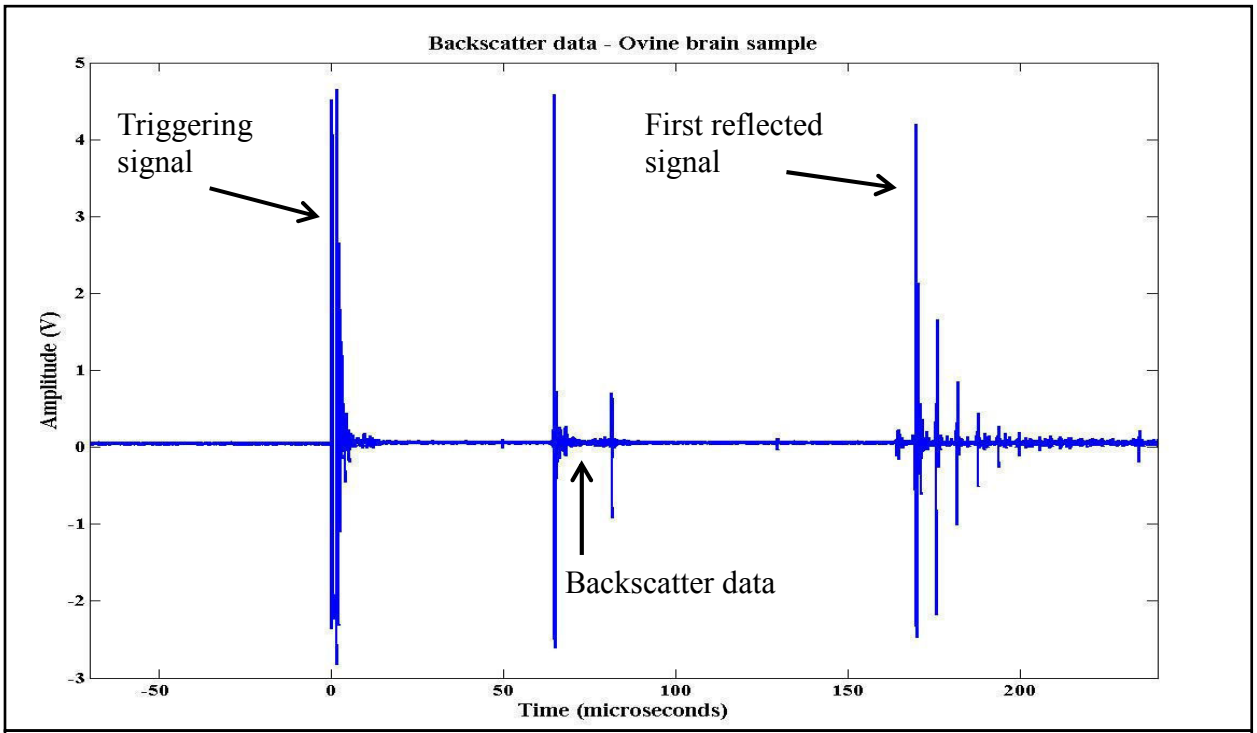

Figure 2.4.1.3: Backscatter data can be easily identified with the steel plate reflections as the reference.

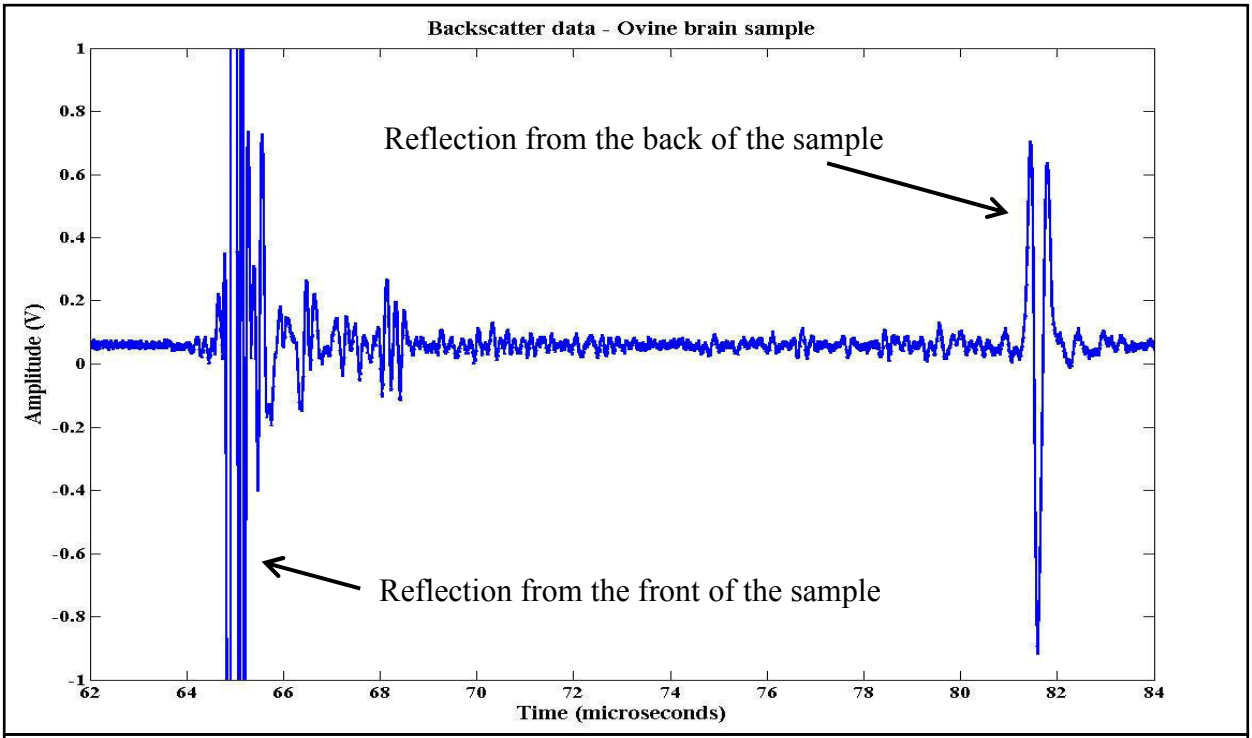

Figure 2.4.1.4: Enlarged backscatter data. We are interested in the backscatter data between the signals from the two boundaries.

2.4.2 Spatial averaging of data

As discussed in section 1.4.6 biological samples are complex media, and a random model is useful to define the acoustic scattering properties of such media. Spatial averaging is the technique that we used during our study to compensate for the randomness of the tissues.

To accomplish spatial averaging, backscatter and attenuation data were collected by moving the sample in 1 mm steps in the *x* and *y* directions as shown in Figure 2.4.2.1. The gain setting of the pulser receiver was adjusted in order to get a clear backscatter pattern while attempting not to saturate the reflected signals when taking the data on each position of the tissue sample. The values obtained were averaged to yield a single spatially averaged value for the apparent backscatter transfer function as well as for the attenuation coefficient.

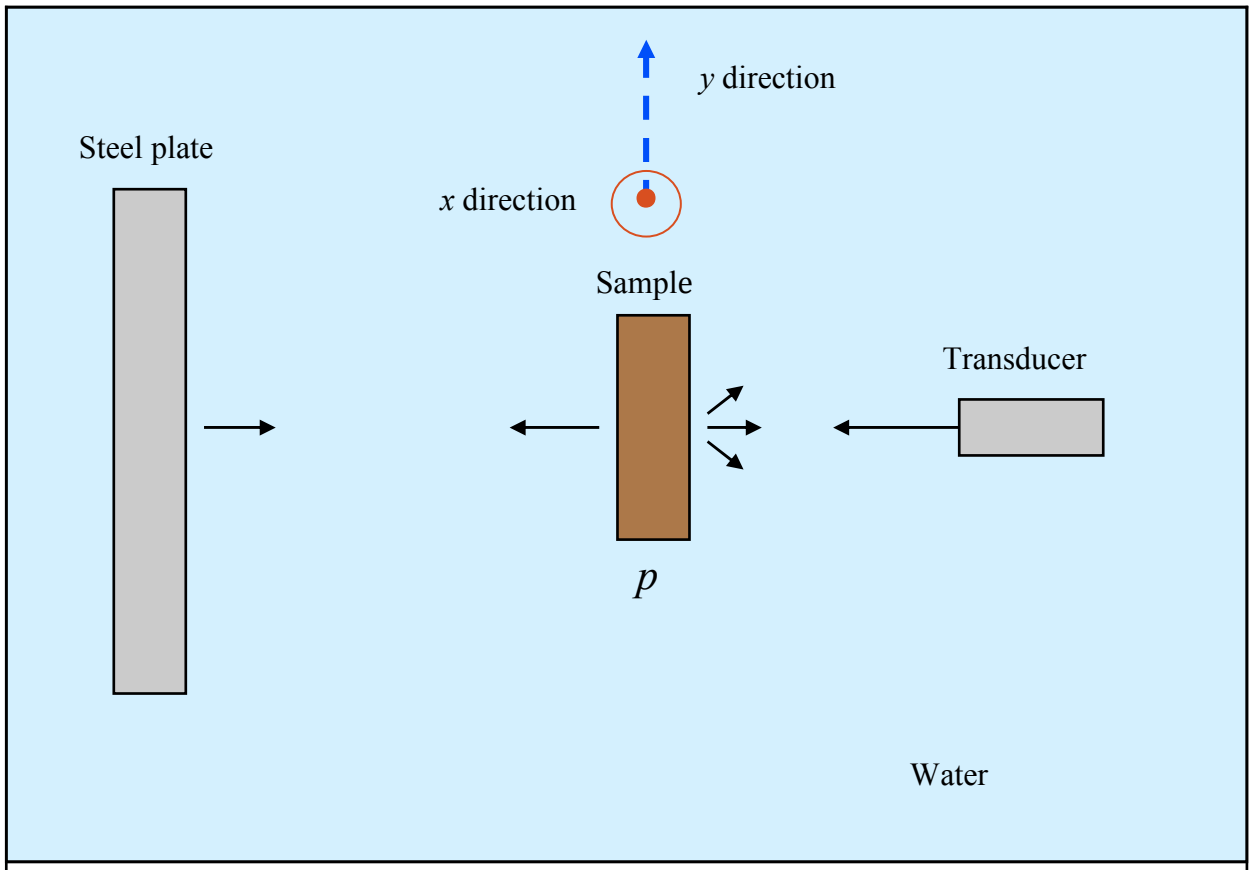

Figure 2.4.2.1: A side view of the diagram for spatial averaging of the backscatter and attenuation data in two perpendicular directions.

Figure 2.4.2.1 shows a diagram depicting the spatial averaging of backscatter and attenuation data in x and y directions. First the data was collected over a grid by moving the tissue sample horizontally in 1 mm steps and then in the vertical (y) direction. The backscatter and attenuation data were collected at 15 positions in one direction of the tissue samples used for this study. While collecting the data, special care was taken to maintain the alignment of the ultrasonic system.

2.4.3 Orientation dependence of data

To investigate the orientation dependence, thirteen measurements of backscatter and attenuation data were made over a range of angles by rotating the cylindrically shaped sample

from 0 degrees to 360 degrees by 30 degree increments. After adjusting the settings as necessary, the zero degree position was marked on the sample to provide the starting orientation for the ultrasonic acquisitions. A diagram of the set up for the orientation dependence is shown in Figure 2.4.3.1. It is clear from Figure 2.4.3.1 that the axis of the cylindrically shaped sample must be perpendicular to the ultrasonic beam in order for the beam to propagate through the same plane of the tissue sample at each orientation. Figure 2.4.3.2 shows a diagram for the top view of the plane of the tissue sample.

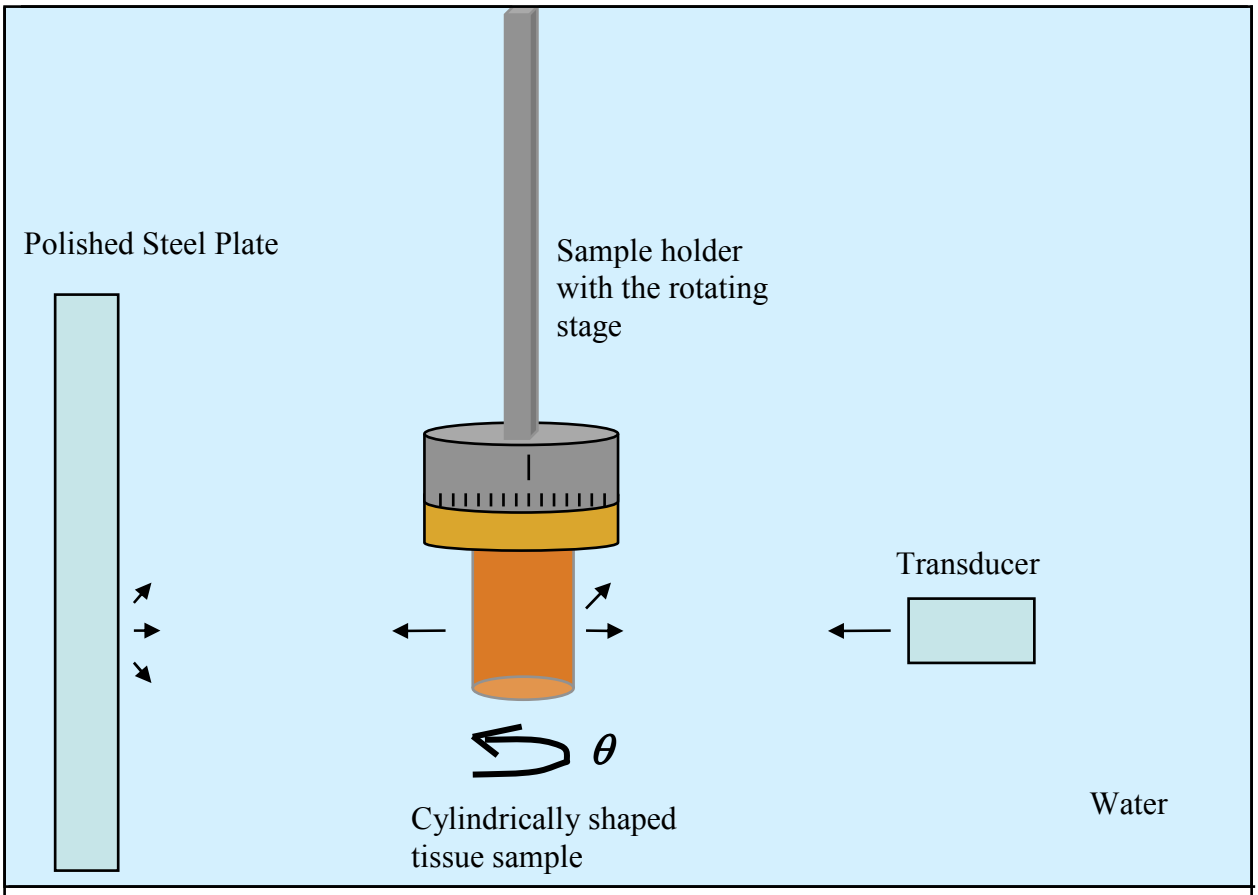

Figure 2.4.3.1: The diagram represents the orientation dependence of the tissue sample with the use of rotating stage.

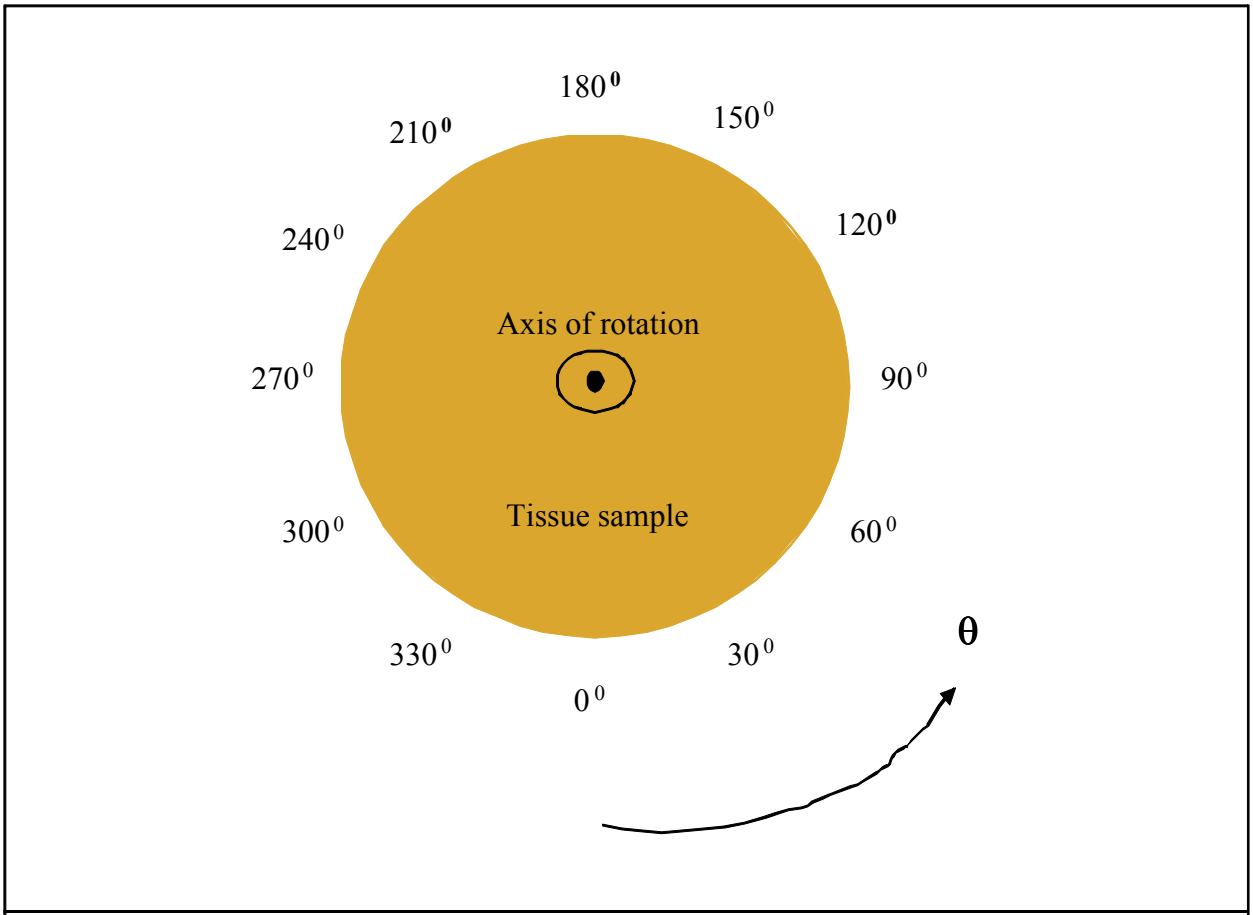

Figure 2.4.3.2: Illustration of top view of the plane of tissue sample when collecting data on 30 degree increments.

2.4.4 Normalization

Once the data was acquired, the signals of interest were isolated by gating and then Fourier transformed yielding a spectrum for that signal. The spectra extracted from the sample signals can be normalized using the spectrum of the polished steel plate reflection in order to compensate for the effects due to the measurement system as a whole [15]. After acquiring the backscatter data from the tissues, the sample was removed from the system and the steel plate was moved to the new position P as shown in Figure 2.4.2.1. This position is where the central axis of the sample was positioned and the reflected data was obtained for the steel plate [15].

2.5 Analysis

The backscatter and reflection data were downloaded from the LeCroy Oscilloscope to a computer (DELL Windows XP). All of the acquisition control and signal processing operations were done using MATLAB (R2011a). Figure 2.4.1.4 represents the enlarged backscatter data along with the reflections from the front and rear boundaries of the sample. Initially a Hanning window with a gate width 1.10 μs (1200 points) was applied to select a subset of the backscatter data as shown in Figure 2.5.1. The Hanning window is a good selection for gating a data set because its Fourier transform has much lower side lobes that provides a relatively smooth convolution curve in the frequency domain and also helps to reduce noise.

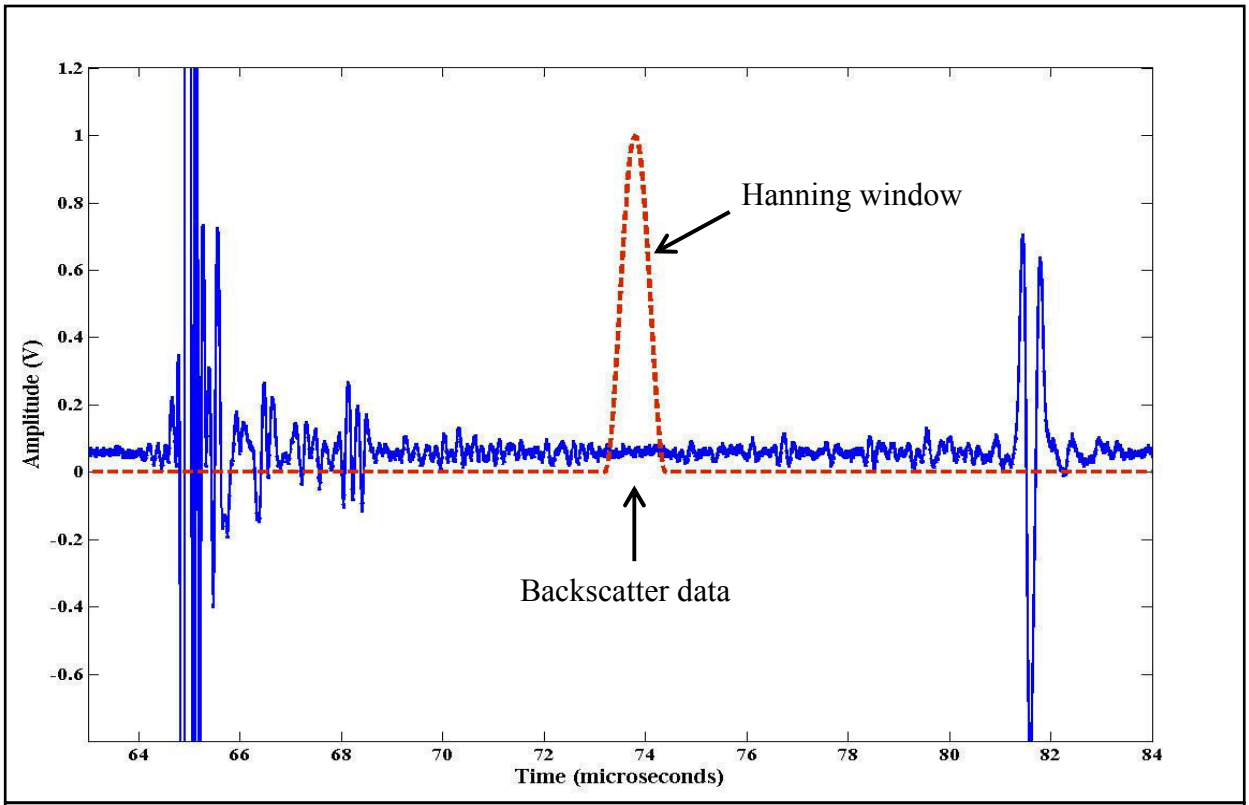

Figure 2.5.1: Applying the gate to the backscatter data between the two boundaries. A Hanning window was used as the gate for this study.

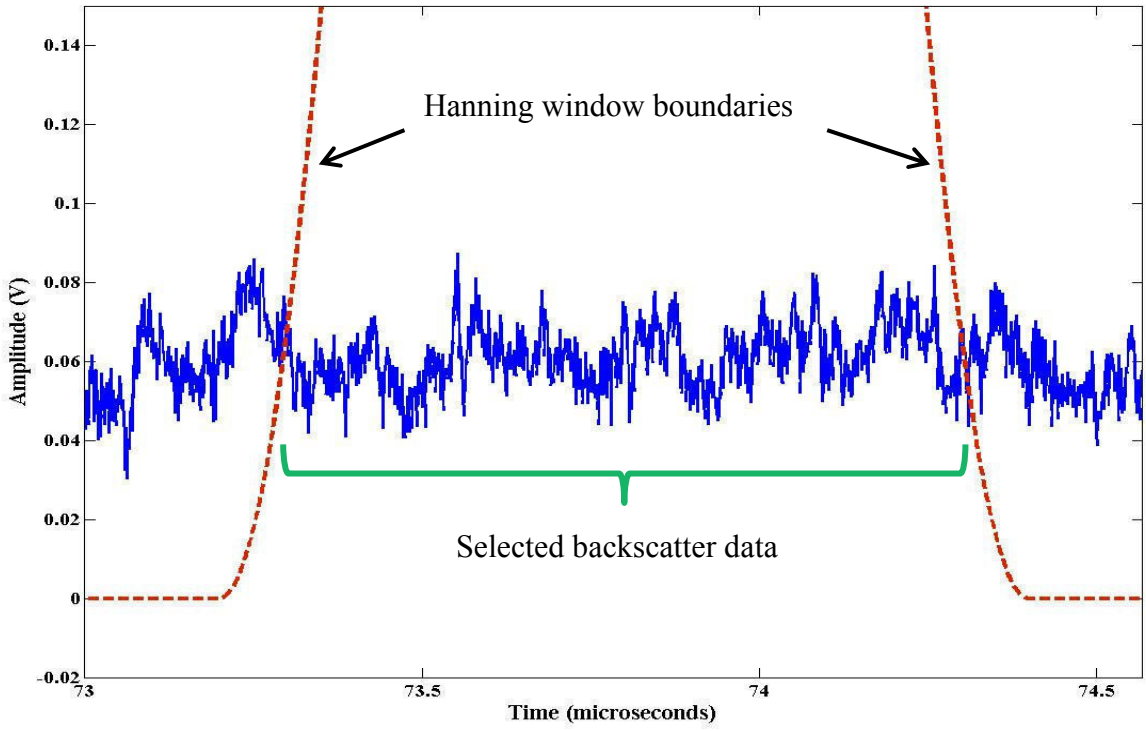

Figure 2.5.2: Close representation of the selected backscatter data using the Hanning window.

Figure 2.5.2 shows a close-up of the backscatter data identifying the portion of the signal selected for further analysis. We used the Hanning window as a sliding window that covered almost all of the backscatter data from the tissue sample starting from backscatter data just beyond the front sample echo to just before the back echo. The spectra were then averaged. Figure 2.5.3 shows how the sliding window works for the selection of backscatter data. Before applying the sliding window, backscatter data were selected manually by defining the end points for the analysis. Then those two points were used as parameters in a MATLAB script along with other information such as gate width and step size. The script slides a Hanning window through the backscatter data. A number of different windowing techniques were tried, and the sliding window approach provided the most stable results for the apparent backscatter transfer function (ABTF).

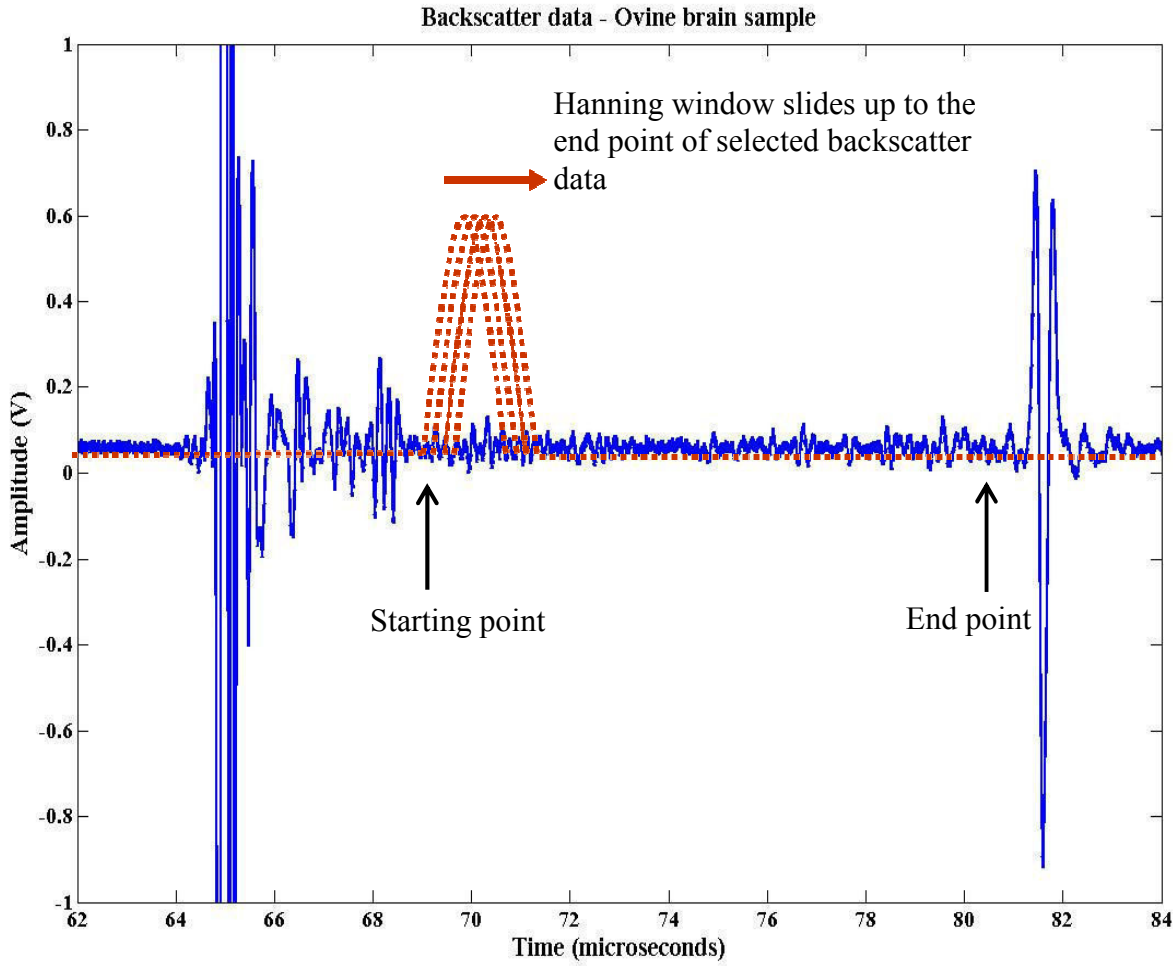

Figure 2.5.3: Applying the Hanning window as a sliding window on to a selected backscatter data.

For the analysis of the reflected signals, a Hanning window of gate width 1.10 μs (1200 points) was applied as shown in Figure 2.5.4. The gate width of 1.10 μs was selected as the best gate size for both backscatter and reflected data. Figure 2.5.4 shows the Hanning window applied to the first reflected signal, when the steel plate at the focal zone of the transducer that is the reference for backscatter data. The same procedure was done for the first reflected signal through the water path which is used as the reference for the attenuation data. Once the signals of interest were isolated by gating, they were Fourier transformed to yield a spectrum for that signal. The

ABTF is determined using the following equation by comparing the scattered signal from the brain tissue sample with the reflected signal from the steel plate that use as a reference, [3]

$$\left|S(\omega)\right|^2 = \frac{\left|F_{tissue}(\omega)\right|^2}{\left|F_{steelplate}(\omega)\right|^2} \tag{2.5.1}$$

where $\left|S(\omega)\right|^2$ is the apparent backscatter transfer function, $\left|F_{tissue}(\omega)\right|^2$ is proportional to the Fourier power spectrum for the brain tissue scattering signals in a given position or orientation and $\left|F_{steel\ plate}(\omega)\right|^2$ is proportional to the Fourier power spectrum for the reference plate reflection signal.

The attenuation coefficient was calculated by comparing the amplitudes of the first reflected signals from the polished steel plate through the water path and the sample using Eq. 2.5.2,

$$\alpha = \frac{20\log_{10}\left(\frac{4Z_1Z_2}{(Z_1+Z_2)^2}\right)}{d} - \frac{20\log_{10}\left(\frac{A_2}{A_1}\right)}{2d} \tag{2.5.2}$$

$$Z_1 = \rho_1 v_1 \tag{2.5.3}$$

$$Z_2 = \rho_2 v_2 \tag{2.5.4}$$

where α is the attenuation coefficient, A_1 is the amplitude of the reflected signal through water path only, A_2 is the amplitude of the reflected signal through tissue sample, Z_1, Z_2 are the acoustic impedances, ρ_1 is the density of water (999.7026 Kg/m^3 at 20 ^{o}C) [16], ρ_2 is the density of tissue (white matter-1043 Kg/m^3) [17], v_1 is the speed of sound through water (1482 m/s at 20 ^{o}C) [18], v_2 is the speed of sound through tissue (1560 m/s) [19] and d is the sample thickness. For the cylindrically shaped samples, the diameter is the same as the sample thickness. For each position and/or orientation, the apparent backscatter transfer function and the attenuation

coefficient were calculated and averaged. Figure 2.5.5 shows a diagram for the reflected data through the water path only and the tissue sample. It is clear from the figure that the amplitude of the reflected signal was reduced when it passed through the tissue sample.

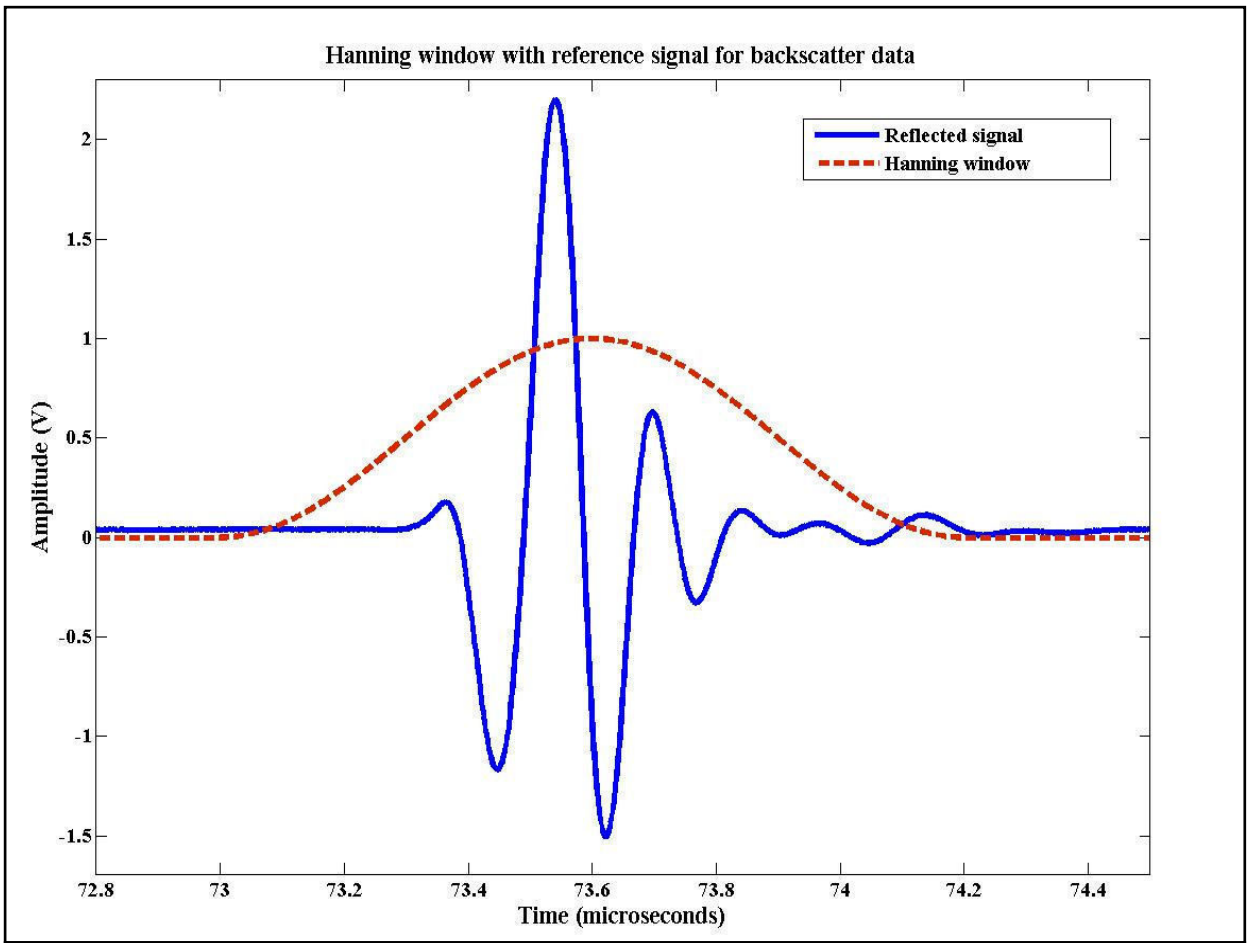

Figure 2.5.4: Applying the Hanning window on to a reflected signal.

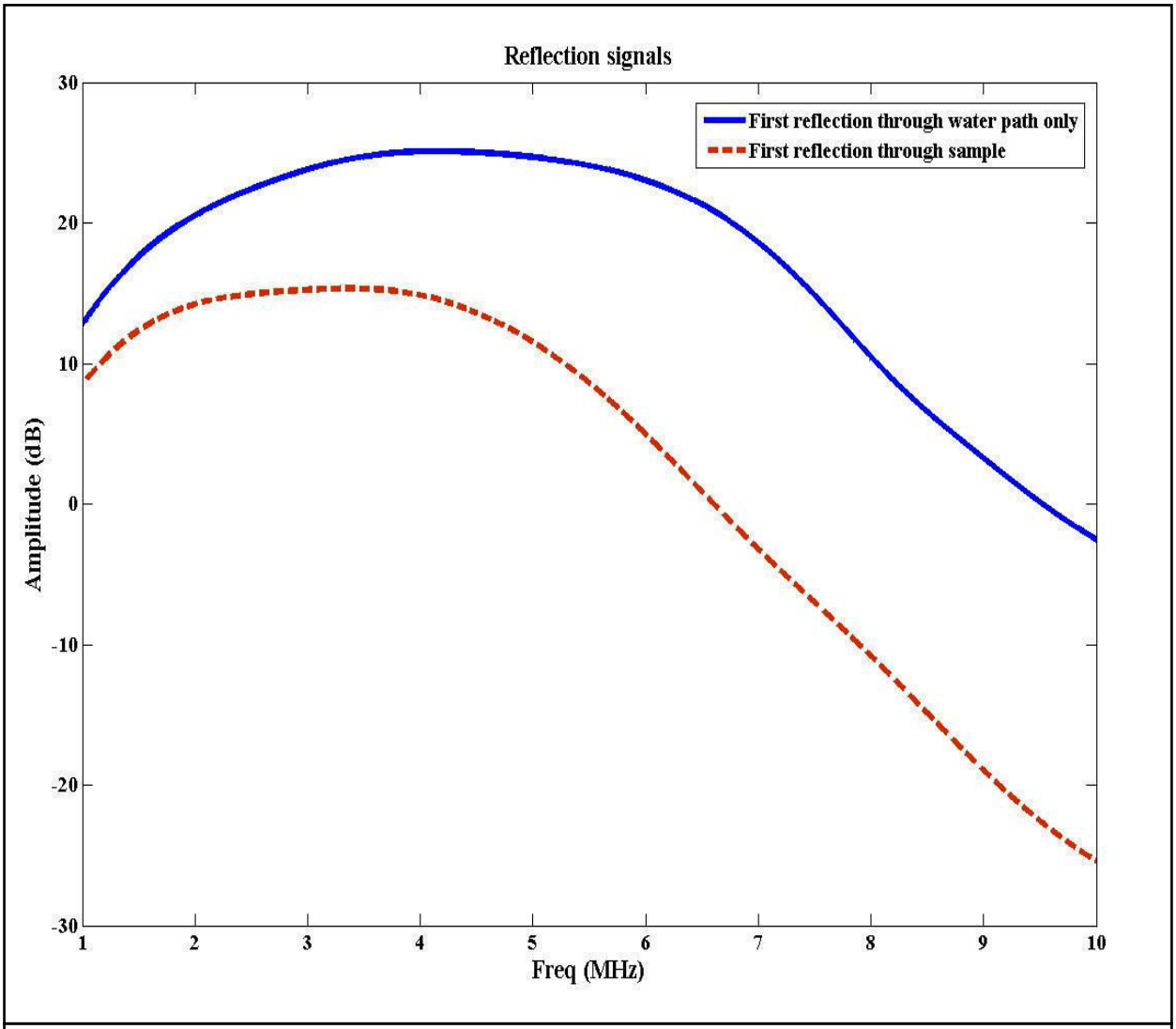

Figure 2.5.5: Comparison of first reflection signals through water path only and tissue.

The backscatter coefficient (μ_{bs}) can be expressed using the terms apparent backscatter transfer function ($|S(\omega)|^2$), the attenuation coefficient (α) and some correction factors, [15]

$$\mu_{bs}(\omega) = \frac{\Gamma^2}{4T^4} R^2 F(\alpha, \tau) \frac{1}{V(\omega)} \left\langle |S(\omega)|^2 \right\rangle \tag{2.5.5}$$

where $\mu_{bs}(\omega)$ is the frequency-dependent backscatter coefficient, Γ is the amplitude reflection coefficient of steel plate reflector, T is the transmission coefficient between water and the tissue,

R is the focal length of the transducer, $V(\omega)$ is the frequency-dependent beam volume and $F(\alpha,\tau)$ is an attenuation correction factor that given in equation 2.5.6, [6]

$$F(\alpha,\tau) = e^{4\alpha(f)x} e^{\alpha(f)c\tau} \frac{2\alpha c\tau}{e^{\alpha c\tau} - e^{-\alpha c\tau}} \tag{2.5.6}$$

where α is the frequency-dependent attenuation coefficient, c is speed of sound through the tissue sample, x is the position of the window after the front wall of the sample and τ is the gate duration.

3 RESULTS

3.1 Spatially averaged backscatter and attenuation data of ovine brain tissue

Spatial averaging is used in this study to overcome the small-scale inhomogeneity of biological tissue samples. Backscatter and attenuation data were obtained for four ovine brain tissue samples that covered regions of mixed white and grey matter on 30 positions of a sample in two perpendicular directions *x* and *y* as in Figure 2.4.2.1. The attenuation coefficient and the backscatter coefficient (BSC) were measured for the 1-5 MHz frequency range and the apparent backscatter transfer function (ABTF) was measured for the 1-10 MHz range.

3.1.1 Apparent backscatter transfer function (ABTF)

The apparent backscatter transfer function that is given by equation 1.4.3.1 was determined by comparing the scattered signal from the brain tissue sample with the reflected signal from the steel plate that was used as the reference reflector. The term "apparent" in ABTF indicates that the backscatter signals are not compensated for frequency-dependent effects. Figures 3.1.1.1 and 3.1.1.2 represent the ABTF on 15 measurement sites of sample 1 in x and y directions respectively. The sample was moved in 1 mm increments using rails as shown in Figures 2.2.1.3 and 2.2.1.4 starting at the 0 mm position up to the 14 mm position in both directions. Each line in the plots represents the ABTF for one particular position. Both Figures 3.1.1.1 and 3.1.1.2 show a similar behavior in ABTF curves with small differences in the 1-10 MHz frequency range; and this difference may be due the site-to-site variations. Each ABTF curve in Figures 3.1.1.1 and 3.1.1.2 was analyzed to determine the backscatter coefficient. Figure 3.1.1.3 shows the spatially averaged ABTF in each direction. Both plots having almost the same

pattern indicates that our model is effective in averaging out the microstructural inhomogeneity. Figure 3.1.1.4 represents the single spatially averaged ABTF for sample 1 that is obtained by averaging the ABTFs of all 30-measurement sites of the tissue sample.

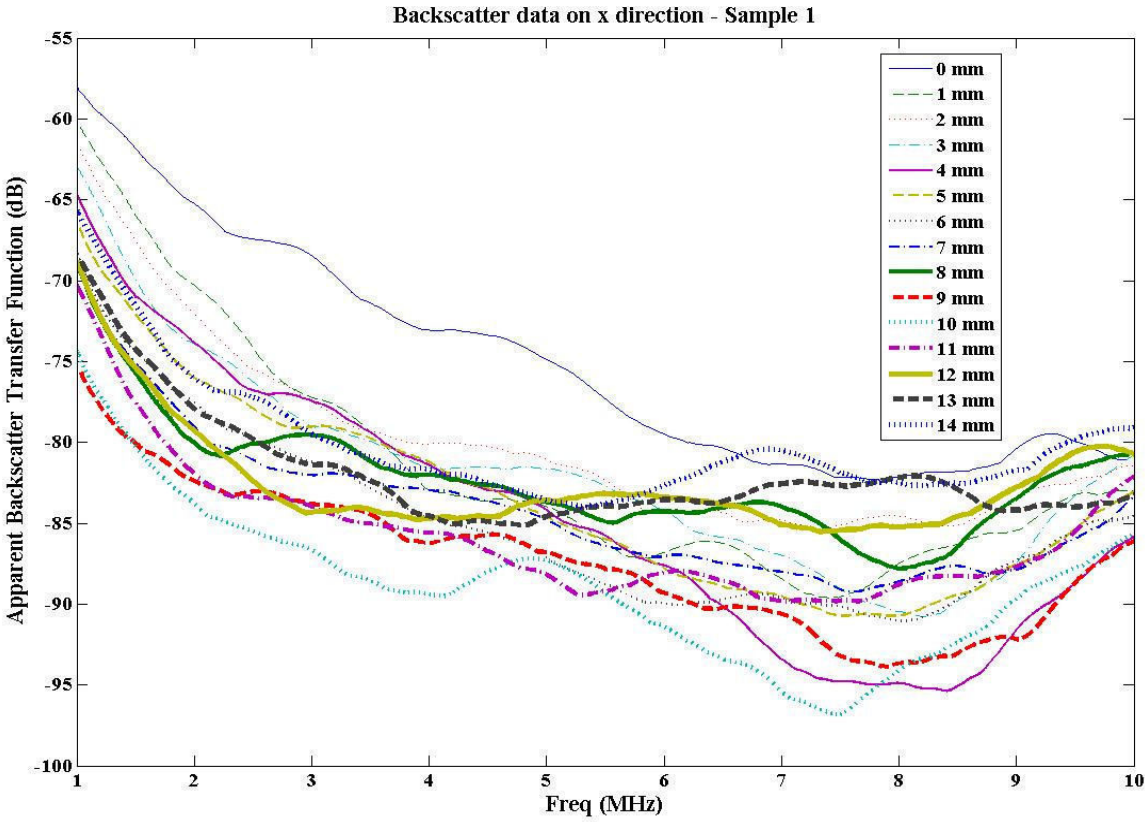

Figure 3.1.1.1: ABTF on 15 positions of x direction-Sample 1.

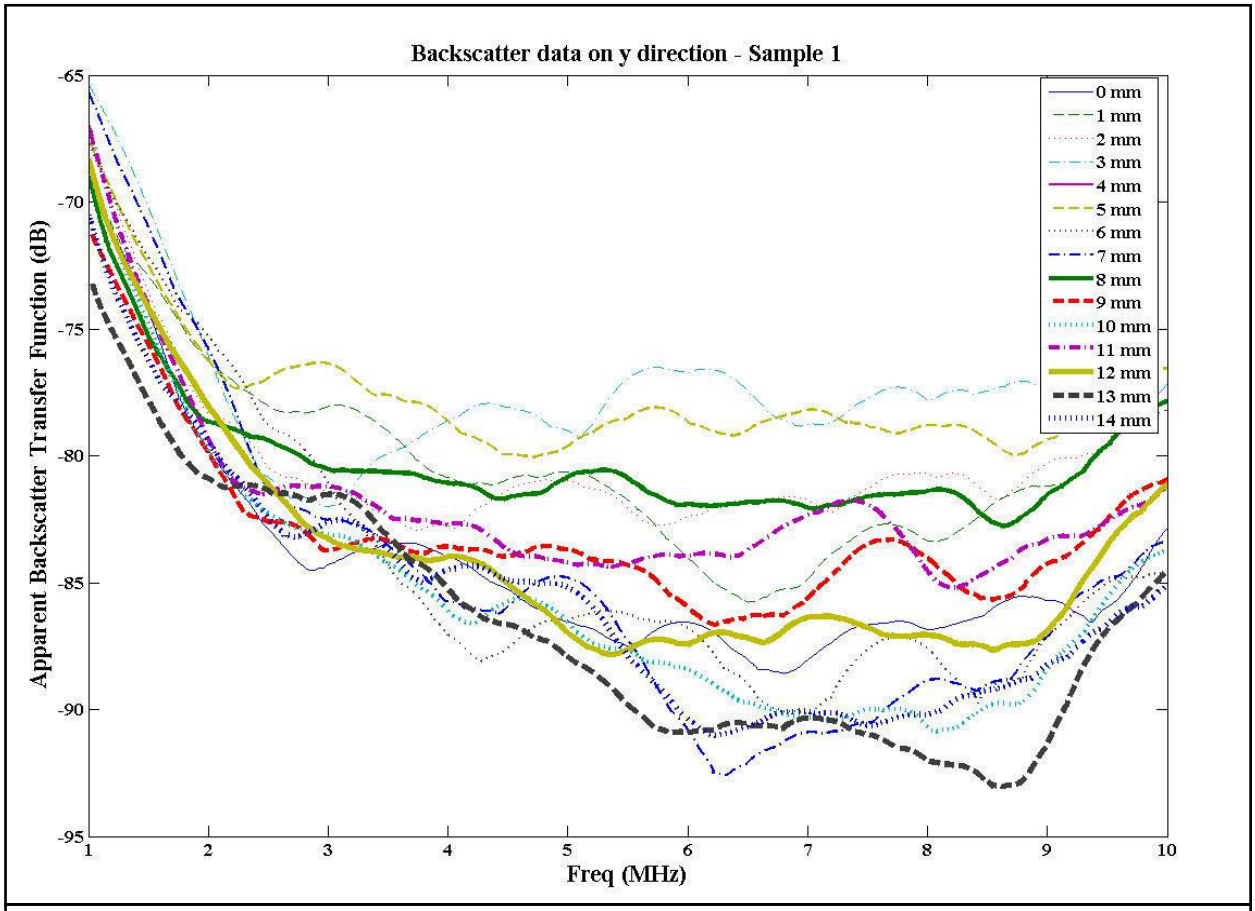

Figure 3.1.1.2: ABTF on 15 positions of y direction-Sample 1.

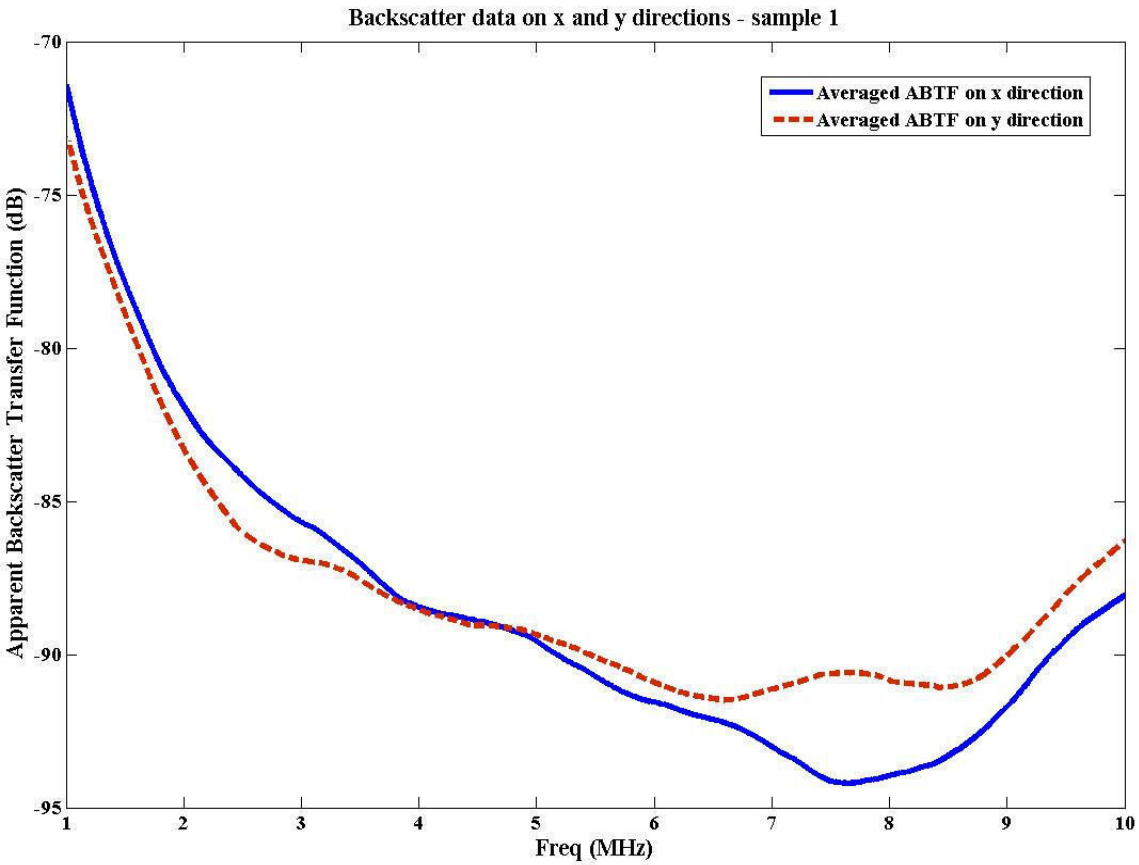

Figure 3.1.1.3: Averaged values of ABTF on two perpendicular directions x and y -Sample 1.

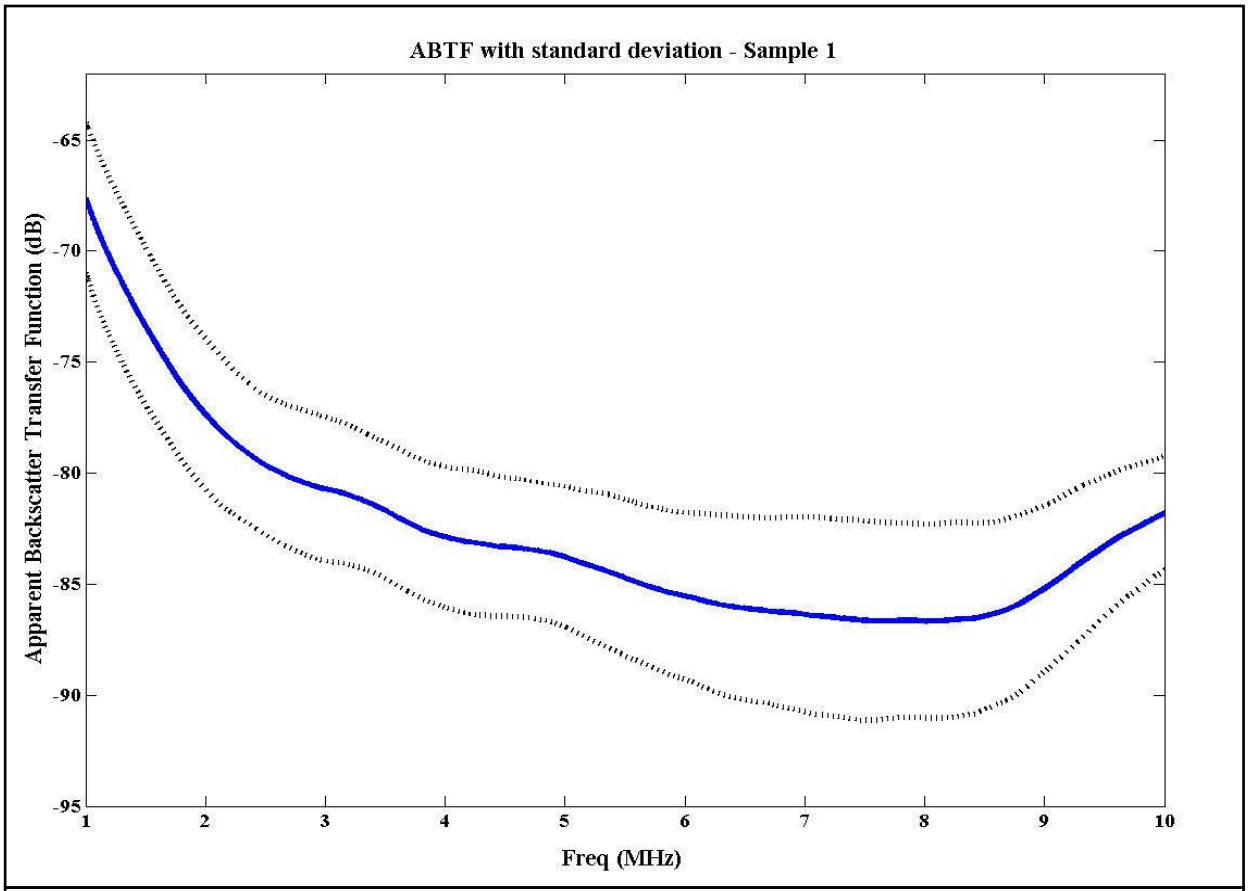

Figure 3.1.1.4: Spatially averaged ABTF with standard deviation-sample 1.

Figure 3.1.1.5 represents the spatially averaged ABTFs for four different samples of tissue. The figure shows that the magnitude of ABTF for sample 1 is the lowest, while samples 3 and 4 are the highest in this frequency range. Figure 3.1.1.6 illustrates the averaged ABTF for all 4 samples with standard deviation limit curves. It shows a monotonically decreasing function of frequency over the range of 1-10 MHz.

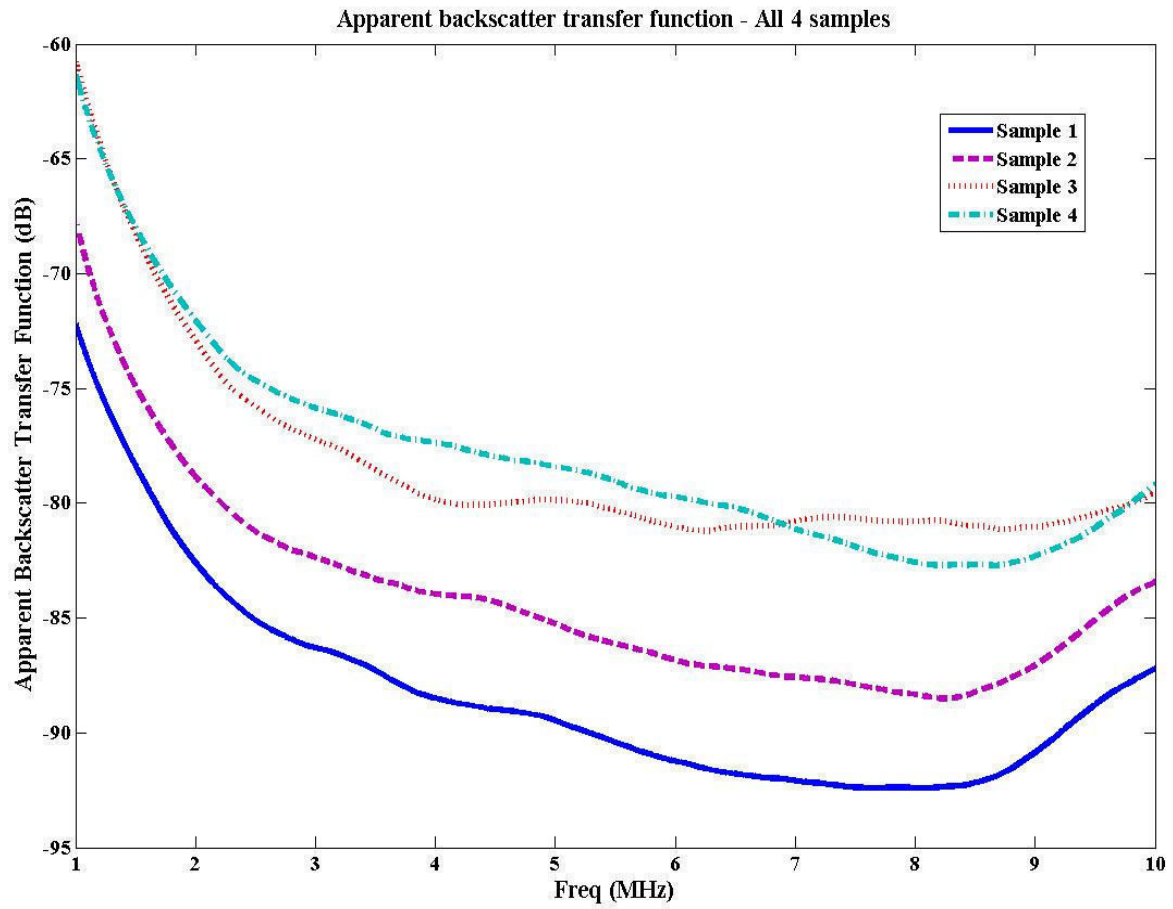

Figure 3.1.1.5: Spatially averaged ABTF-all 4 samples

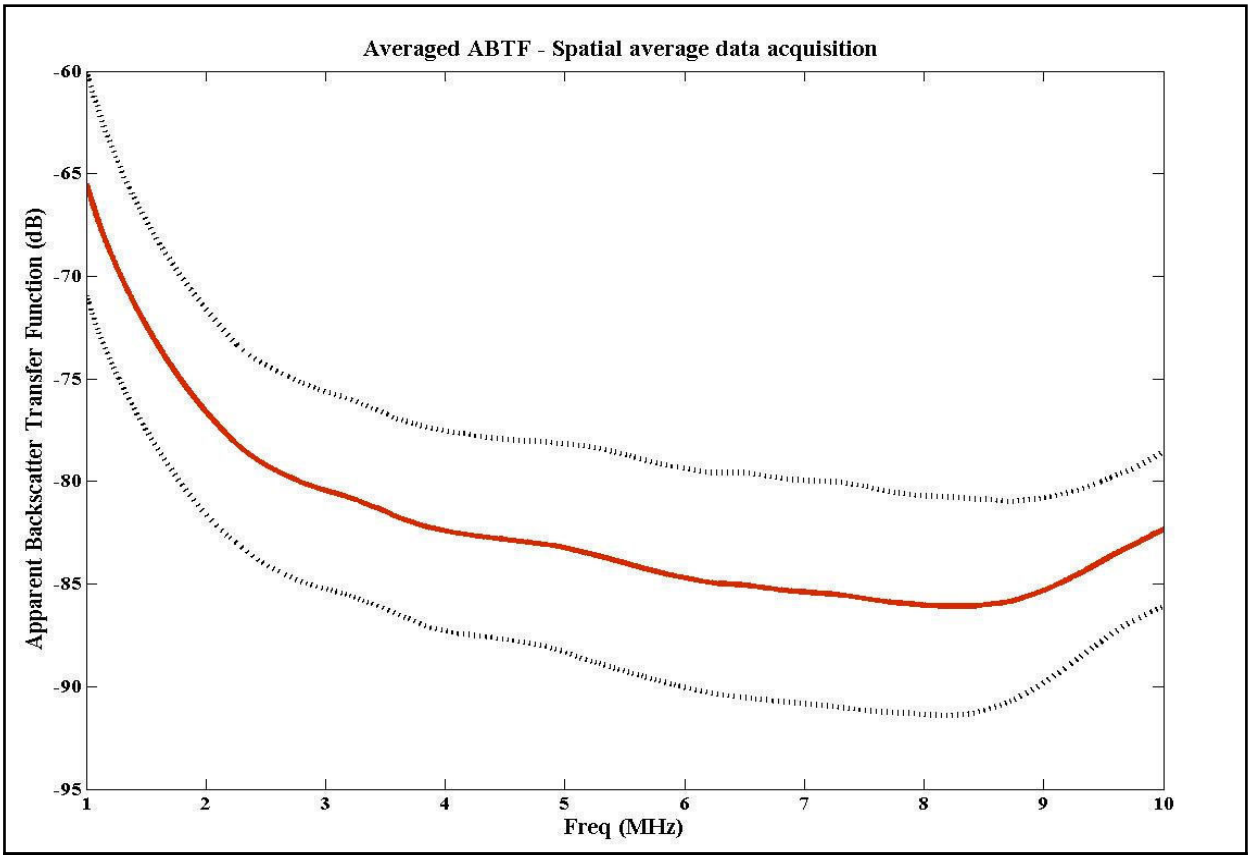

Figure 3.1.1.6: ABTF averaged over all 4 samples with standard deviation.

3.1.2 Attenuation coefficient

The attenuation coefficient (α) is an important parameter that quantifies the reduction in the amplitude of ultrasound as it passes through a medium. The attenuation coefficient from 1 to 10 MHz at 30 sites of the sample in two perpendicular directions is shown in Figures 3.1.2.1 and 3.1.2.2. These two diagrams show relatively uniform behavior up to 5 MHz, while at higher frequency they show markedly larger variations. This indicates that the 1 to 5 MHz range can be considered as the valid frequency range for the attenuation coefficient. Figures 3.1.2.3 and 3.1.2.4 show the attenuation coefficient for that range of frequency. It can be seen that the

magnitudes of the attenuation coefficient lie between 0.5 to 6 dB/cm in most of the curves. Each curve in Figures 3.1.2.3 and 3.1.2.4 was used in the determination of the backscatter coefficient.

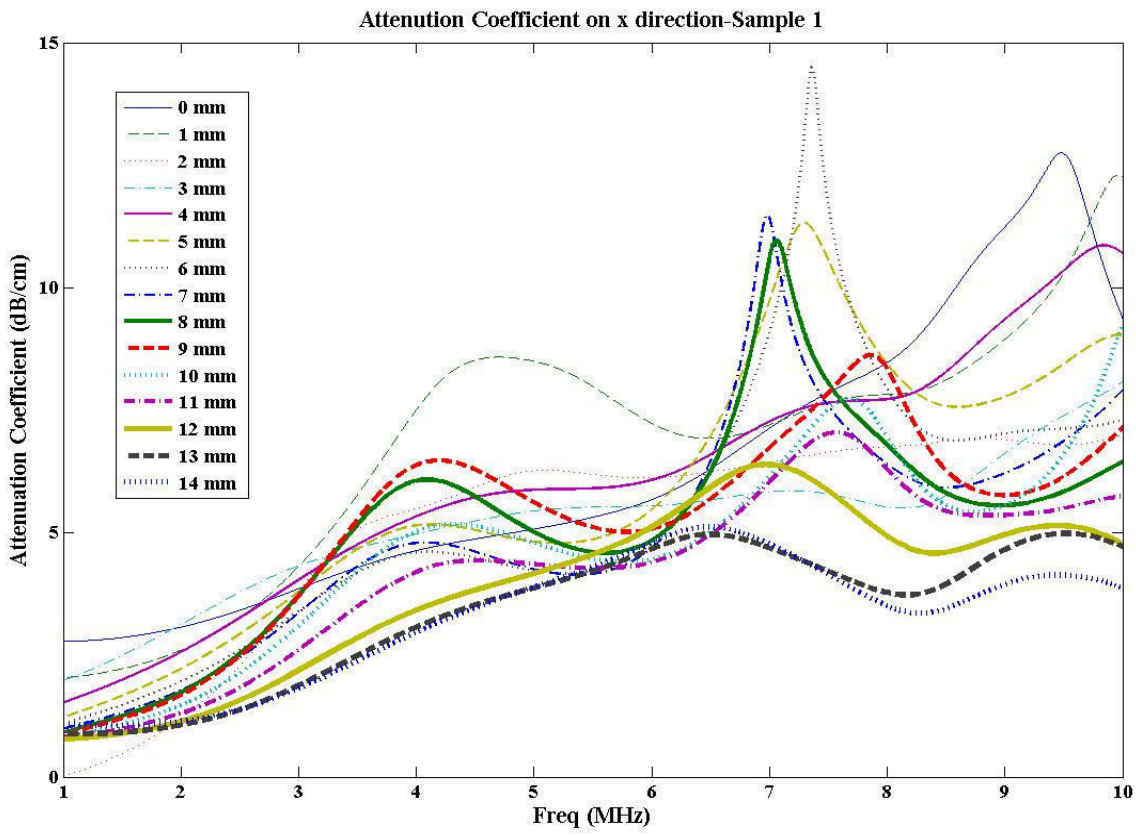

Figure 3.1.2.1: Attenuation coefficient on 15 positions of x direction-Sample 1.

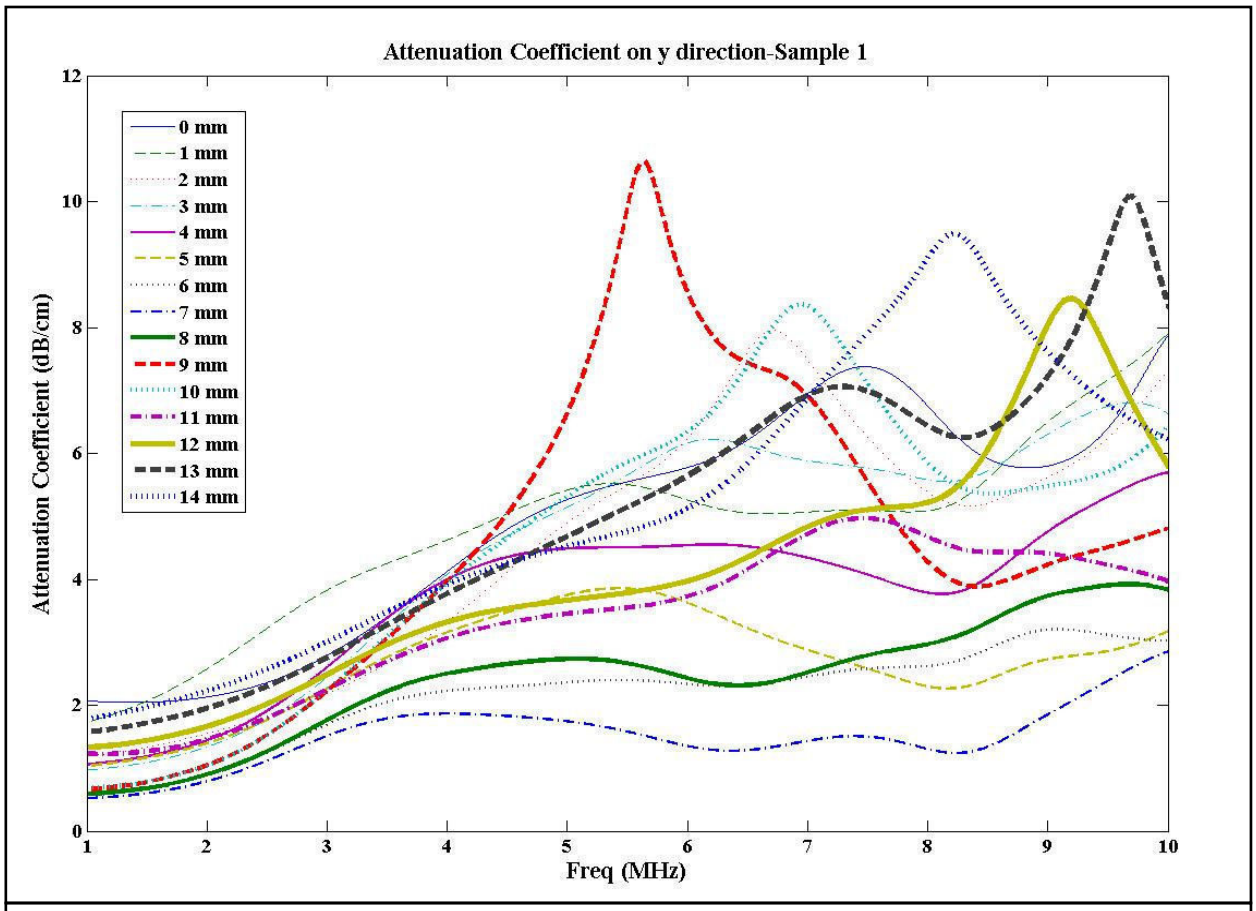

Figure 3.1.2.2: Attenuation coefficient on 15 positions of y direction-Sample 1.

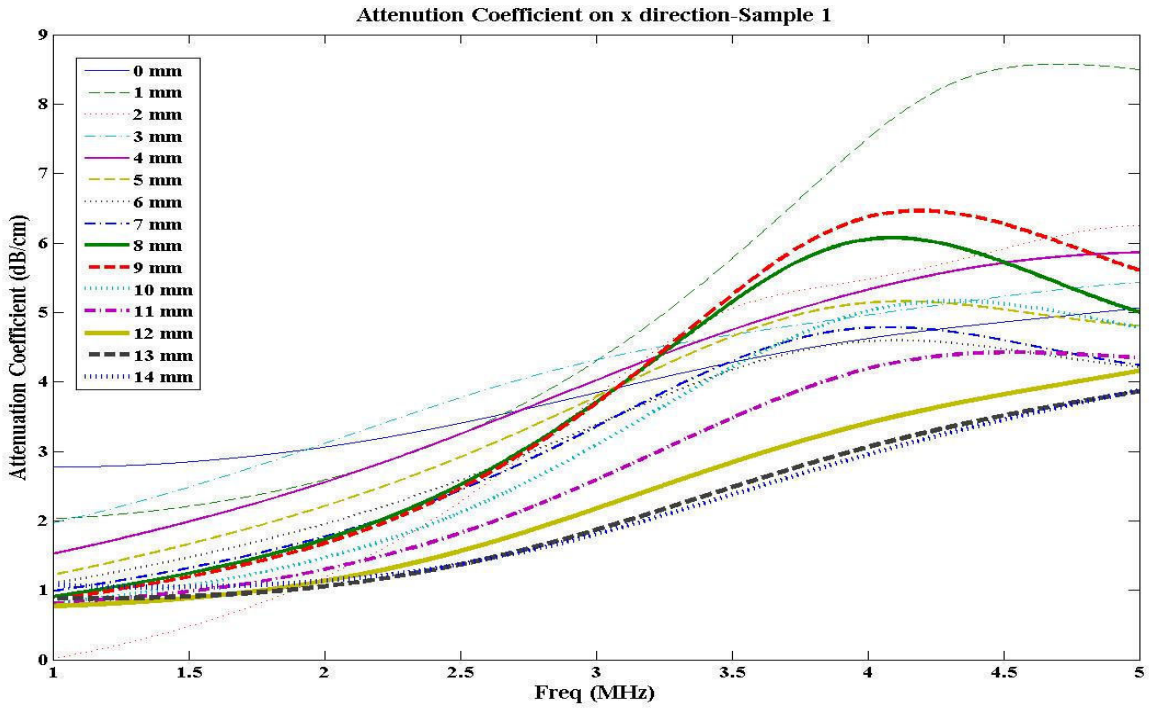

Figure 3.1.2.3: Best frequency range - attenuation coefficient (on x direction-Sample 1)

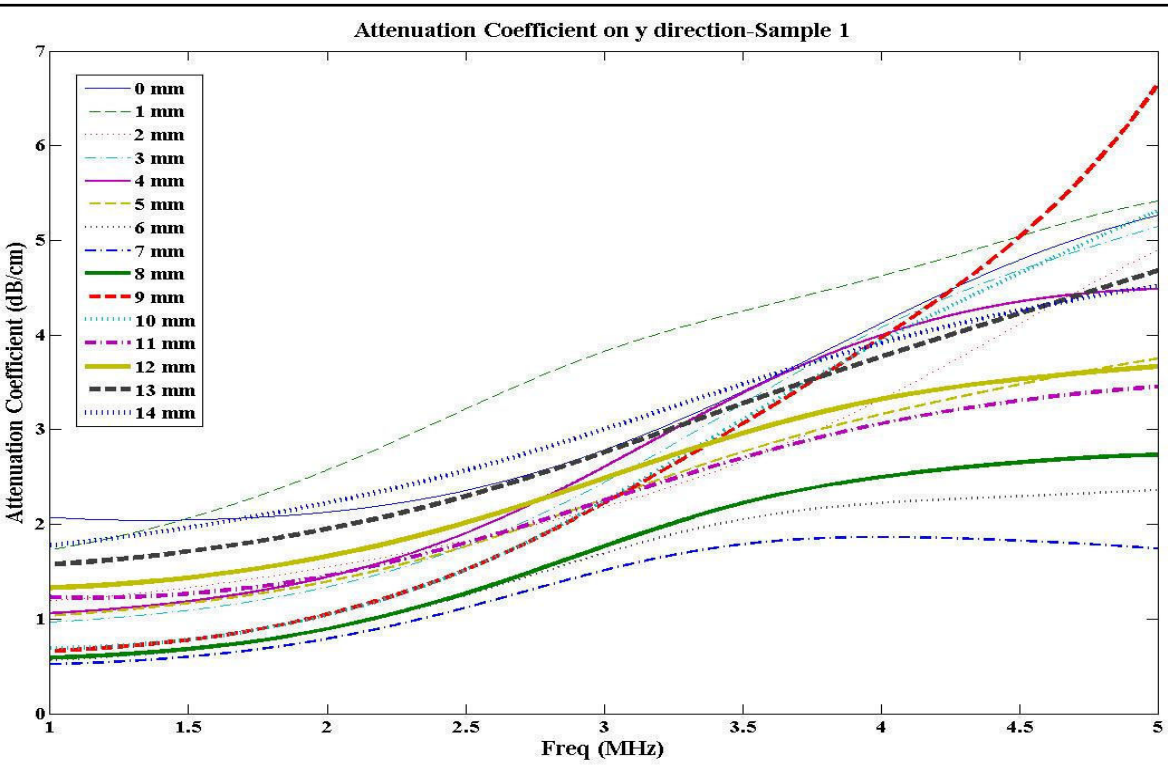

Figure 3.1.2.4: Best frequency range - attenuation coefficient (on y direction-Sample 1)

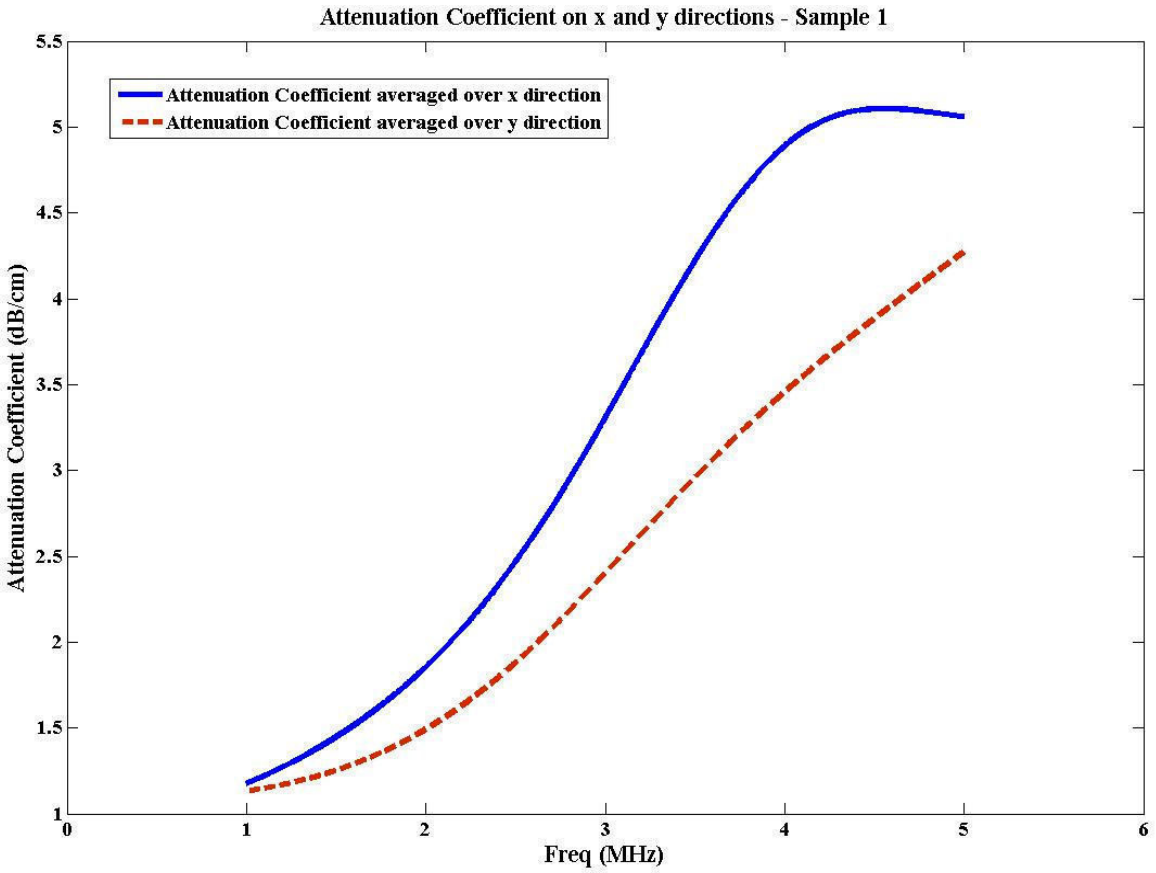

Figure 3.1.2.5: Attenuation coefficient averaged over x and y directions-Sample 1.

Figure 3.1.2.5 represents the average values of attenuation coefficient on 15 sites in each perpendicular direction. The magnitude of the attenuation coefficient in the *x* direction is higher than that of the *y* direction. This may be due to site-to-site variations in the tissue sample. Figure 3.1.2.6 shows the spatially averaged attenuation coefficient on 30 sites of sample 1 and the standard deviation limit curves.

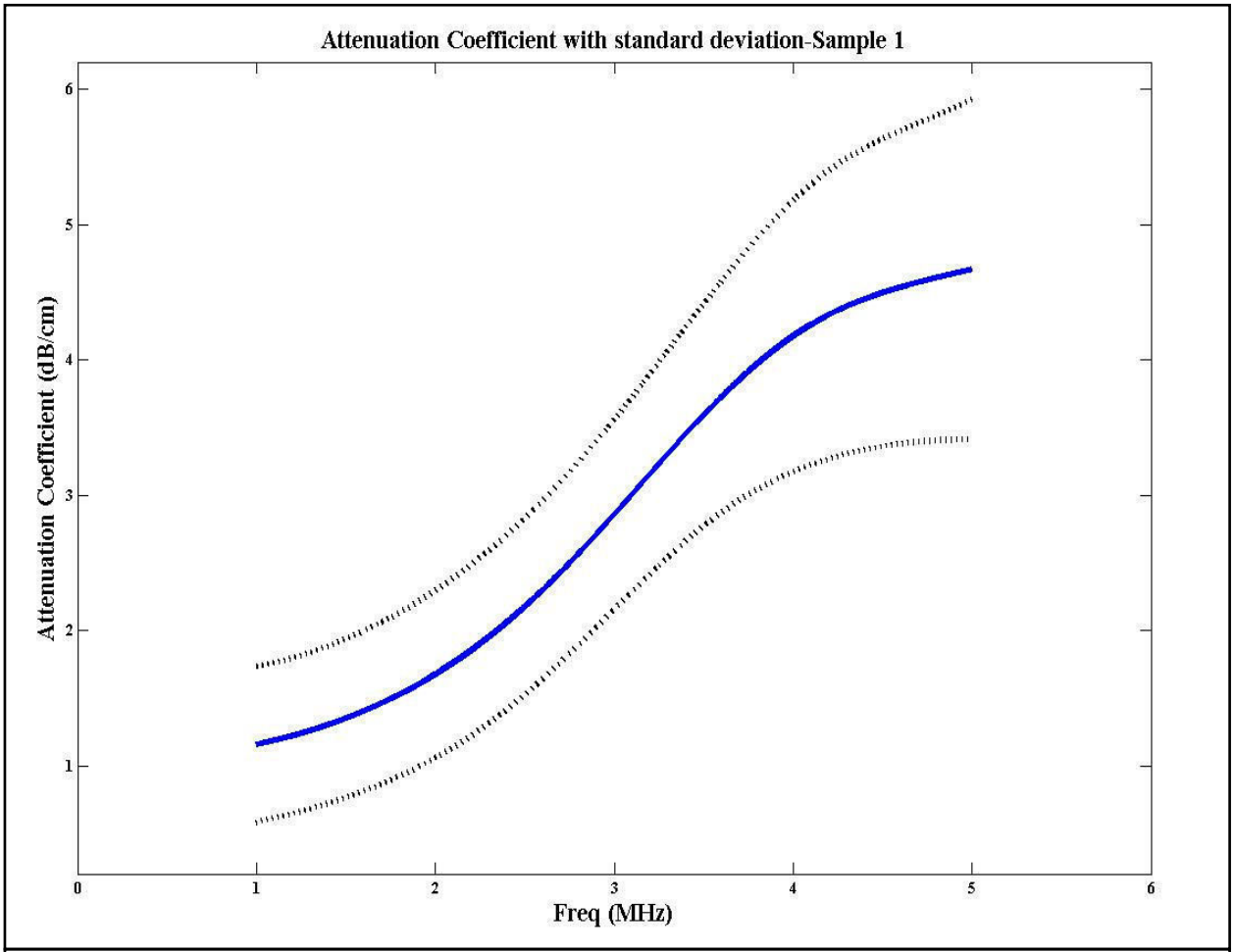

Figure 3.1.2.6: Attenuation coefficient with standard deviation- Sample 1.

Figure 3.1.2.7 illustrates the spatially averaged attenuation coefficient of four different samples. All four samples show that the attenuation is a monotonically increasing function of frequency in the 1-5 MHz range and can be reasonably approximated as a linear relationship with frequency. Figure 3.1.2.8 shows the average of the attenuation coefficient over all 4 samples, which exhibit approximately linear frequency dependence. The frequency dependence of the attenuation coefficient agrees reasonably well with previous results [3, 6] that show the attenuation coefficient rises linearly with frequency. The attenuation coefficient on ovine brain white matter in the frequency range 2-9 MHz in two orientations of the tissue sample 90^{o} and 0^{o}

has been reported in previous work [3]. Results for the attenuation coefficient in 90^{o} orientation show some higher values than ours but in both orientations the attenuation coefficient shows a linear relationship with frequency. The attenuation coefficient in white, grey and mixed matter of human brain in the frequency range 1-5 MHz is reported in [6]. Here also the attenuation coefficient shows a linear relationship with frequency for all three types of tissues.

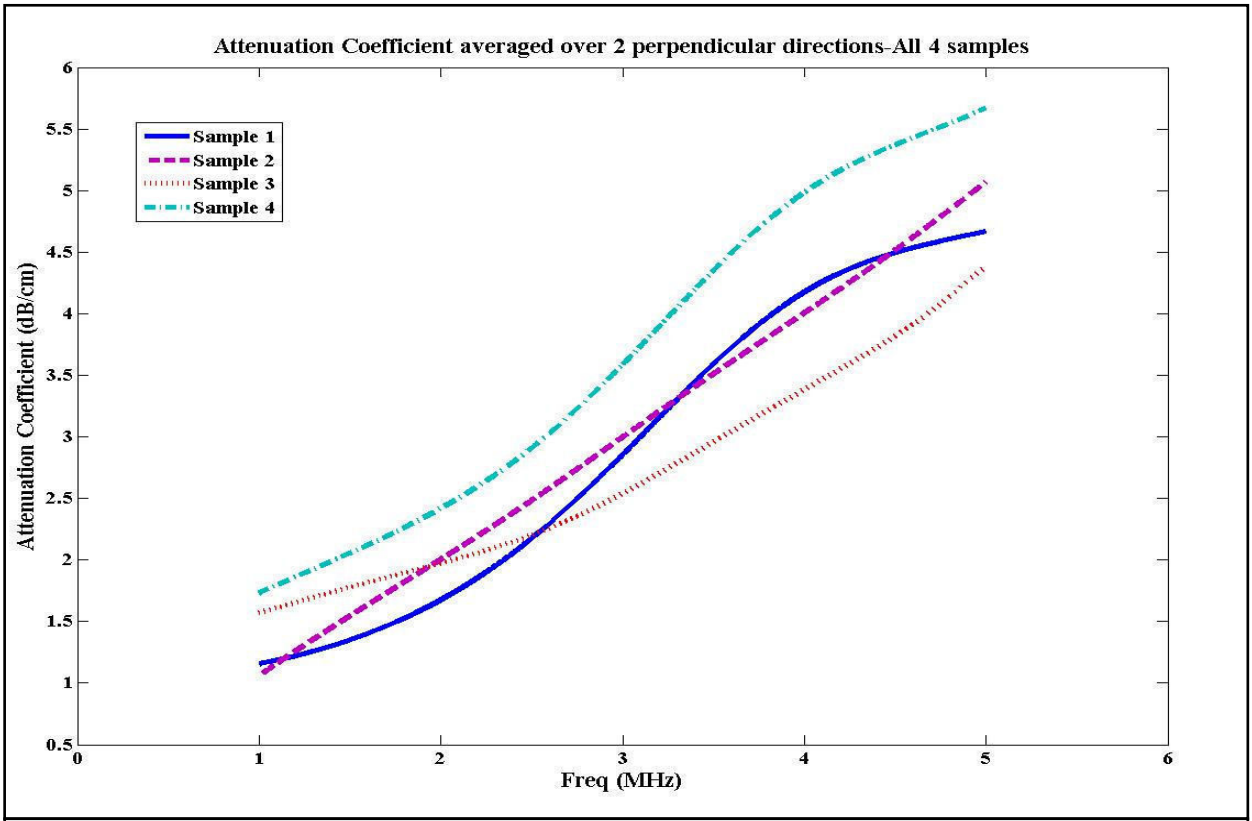

Figure 3.1.2.7: Attenuation coefficient averaged over 2 perpendicular directions -All 4 samples.

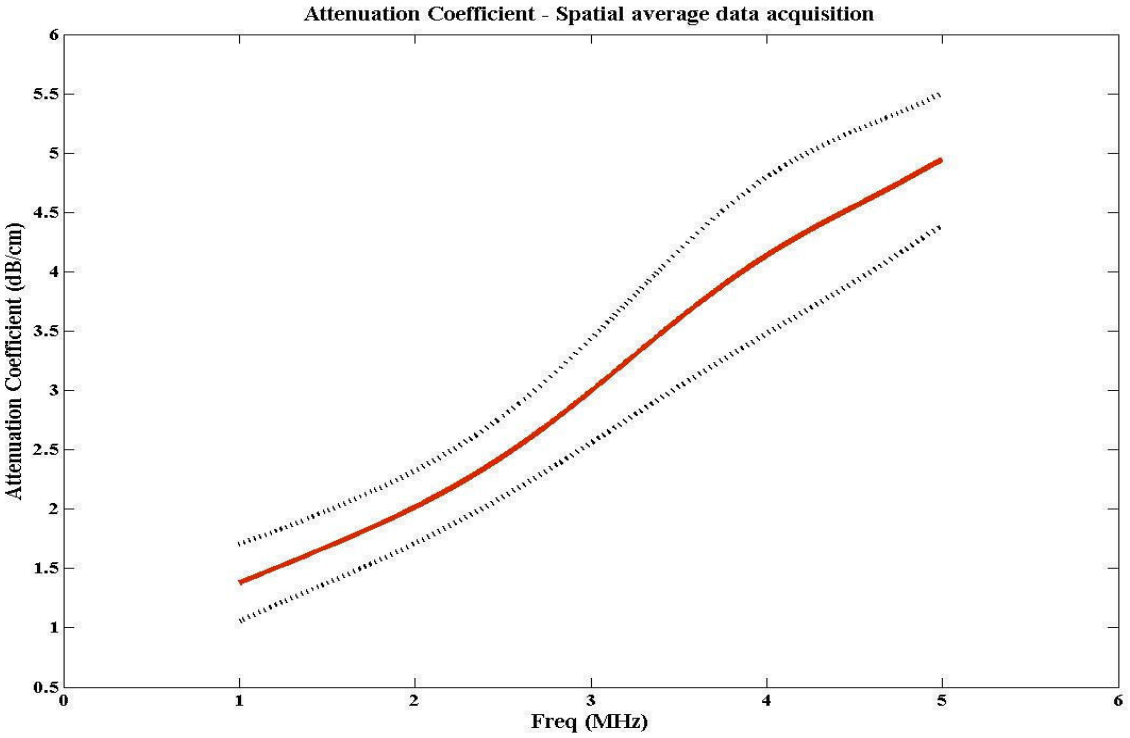

Figure 3.1.2.8: Attenuation coefficient averaged over 4 samples with standard deviation.

3.1.3 Backscatter Coefficient (BSC)

The backscatter coefficient can be expressed in terms of the apparent backscatter transfer function (ABTF), the attenuation coefficient (α) and some correction factors as given by Equation 1.4.5.1. The backscatter coefficient from 1 to 10 MHz at 30 sites of sample 1 in two perpendicular directions is shown in Figures 3.1.3.1 and 3.1.3.2. As mentioned earlier most curves in both diagrams show relatively uniform behavior up to 5 MHz. At higher frequencies, they show variations that are indicative of diffraction artifacts, which are not due to the inherent scattering properties of the tissue. Figure 3.1.3.3 represents the spatially averaged backscatter coefficient in those two directions. Again it is clear from Figure 3.1.3.3 that the backscatter coefficient shows relatively uniform behavior up to 5 MHz. This can be clearly illustrated by taking the standard deviation as shown in Figures 3.1.3.4 and 3.1.3.5.Figure 3.1.3.4 shows a low standard deviation up to 6 MHz for the x direction data and Figure 3.1.3.5 shows that for the y direction data up to 5 MHz. This indicates that the bandwidth from 1 to 5 MHz is the valid range for reporting the backscatter coefficient for our tissue samples. Figure 3.1.3.6 shows the spatially averaged backscatter coefficient from 1 to 5 MHz for 30 sites in sample 1.

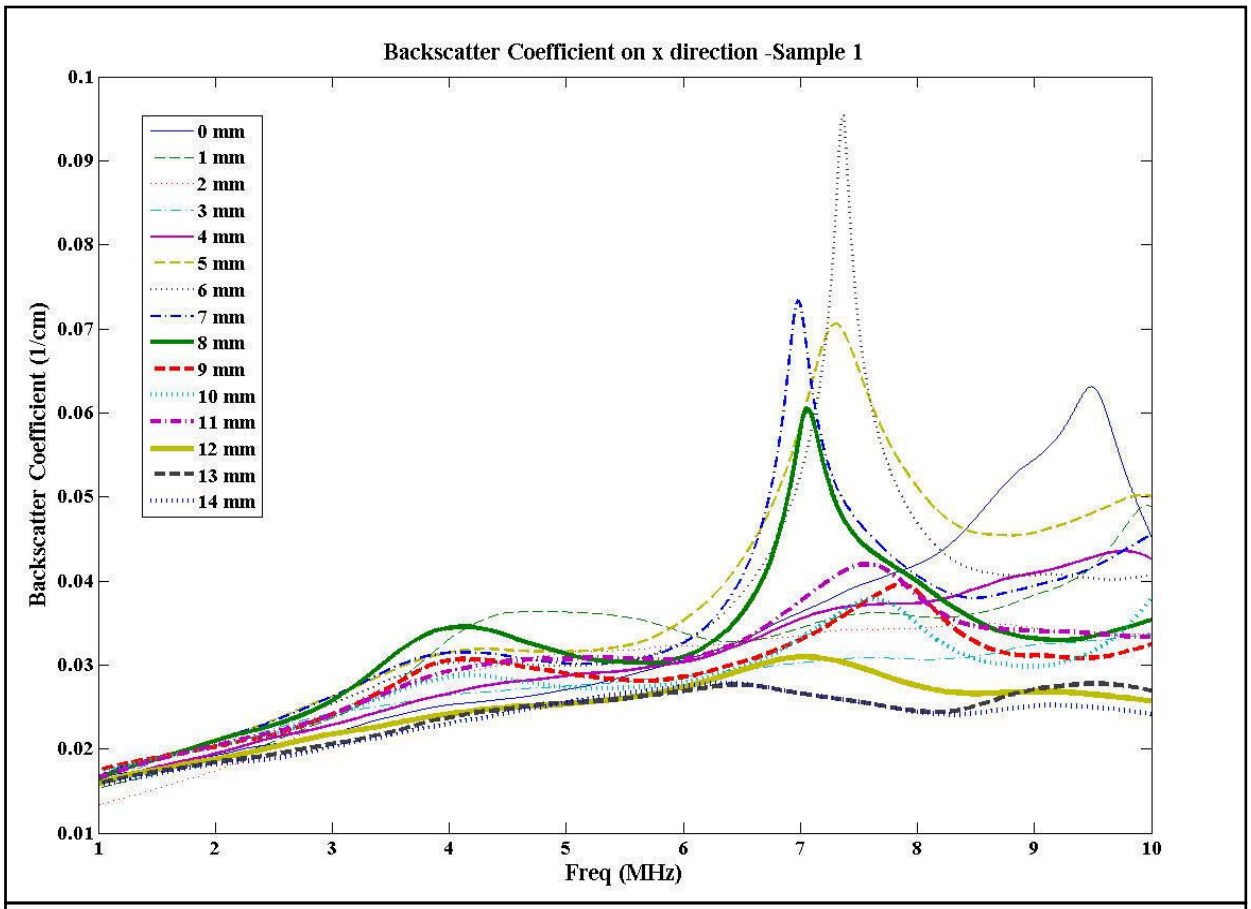

Figure 3.1.3.1: Backscatter coefficient on 15 positions of x direction-Sample 1.

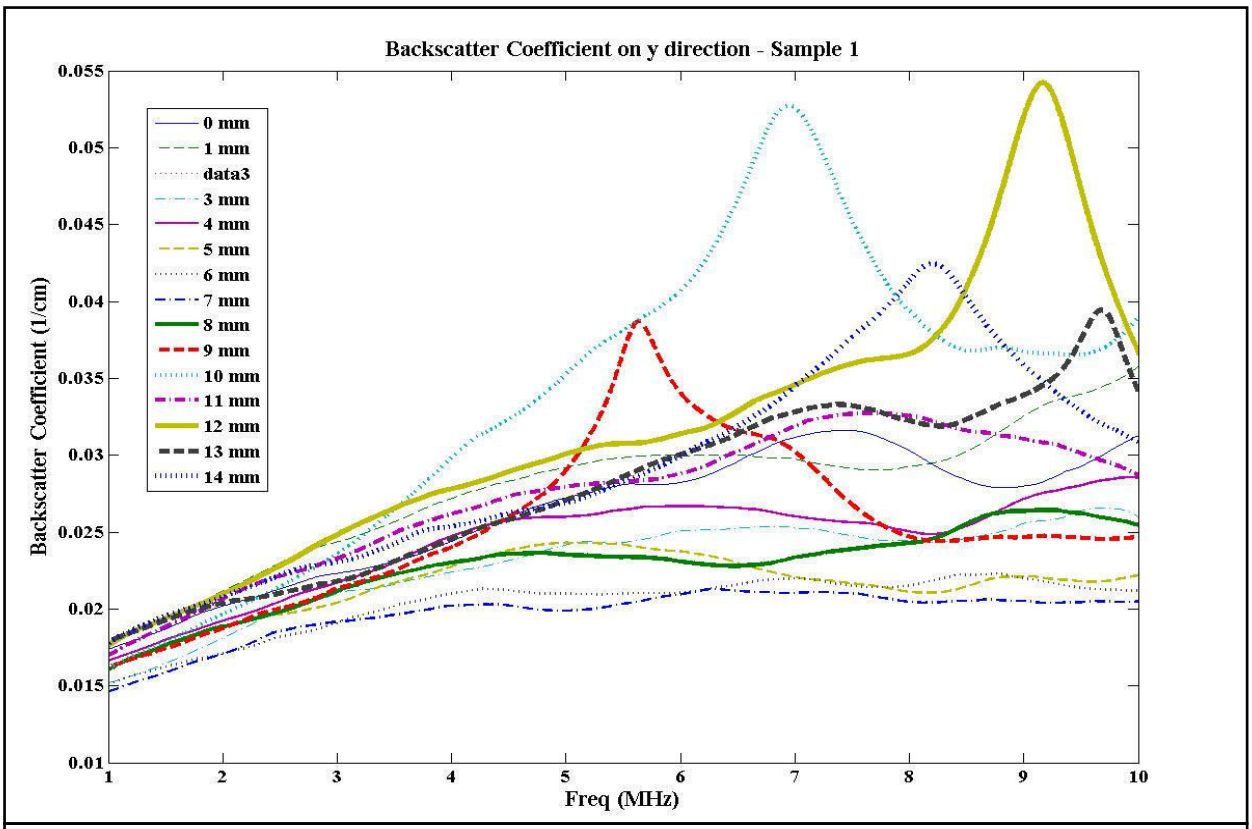

Figure 3.1.3.2: Backscatter coefficient on 15 positions of y direction-Sample 1.

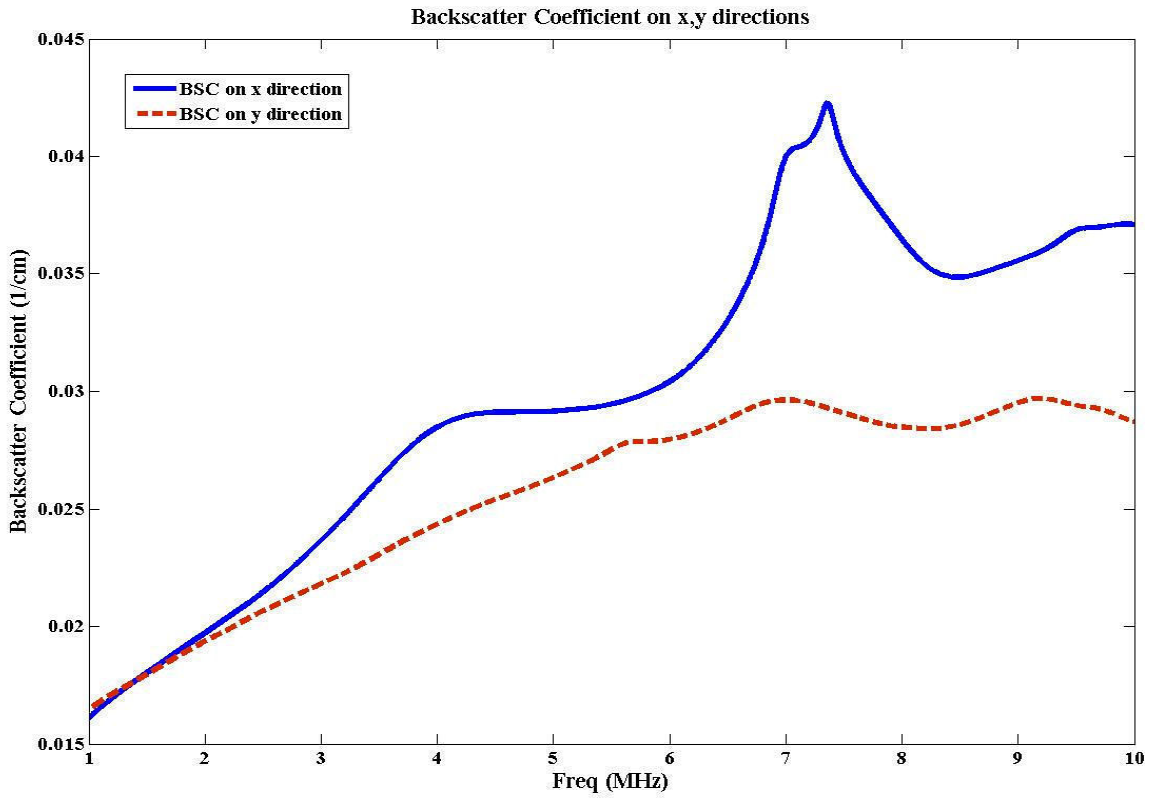

Figure 3.1.3.3: Averaged values of BSC on two perpendicular directions-Sample 1.

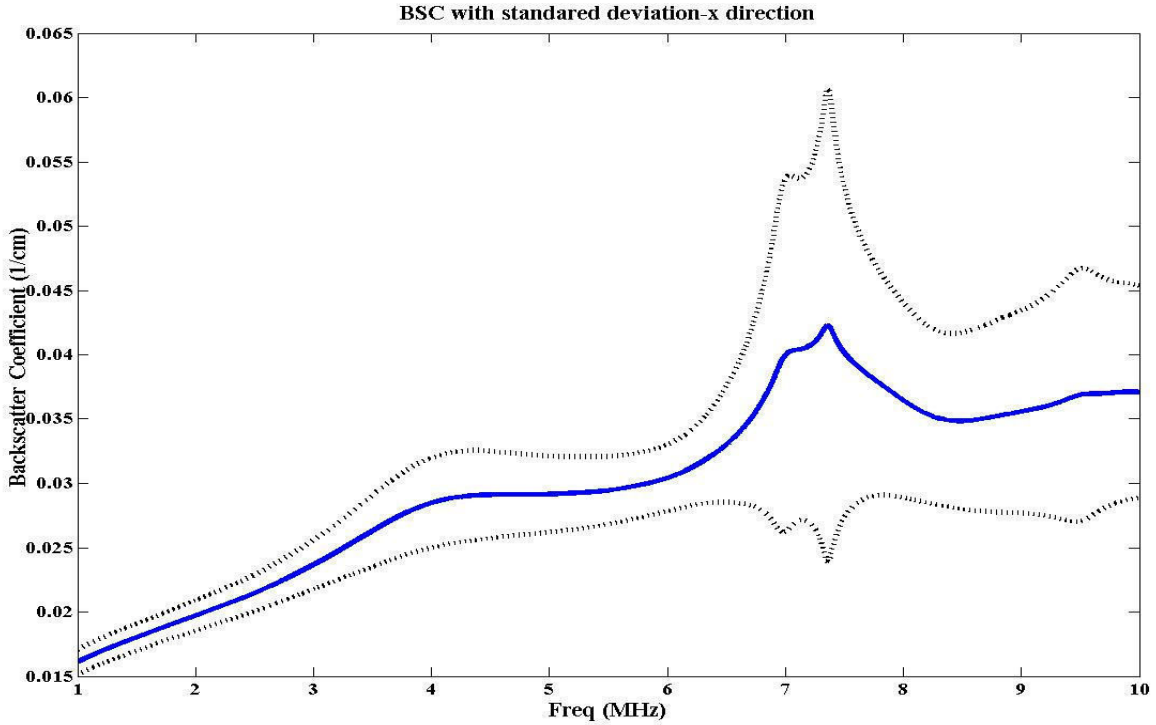

Figure 3.1.3.4: BSC with standard deviation – x direction.

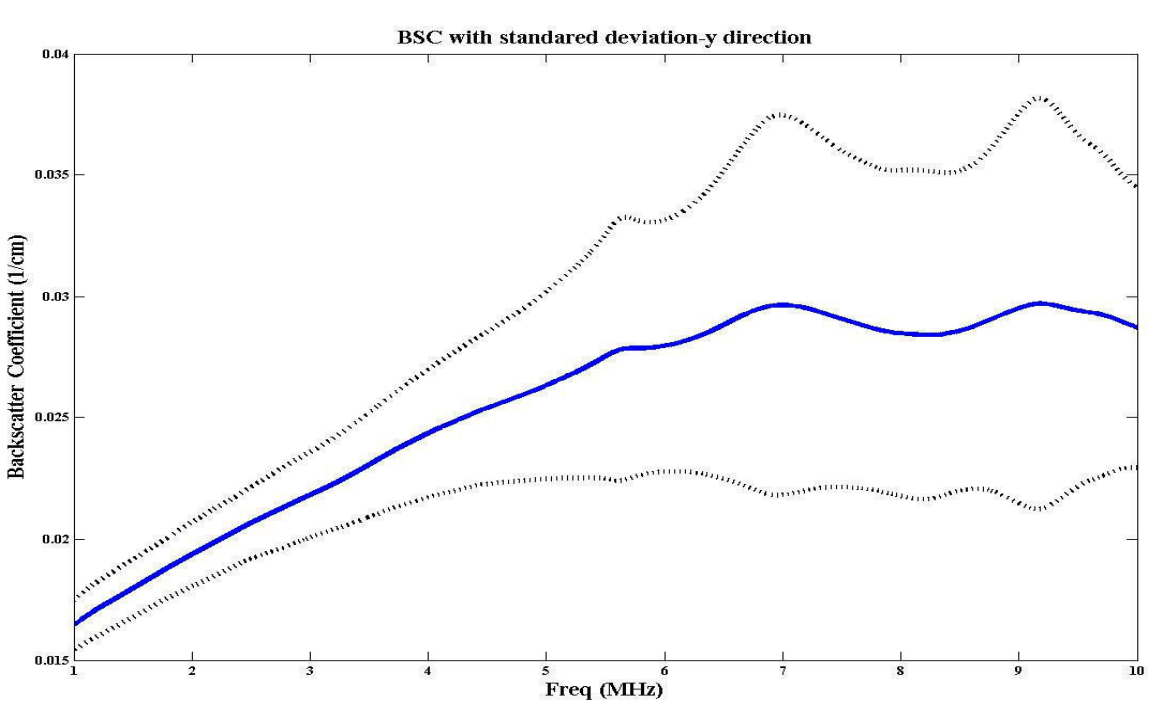

Figure 3.1.3.5: BSC with standard deviation – y direction.

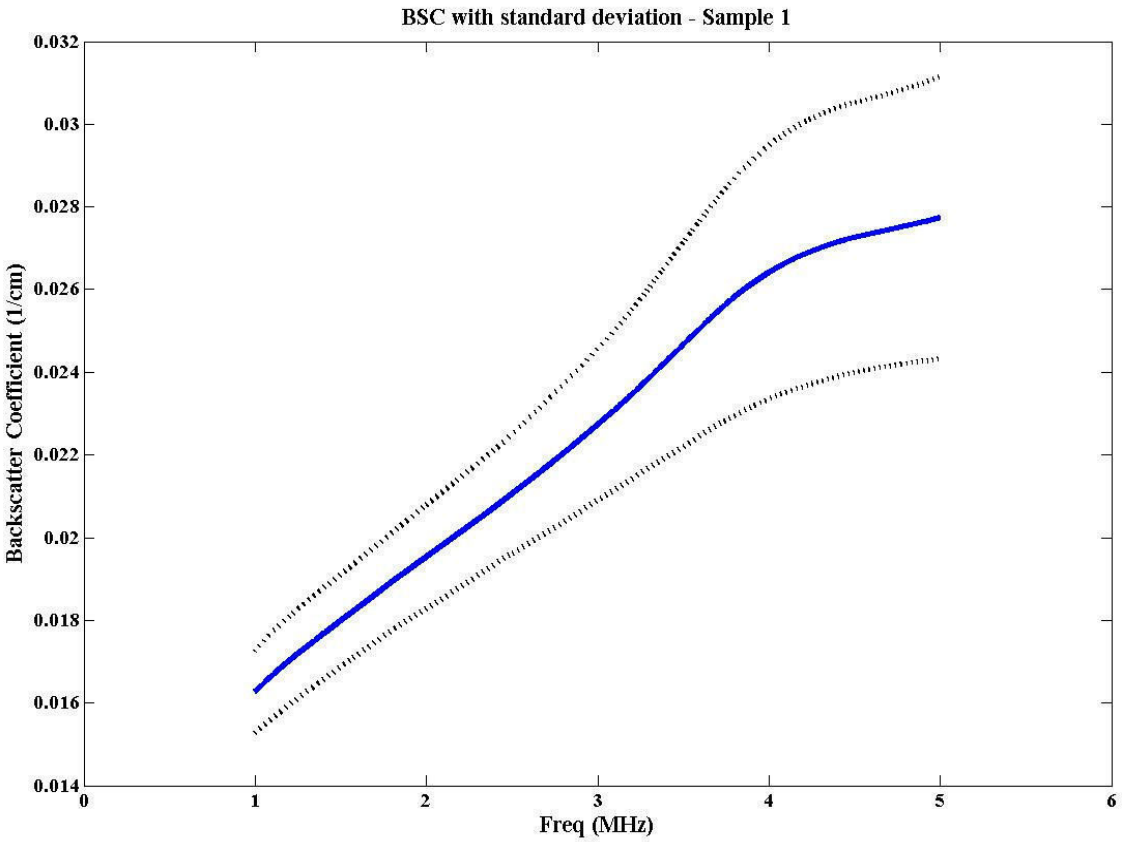

Figure 3.1.3.6: BSC with standard deviation – Sample 1.

Figure 3.1.3.7 illustrates the spatially averaged backscatter coefficient on four different samples. The same sample was used to measure the ABTF, the attenuation coefficient and the backscatter coefficient. As shown in Figure 3.1.3.7 the magnitude of the backscatter coefficient for sample 1 is the highest, while sample 3 shows the lowest in this frequency range. Figure 3.1.3.8 shows the averaged backscatter coefficient over all 4 samples. The backscatter coefficient for the mixed matter from ovine brain tissues is an increasing function of frequency from 1 to 5 MHz. The behavior for the backscatter coefficient on ovine brain tissues agrees reasonably well with the results obtained by [10, 20] that show the backscatter coefficient increases gradually with the frequency. The frequency dependence of the backscatter coefficient of bovine liver,

pancreas, kidney, heart and spleen from 2 to 7 MHz is reported in [10] and [20] shows that of the human liver and kidney in the range of 2 to 4 MHz. Our results for the backscatter coefficient of ovine brain tissue show a similar frequency dependence as in [10, 20] with some higher values for the magnitude of the backscatter coefficient. This may be due to the beam characteristics of the transducers used for data collection; ultrasonic data acquisition systems used and also may be due to the different tissue types.

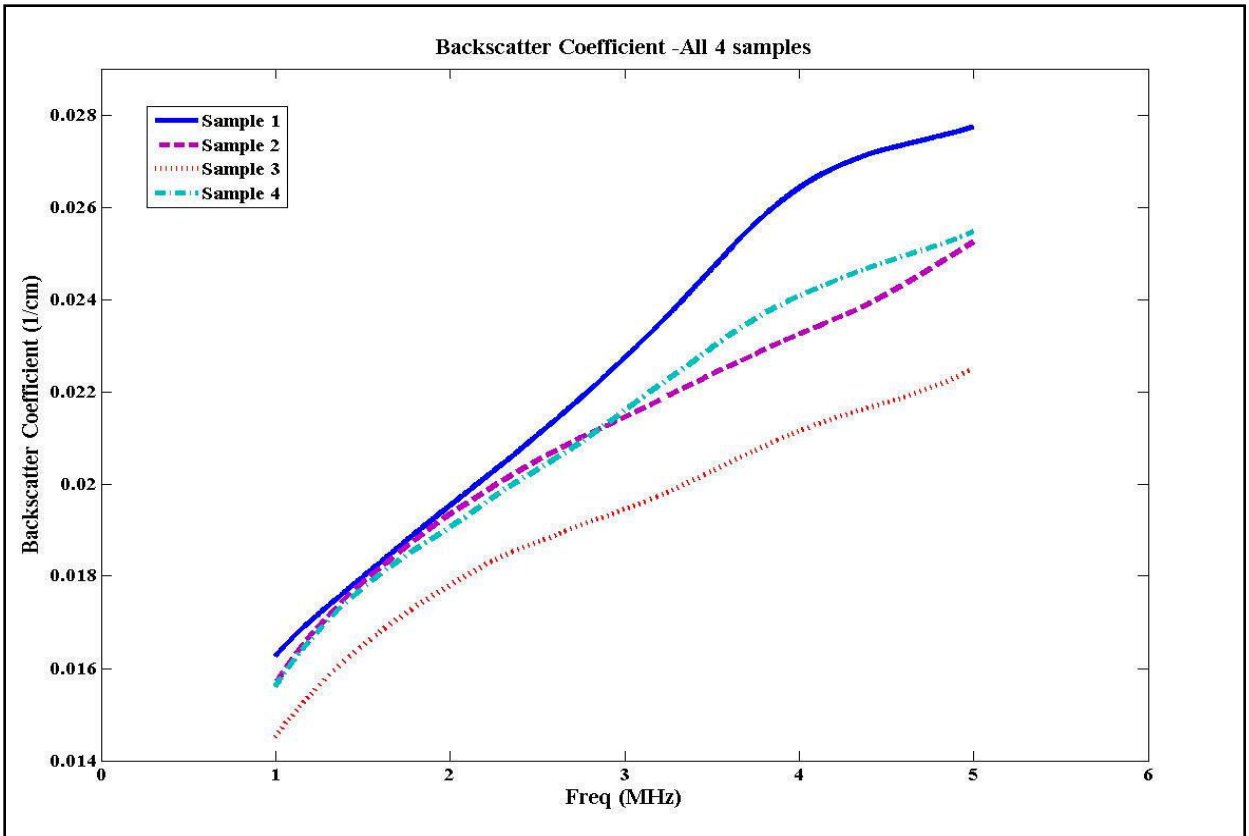

Figure 3.1.3.7: Backscatter coefficient averaged over 2 perpendicular directions - All 4 samples.

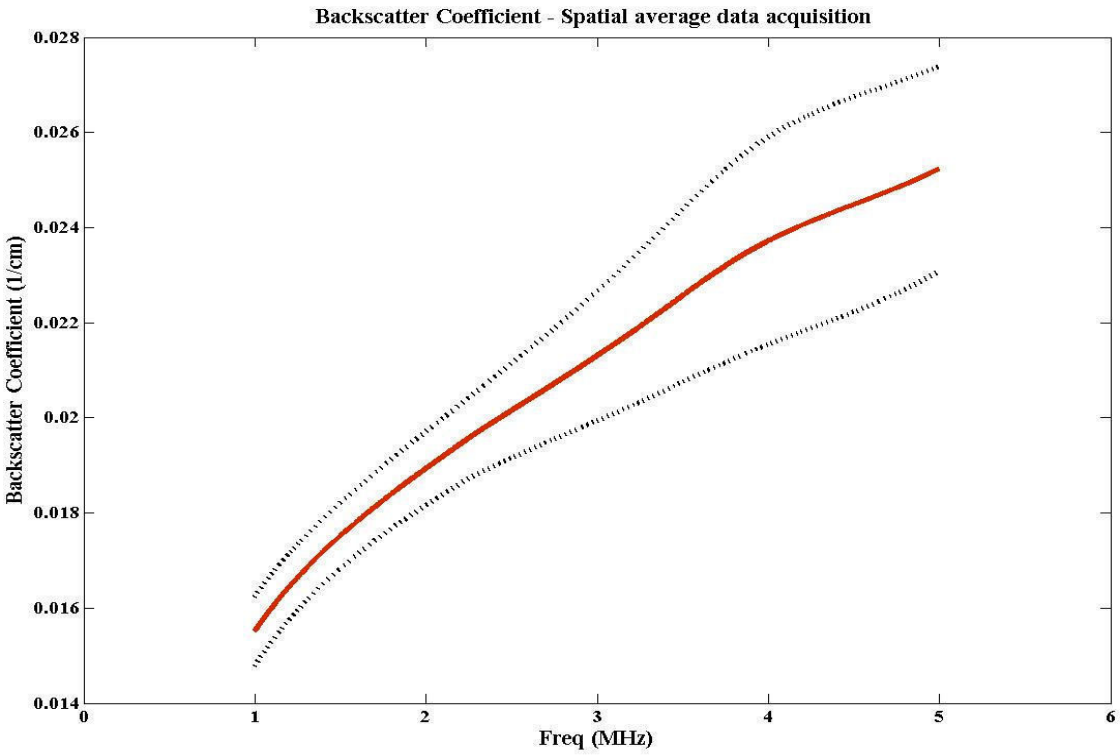

Figure 3.1.3.8: Backscatter coefficient averaged over 4 samples with standard deviation.

3.2 Orientation dependence of backscatter and attenuation data of ovine brain tissues

In this study, the orientation dependence of backscatter and attenuation data were examined on 5 cylindrically shaped ovine brain tissue samples with mixed matter that covered from 0^o to 360^o by rotating the sample with 30^o increments using a rotating stage as shown in Figures 2.2.2.5 and 2.2.2.6. As mentioned in section 3.1, the attenuation coefficient and the backscatter coefficient (BSC) were measured for the 1-5 MHz frequency range, and the apparent backscatter transfer function (ABTF) was measured for the 1-10 MHz range.

3.2.1 Apparent backscatter transfer function (ABTF)

Figure 3.2.1.1 shows the ABTF for 13 orientations of cylindrically shaped tissue sample 2. In Figure 3.2.1.1 each curve represents the ABTF at one orientation for the frequency range 1-10 MHz. All the curves show similar behavior, a result consistent with section 3.1 in the same frequency range. Figure 3.2.1.2 represents the averaged value of ABTF over the angles with standard deviation limit curves.

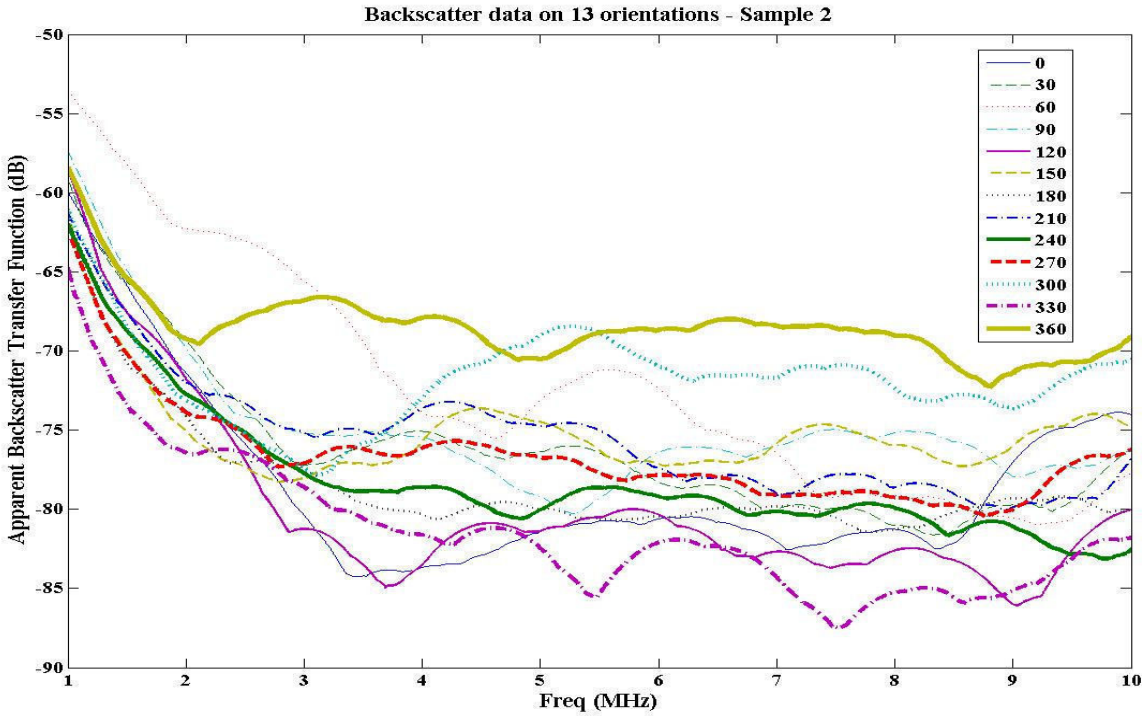

Figure 3.2.1.1: ABTF on 13 orientations – Sample 2.

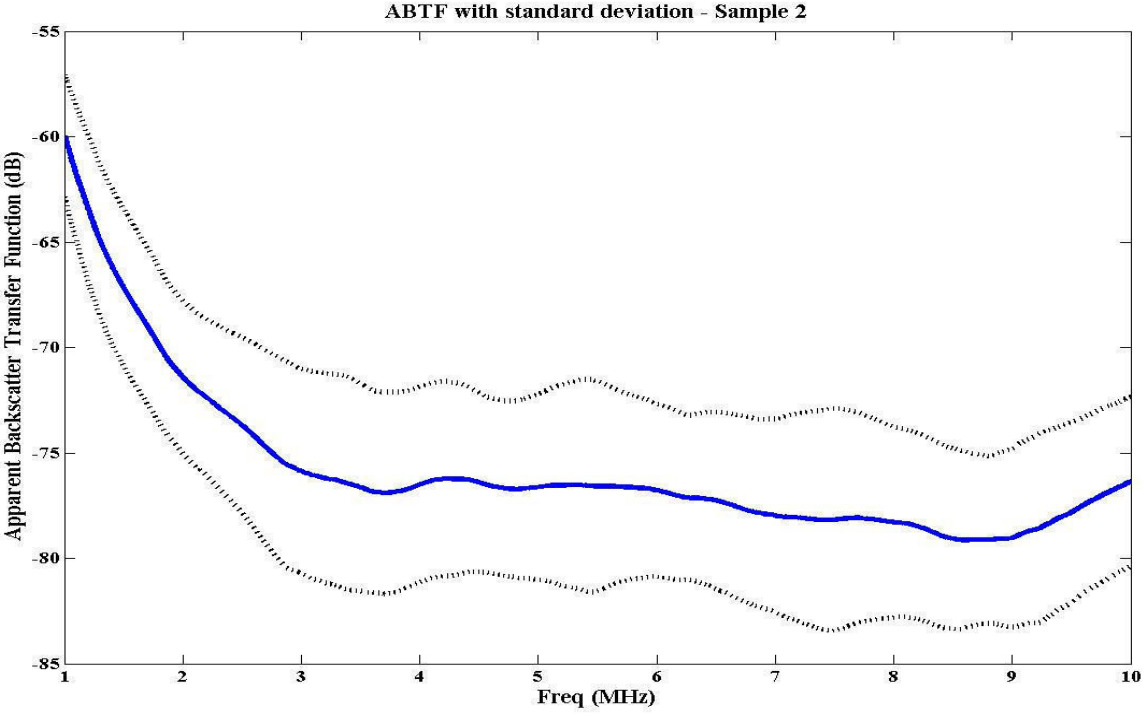

Figure 3.2.1.2: ABTF averaged over angles with standard deviation–Sample 2.

The same procedure was repeated for 4 more samples and Figure 3.2.1.3 shows the ABTF averaged over angles for all 5 samples. There is no significant difference in ABTF for the upper 4. Figure 3.2.1.4 represents the averaged value of ABTF for samples 2, 4, 5 and 6. As discussed earlier, it shows a monotonically decreasing function of frequency over the range of 1-10 MHz, and there is no appreciable difference with the values obtained from the spatial averaging method in section 3.1.1.

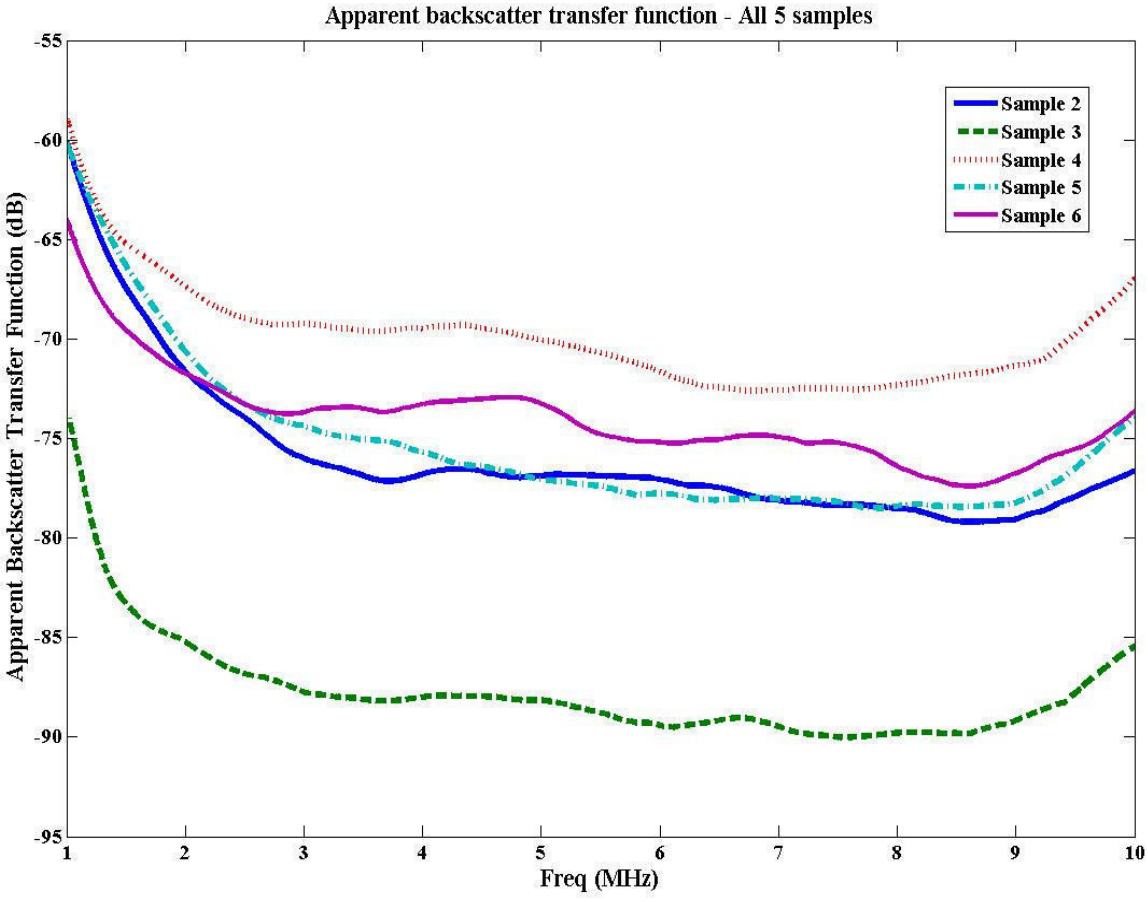

Figure 3.2.1.3: ABTF averaged over angels-All 5 samples.

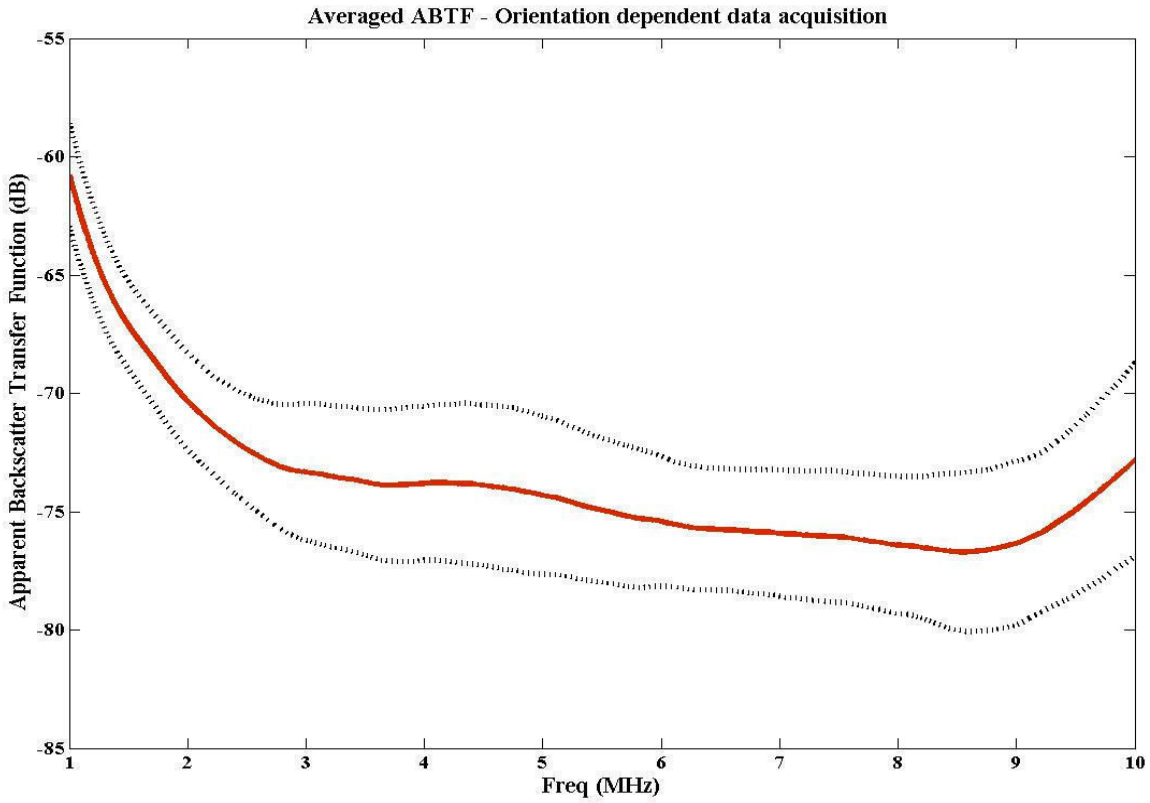

Figure 3.2.1.4: ABTF averaged over 4 samples with standard deviation.

3.2.2 Attenuation coefficient

The attenuation coefficient as a function of frequency from 1 to 10 MHz at 13 orientations of sample 2 is shown in Figure 3.2.2.1. As discussed earlier, most of the curves in Figure 3.2.2.1 are relatively consistent up to 5 MHz. So the 1 to 5 MHz range can be considered as the best frequency band for the attenuation coefficient, and Figure 3.2.2.2 shows the attenuation coefficient for that region of the spectrum. Figure 3.2.2.3 illustrates the averaged attenuation coefficient for sample 2, which has monotonically increasing frequency dependence from 1-5 MHz with standard deviation limit curves.

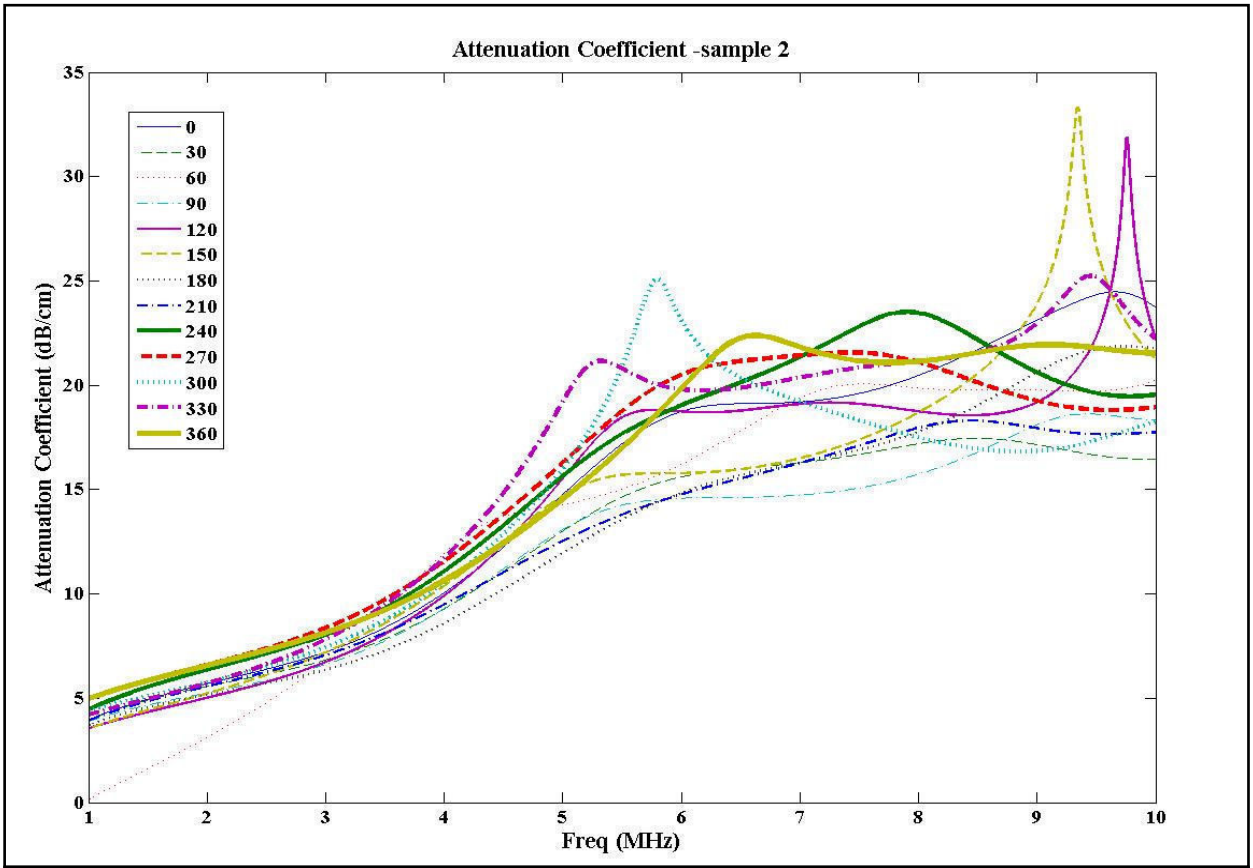

Figure 3.2.2.1: Attenuation coefficient on 13 orientations - Sample 2.

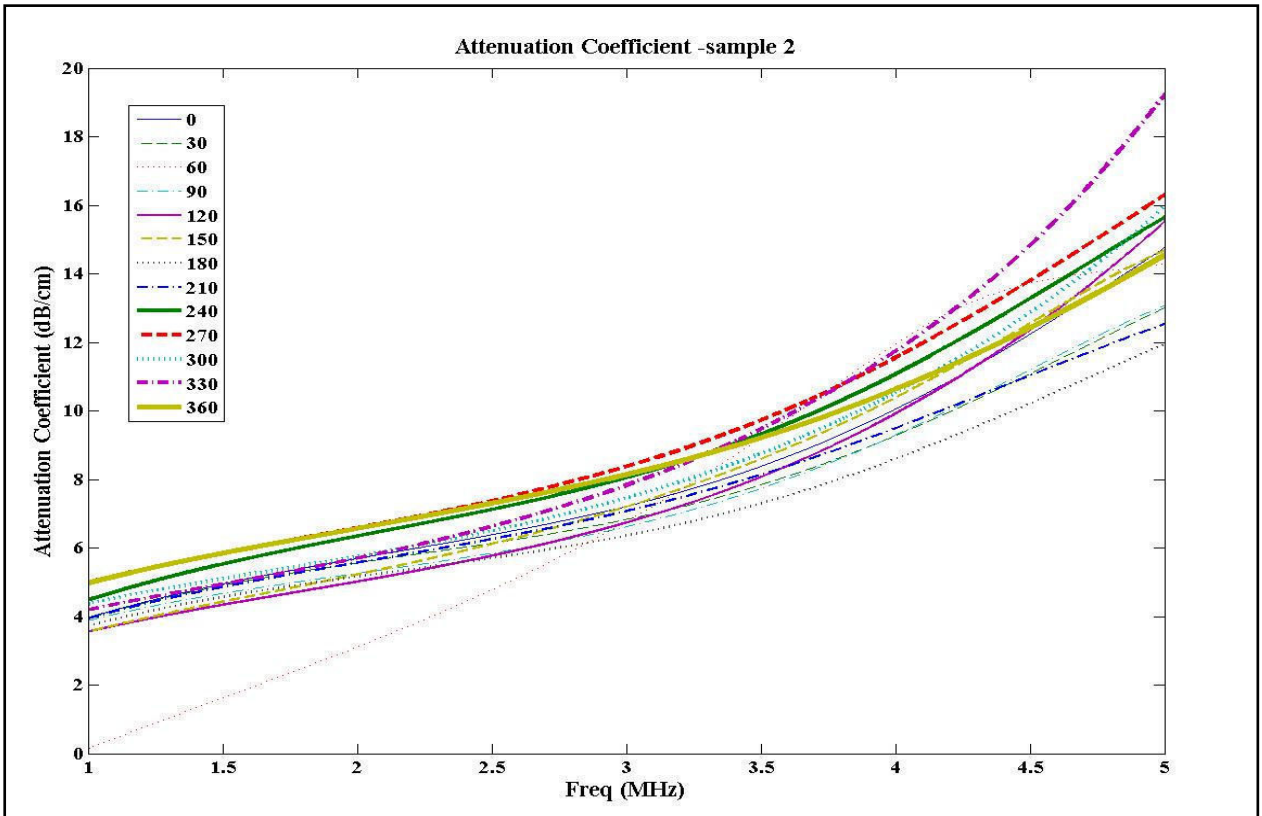

Figure 3.2.2.2: Best frequency range for the attenuation coefficient.

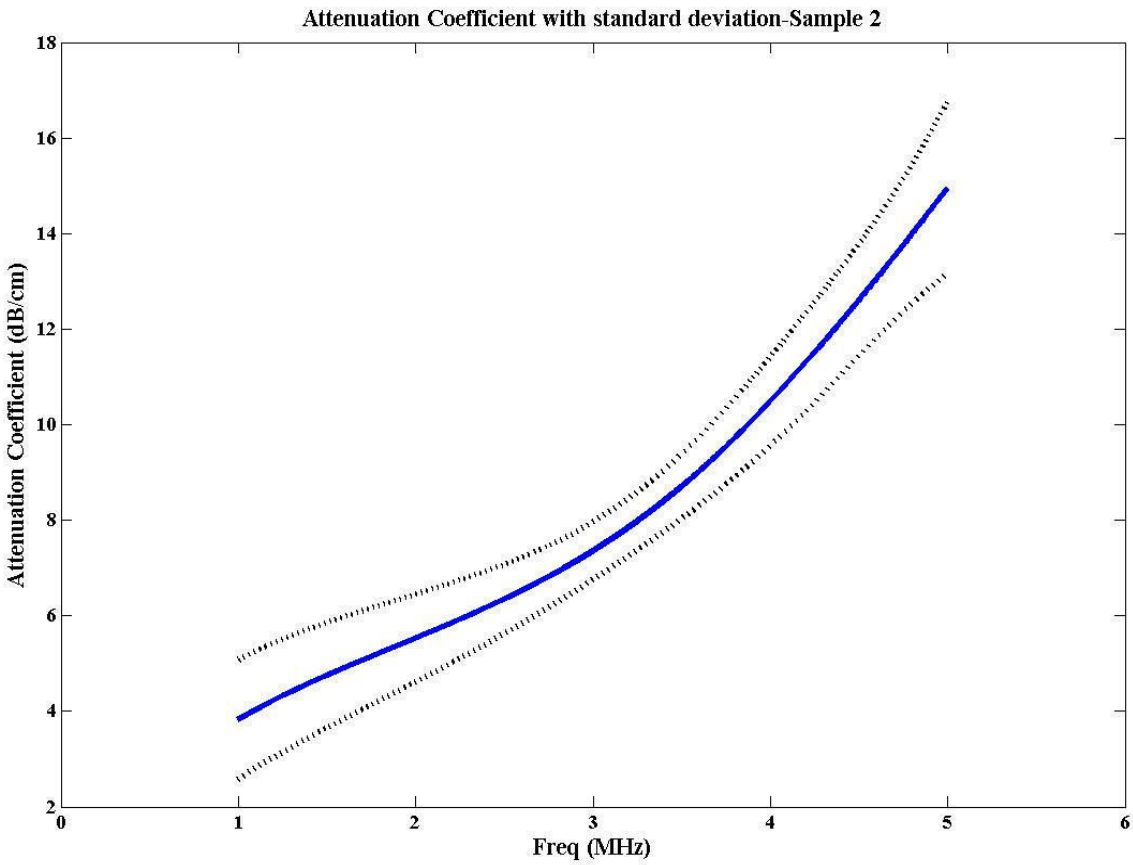

Figure 3.2.2.3: Attenuation coefficient averaged over angles –Sample 2.

Figure 3.2.2.4 represents the averaged attenuation coefficient over angles as a function of frequency for all 5 samples in the frequency range 1 to 5 MHz. Sample 3 shows the highest attenuation coefficient values as with the ABTF but here it does not show a considerable difference with the other 4 curves. Figure 3.2.2.5 represents the averaged attenuation coefficient of all 5 samples for the 1 to 5 MHz range. When compared with the magnitudes of the attenuation coefficient obtained from the spatial averaging method, Figure 3.2.2.5 shows higher values of that in the same frequency range. The reason for this discrepancy is not clear.

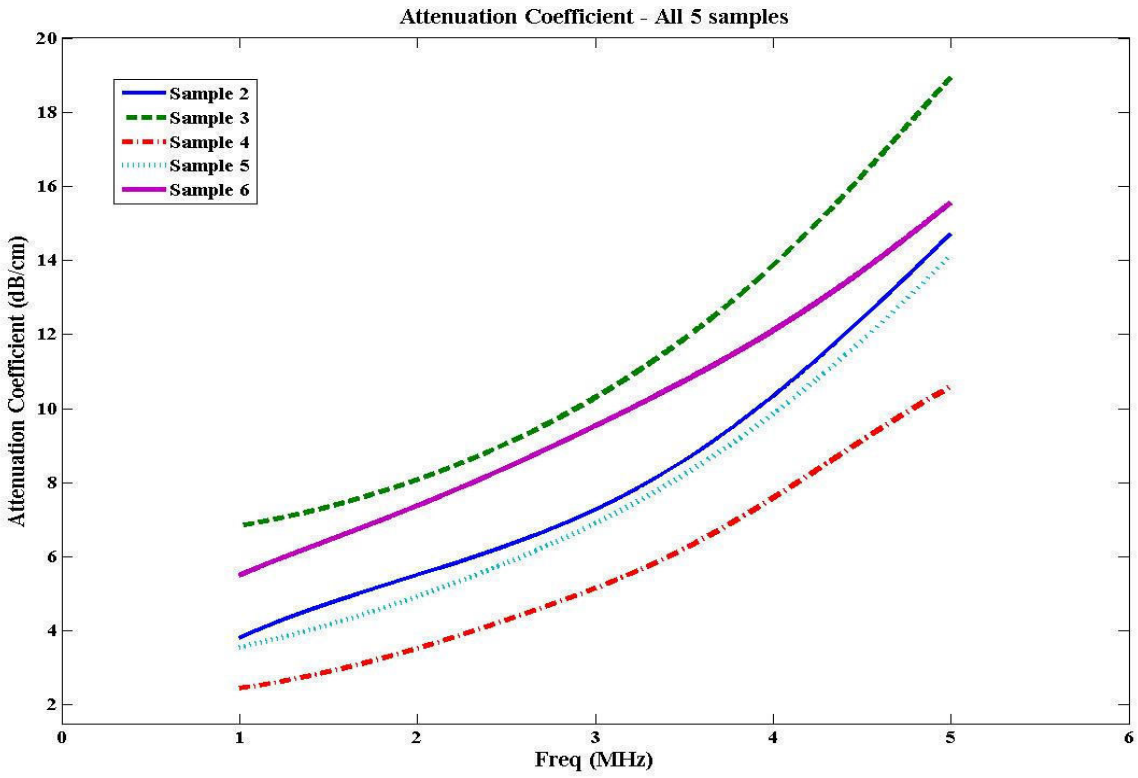

Figure 3.2.2.4: Attenuation coefficient averaged over angels-All 5 samples.

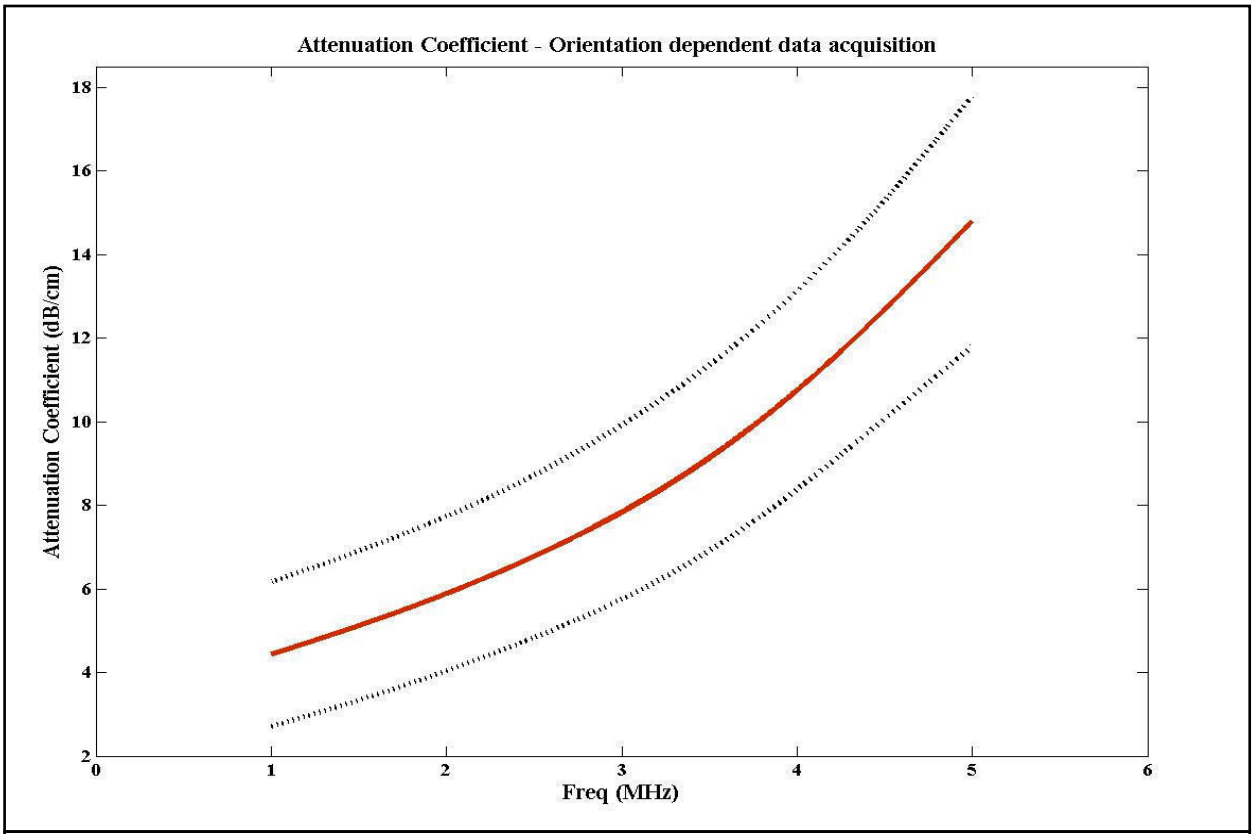

Figure 3.2.2.5: Attenuation coefficient averaged over 5 samples with standard deviation.

3.2.3 Backscatter coefficient

The backscatter coefficient as a function of frequency from 1 to 10 MHz at 13 orientations of sample 2 is shown in Figure 3.2.3.1.As discussed in section 3.1.3, some of the curves on Figure 3.2.3.1 show a relatively uniform pattern up to 5 MHz. So the 1 to 5 MHz range was considered the valid range for the backscatter coefficient as with the attenuation coefficient.

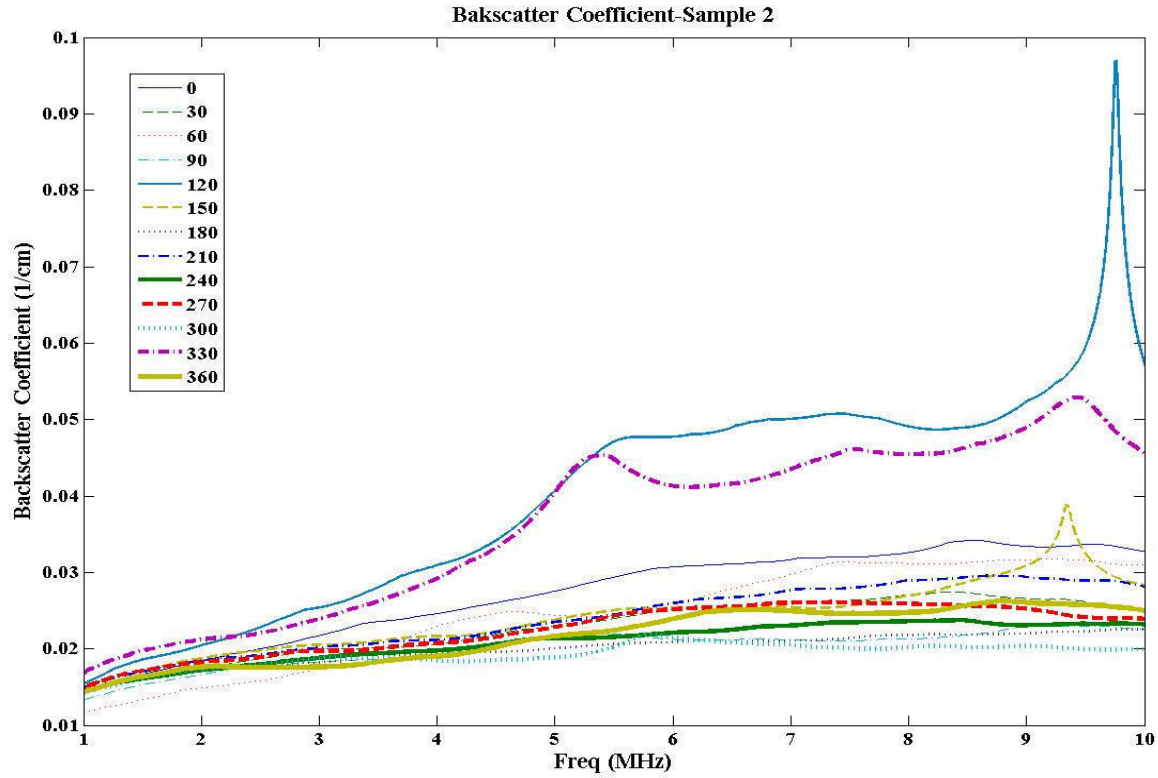

Figure 3.2.3.1: BSC on 13 orientations - Sample 2.

Figures 3.2.3.2 and 3.2.3.3 show the backscatter coefficient for 0^o to 150^o and 180^o to 360^o in the frequency range of 1 to 5 MHz respectively. They are plotted separately so as to allow analysis of the orientation dependence of the BSC, and it is clear from Figures 3.2.3.2 and 3.2.3.3 that almost all of the curves overlap on those two ranges of angles. Thus the 0^o to 150^o range was considered for all the calculations of backscatter coefficient on all 5 samples.

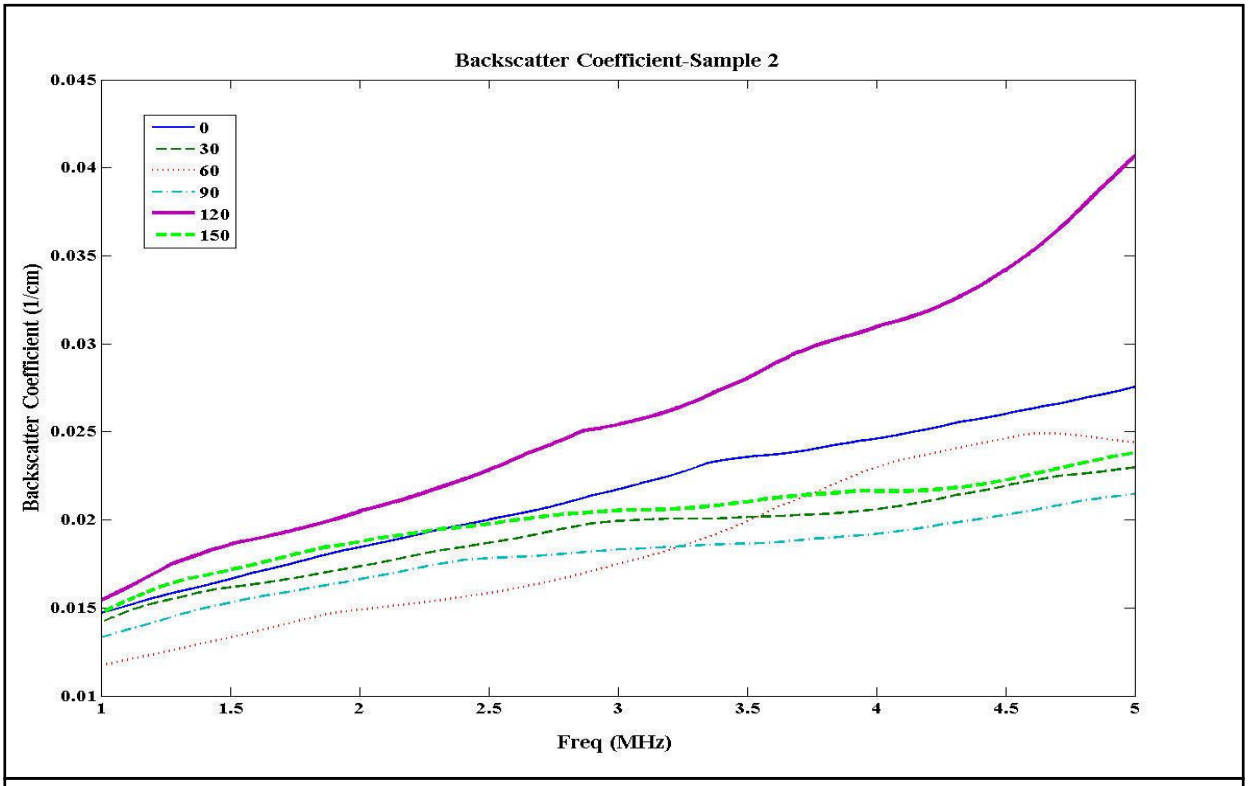

Figure 3.2.3.2: BSC on 0^{0} to 150^{0} - Sample 2.

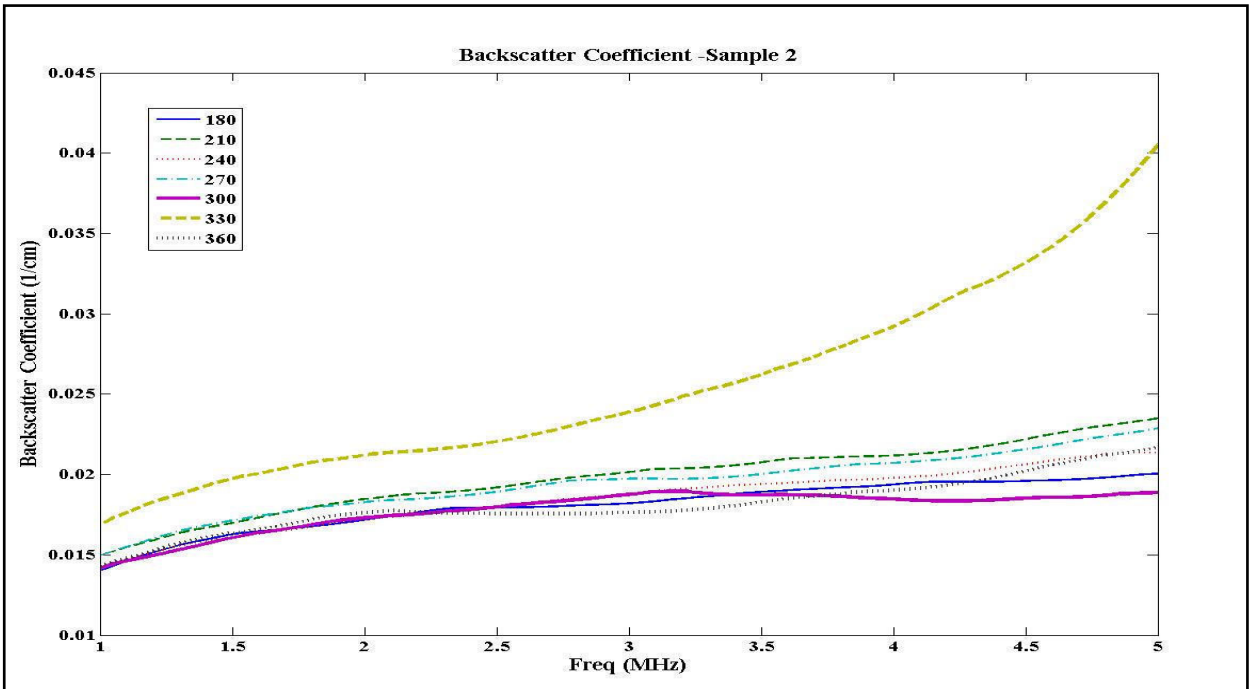

Figure 3.2.3.3: BSC on 180^{0} to 360^{0} - Sample 2.

Figure 3.2.3.4 shows the standard deviation of the averaged BSC for sample 2, and again it is clear that the best range for the backscatter data is 1 to 5 MHz.

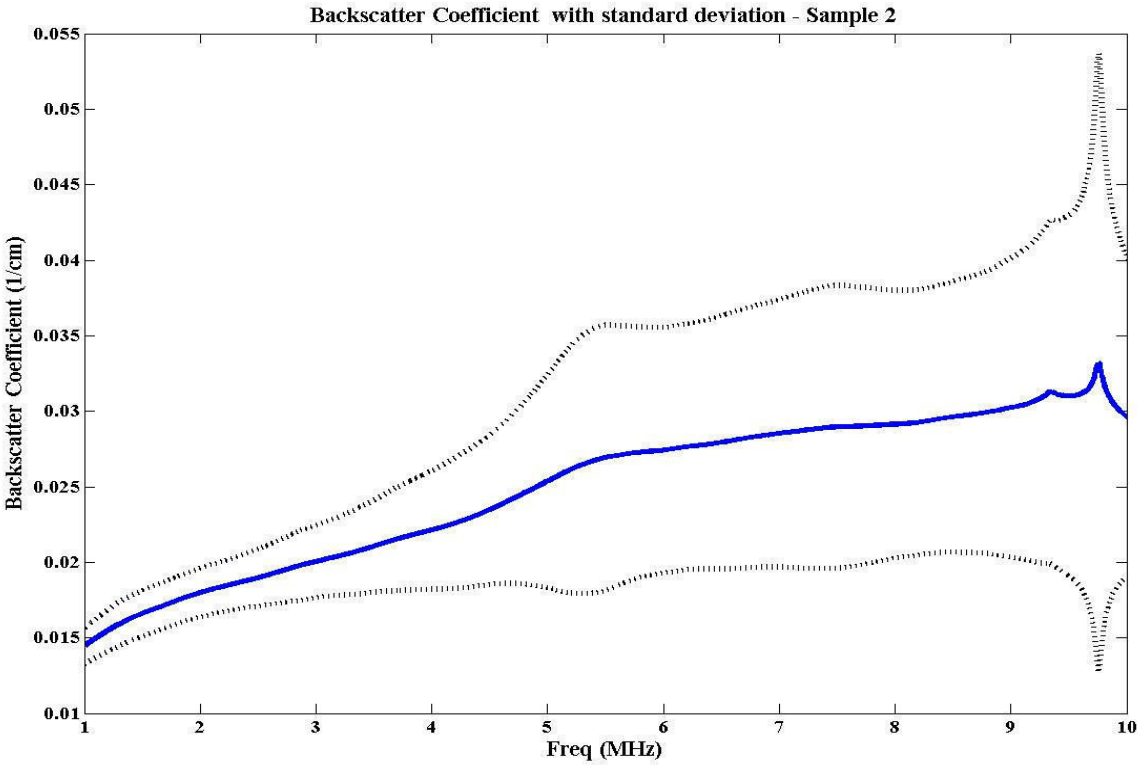

Figure 3.2.3.4: BSC with standard deviation – Sample 2.

Figure 3.2.3.5 shows the averaged backscatter coefficient over angles from 0^o to 150^o in the frequency range of 1 to 5 MHz for sample 2. Figure 3.2.3.6 shows the averaged BSC for all 5 samples for the same range of angles and the frequency. Again sample 3 shows very different values for the magnitude of the backscatter coefficient than the other 4 curves.

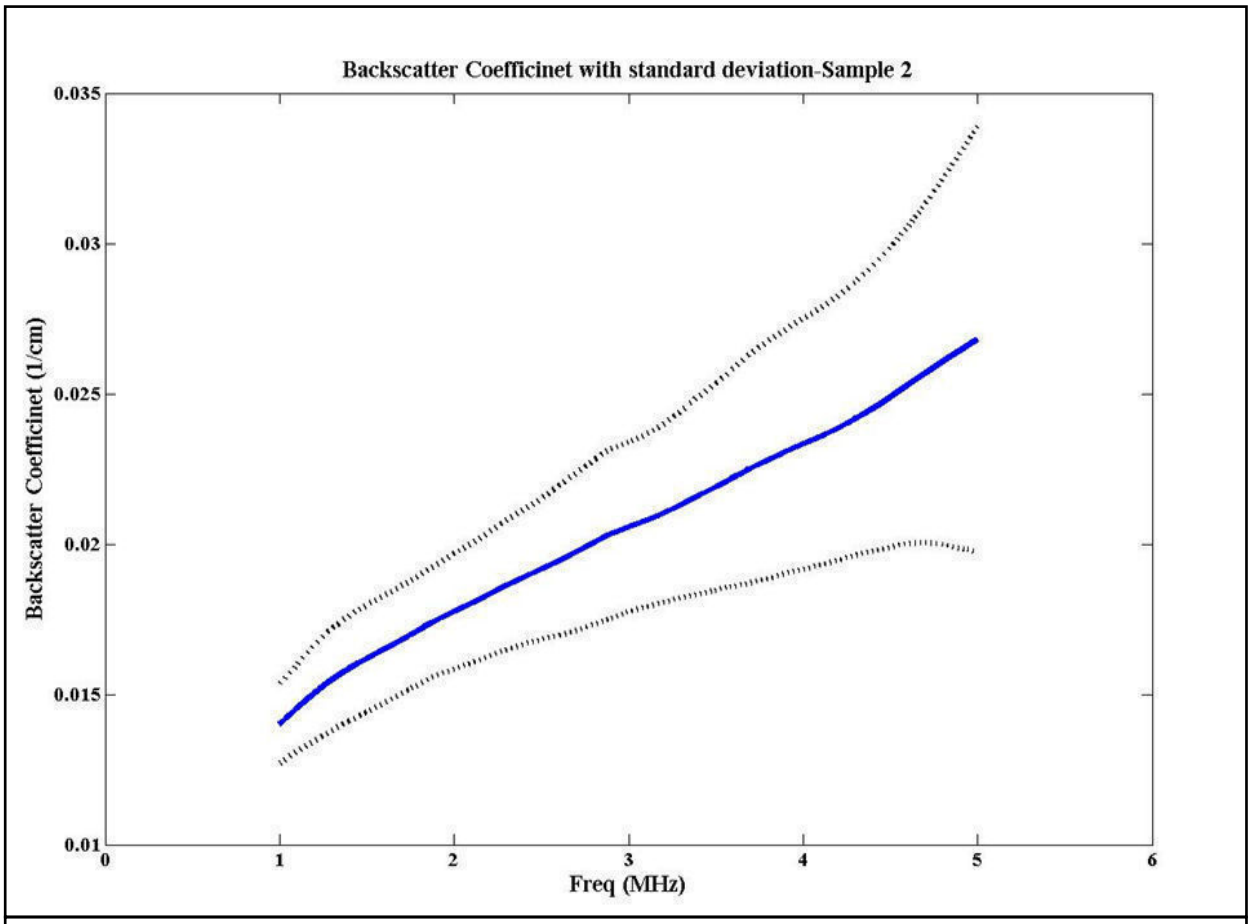

Figure 3.2.3.5: BSC with standard deviation at1-5 MHz – Sample 2.

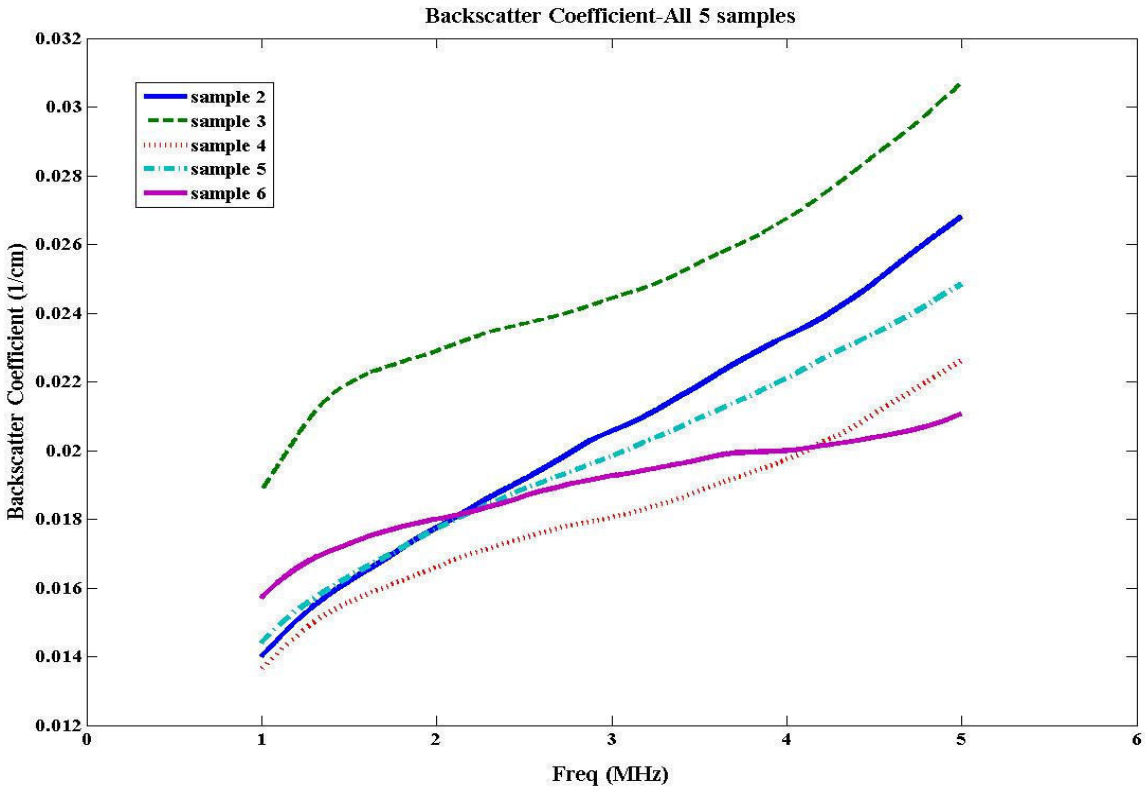

Figure 3.2.3.6: BSC averaged over angels-All 5 samples.

Figure 3.2.3.7 represents the averaged backscatter coefficient on samples 2, 4, 5 and 6 in the frequency range 1 to 5 MHz. The backscatter coefficient shows a gradual increase with frequency in this range of the spectrum. As mentioned in section 3.1.3, our results for the backscatter coefficient from ovine brain tissue show a similar frequency dependence as reported by [10, 20] with some higher values for the magnitude of the backscatter coefficient. The backscatter coefficient illustrates a similar variation with frequency in both spatial averaging and orientation-dependent data acquisitions.

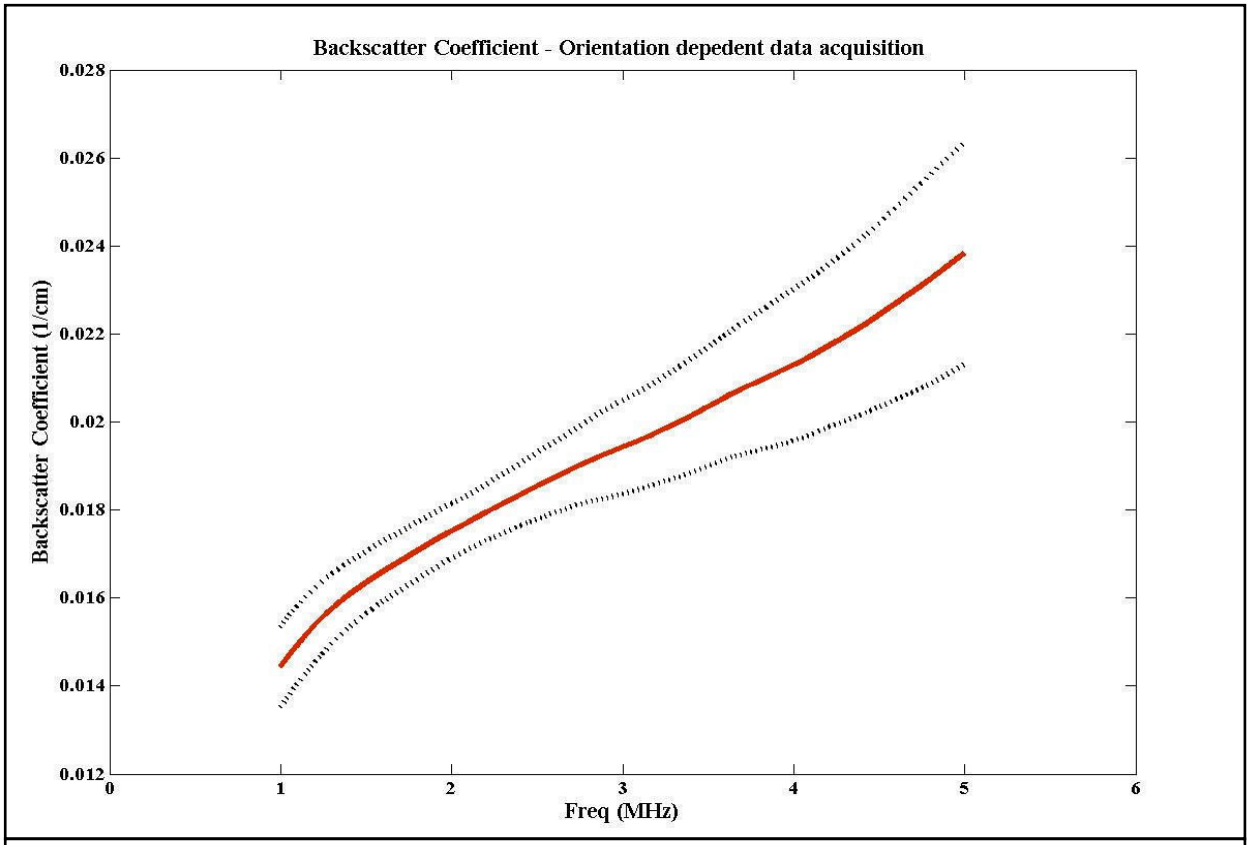

Figure 3.2.3.7: BSC averaged over 4 samples with standard deviation.

4. DISCUSSION

The apparent backscatter transfer function (ABTF) is obtained by subtracting the reference spectrum from the backscatter spectrum. The ABTF plays an intermediate step in analysis of the backscatter coefficient (BSC), which is a useful parameter in tissue characterization. Initially a backscatter spectrum should be obtained from the gated portion of the backscattered signal using a window as shown in Figure 2.5.2. In this study the backscatter data was gated using a Hanning window. As mentioned in section 2.5, the Hanning window is a good selection because its Fourier transform has much lower side lobes that provide a relatively smooth convolution curve in the frequency domain. At the same time, the gate width should be carefully selected so that it accounts for all the characteristic features of the signal of interest. If the gate width is too small it does not cover all the information in a signal that needs to be analyzed and on the other hand with a wide gate width it will include random variations due to interference from other scattering volumes. This can be seen in Figure 4.1. Figure 4.1 represents the first reflected signal from the steel plate, with different gate sizes applied to it. From Figure 4.1, 1200 points that correspond to 1.10 μs was determined as the best gate width for the attenuation data. Figure 4.2 represents the backscatter data after applying three different gate sizes and again 1200 points (1.10 μs) was selected as the best gate width for the backscatter data. So a Hanning window with 1200 points (1.10 μs) was used as the best gate for this study.

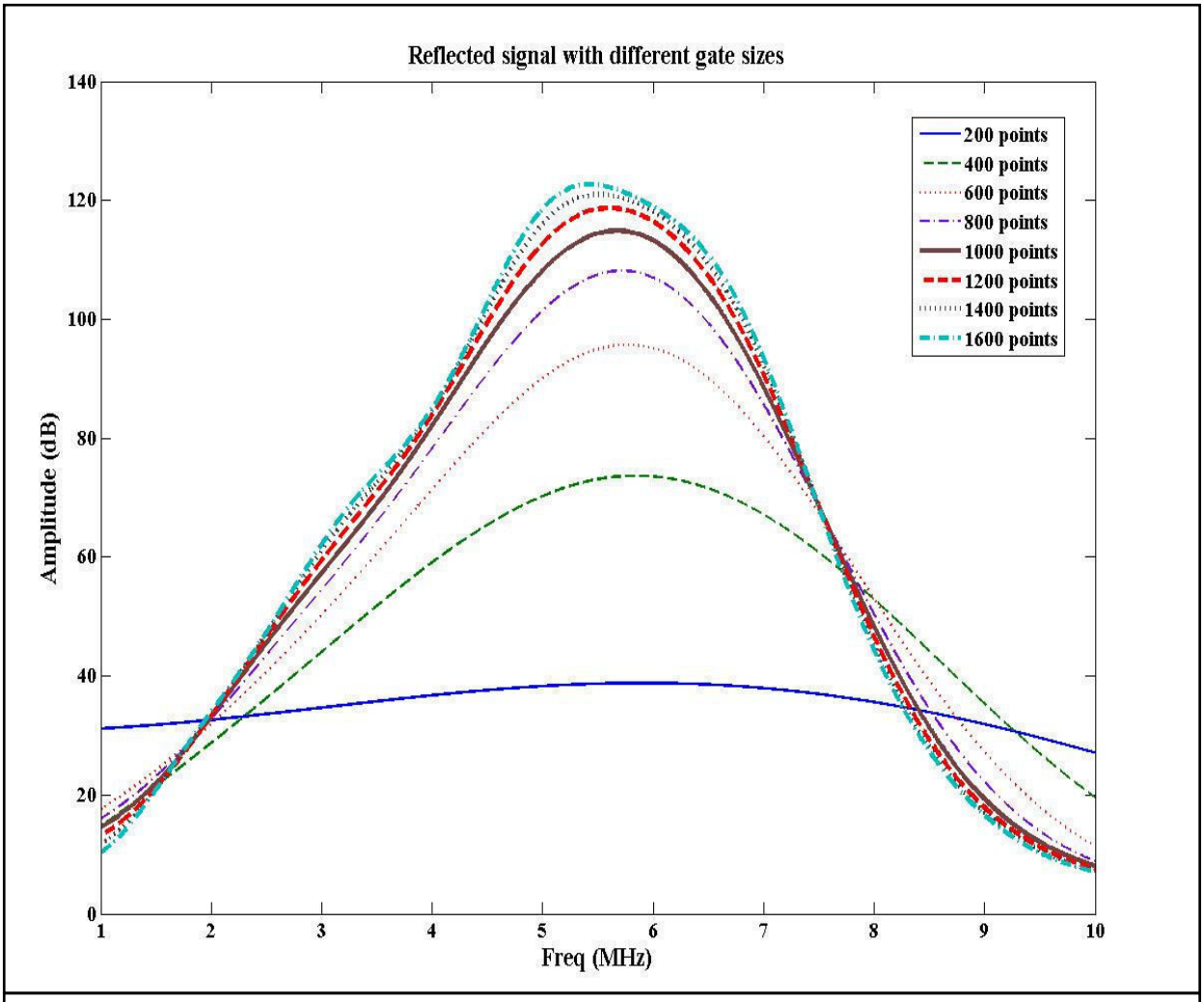

Figure 4.1: Reflected signal with different gate sizes.

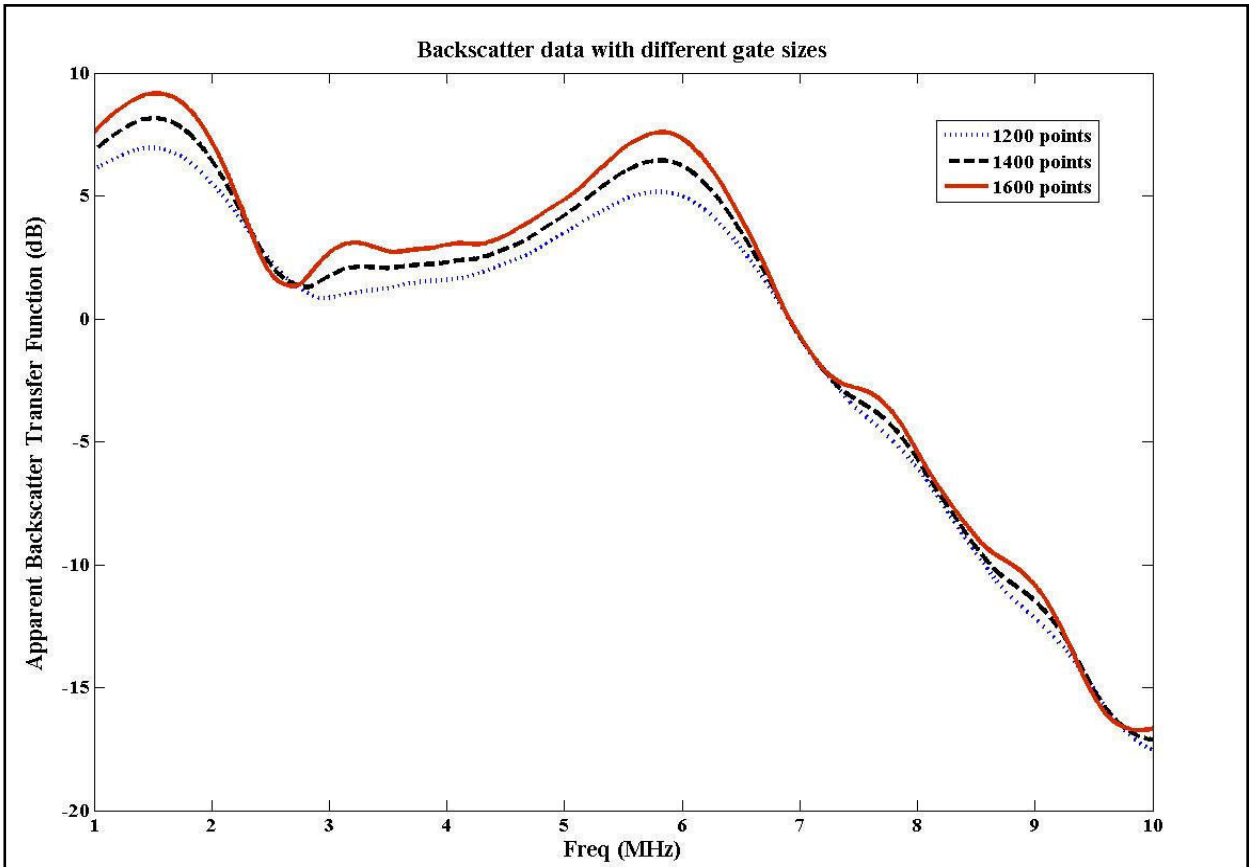

Figure 4.2: ABTF with different gate sizes.

Figures 3.1.1.1 and 3.1.1.2 represent the ABTF curves for 30 measurement sites of sample 1 in two perpendicular directions. The purpose of collecting data on 30 sites is to overcome the complexity of the tissue structure. Figure 3.1.1.4 shows the single spatially averaged ABTF curve for sample 1, and it is clear that by averaging the ABTFs from multiple measurement sites, the complexity of the tissue structure diminishes to reveal interesting features in the backscatter data. Ovine brain tissues were used in this study as the samples, and Figure 3.1.1.5 shows the spatially averaged ABTF curves for four different tissue samples. Each curve in Figure 3.1.1.5 represents the averaged ABTF of 30 measurement sites of the sample. Figure 3.1.1.6 shows the spatially averaged ABTF of all 4 samples that is the average of 120

measurement sites. ABTF represents a similar variation with frequency in the orientation dependence data acquisition as well those shown in Figures 3.2.1.1, 3.2.12, 3.2.1.3 and 3.2.1.4. Here the data were collected from 0^o- 360^o in 30^o increments using cylindrically shaped tissue samples. Each curve in Figure 3.2.1.3 represents the averaged ABTF of 13 orientations of the sample. Sample 3 in Figure 3.2.1.3 shows some lower values of ABTFs than the other 4 curves and this may be due to site-to-site variations. Our results would be more interesting if we could spatially average the data, to get read of the complexity of tissues, along the axis of the cylindrically shaped tissue sample as shown in Figure 4.3.

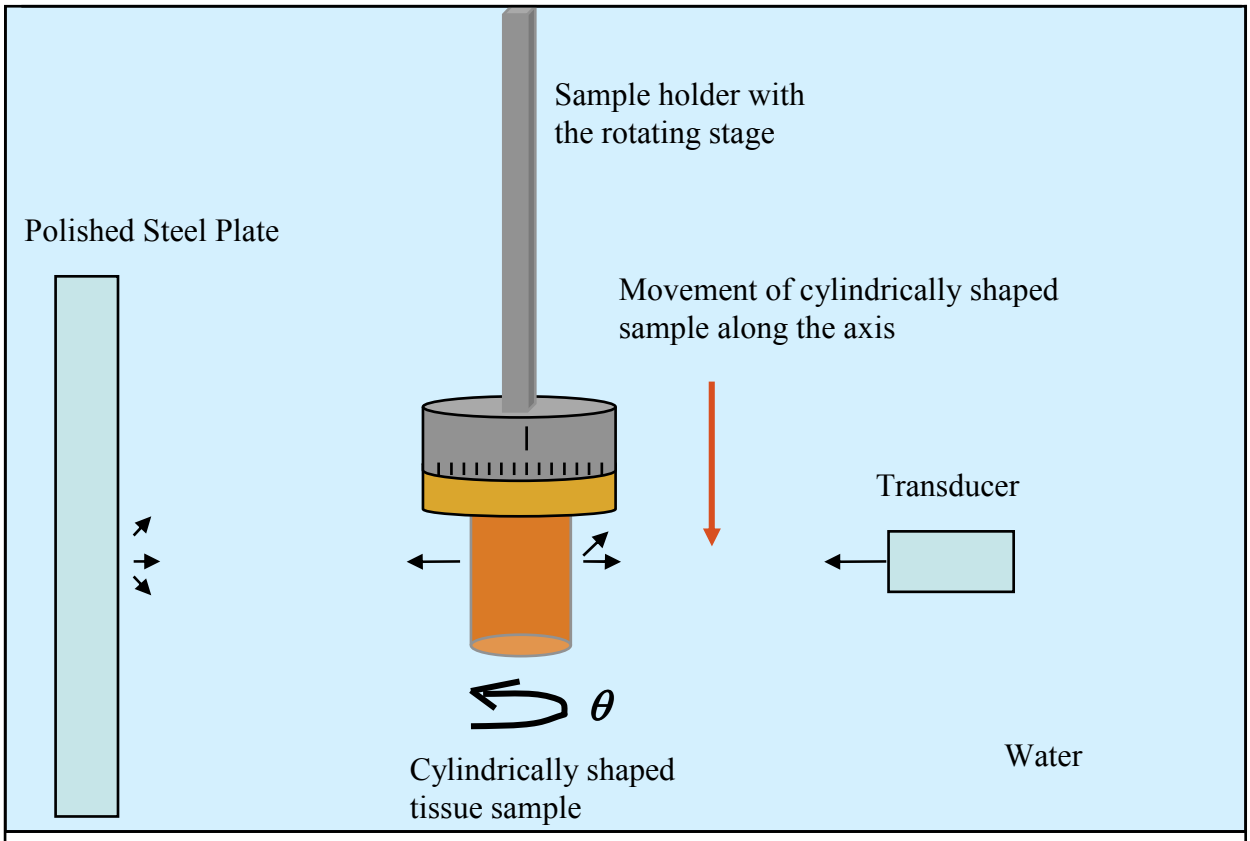

Figure 4.3: The diagram represents the spatial averaging of data while performing the orientation dependence measurements.

As seen in Figures 3.1.1.6 and 3.2.1.4 ABTF, exhibits a monotonically decreasing function of frequency over the range of 1-10 MHz. Our results for the ABTF on mammalian

brain tissues show somewhat lower values than those of [21] that examined the apparent backscatter measurements on human cancellous bone in the same range of frequency. Cancellous bone is one type of osseous tissues that is responsible for the formation of bones. During that study, backscatter measurements on 22 specimens of bone were performed *in vitro* using five transducers, and ABTF was spatially averaged. However for cancellous bone, the ABTF exhibits more complicated frequency dependence between measurement sites than our observations as in Figures 3.1.1.1, 3.1.1.2 and 3.2.1.1. The difference between bone and tissue is probably the reason for this discrepancy.

The attenuation coefficient is again an intermediate step in analysis of the BSC. For this study, the first reflected signals from the steel plate through the water path only and through the sample were compared. Figure 2.5.5 represents a diagram for the reflected data through the water path only and the tissue sample. It is clear from Figure 2.5.5 that the amplitude of the reflected signal reduced when it passed through the tissue sample, partially due to interface effects and partially due to bulk attenuation. Figures 3.1.2.1, 3.1.2.2 show the attenuation data for 30 measurement sites of sample 1 and Figure 3.2.2.1 shows that of 13 orientations of sample 2. It can be seen from Figures 3.1.2.1, 3.1.2.2 and 3.2.2.1 that there is no uniform behavior for the attenuation coefficient above 5 MHz, so 1 to 5 MHz is the best bandwidth for our study. Figures 3.1.2.3, 3.1.2.4 and 3.2.2.2 represent the best frequency range for the attenuation coefficient for samples 1 and 2, respectively. Each curve in those 3 figures was analyzed to determine the BSC. Figure 3.1.2.6 illustrates the single spatially averaged attenuation coefficient for sample 1 at 1 to 5 MHz and Figure 3.1.2.7 shows that of the 4 different samples. Each curve in Figure 3.1.2.7 represents the averaged attenuation coefficient on 30 measurement sites. Figure 3.1.2.8 represents the average of all 4 samples which total 120 measurement sites. Similar behavior

could be observed for the attenuation coefficient at orientation dependence data acquisition as shown in Figure 3.2.2.3 that is the average of 13 orientations for sample 2. Figure 3.2.2.4 shows the averaged attenuation coefficient on 5 different samples for 1 to 5 MHz. Figure 3.2.2.5 shows the averaged attenuation coefficient on all 5 samples in the same range of frequency on 65 measurement sites. Figure 3.2.2.5 shows higher values for the magnitude of the attenuation coefficient than that of Figure 3.1.2.8 for the ovine brain tissues. Those two diagrams show the attenuation data from orientation dependence and spatial averaging data acquisitions respectively. The reason for this discrepancy is not clear. Our results for the attenuation coefficient agree with previous studies [3, 6] that show the attenuation coefficient exhibits an increasing function of frequency for soft tissues. Results obtained from the spatially averaging method agree reasonably well with previous studies done by [6] that examined the ultrasonic attenuation and propagation speed in normal human brain in the same range of frequency, but on the other hand, the orientation dependence method agrees with the results obtained by [3] that shows the attenuation coefficient results of mammalian white matter.

In a tissue or a material, the BSC can be used to describe the scattering efficiency as a function of frequency. The BSC was determined by analyzing the ABTF, attenuation coefficient and some correction factors in the 1-5 MHz range. This range of frequency can be clearly illustrated by taking the standard deviation of the backscatter data as shown in Figures 3.1.3.4, 3.1.3.5 and 3.2.3.4. It can be seen from Figures 3.1.3.4, 3.1.3.5 and 3.2.3.4 there is a low standard deviation up to about a frequency of 5 MHz. The same behavior can be observed from all nine samples used in this study, which was helpful to determine the valid frequency range as 1-5 MHz. The backscatter coefficient as a function of frequency at 1 to 5 MHz is shown in Figure 3.1.3.7 for four different ovine brain samples. Each curve in Figure 3.1.3.7 represents the

spatially averaged BSC on 30 measurement sites. Figure 3.1.3.8 shows the averaged BSC on all 4 samples in the same frequency range that gives the average of 120 measurement sites. It is clear from Figure 3.1.3.8 that the backscatter coefficient for the mixed matter from ovine brain tissues shows an increasing function of frequency over the range of 1 to 5 MHz. Similar behaviors could be observed for the BSC on orientation dependence data acquisition as shown in Figures 3.2.3.6 and 3.2.3.7. Each curve in Figure 3.2.3.6 shows the averaged BSC as a function of frequency on 13 orientations and Figure 3.2.3.7 shows that of 52 measurement sites. It appears from Figure 3.2.3.6 that sample 3 shows higher values for the BSC than the other 4 curves, and again this may be due to the site-to-site variations throughout the tissue sample. As mentioned above, the BSC for ovine brain tissues shows a gradual increase with frequency over the range of 1 to 5 MHz that agrees reasonably well with the results obtained by [10] which shows the backscatter coefficient of bovine liver, pancreas, kidney, heart and spleen as a function of frequency from 2 to 7 MHz and also [20] which shows the ultrasonic backscatter coefficients in human liver and kidney in the range of 2 to 4 MHz. However our results for the backscatter coefficient on ovine brain tissues are somewhat higher than those reported by [10, 20]. The reasons may be due to the difference in propagation speed in different tissue types, fiber orientation in different samples, beam characteristics of the transducers used for data collection and the ultrasonic data acquisition systems used. It was mentioned in [10] that greater values of backscatter data were observed with the use of a focused transducer for data collection rather than an unfocussed one on the same specimen. During our study we used a focused transducer for the data collection procedure. In the reported study [10], an unfocussed transducer was used, in [20] two transducers were used for data collection, a circular focused transducer and an annular array transducer.

Normally scattering from brain tissues is very small compared with other soft tissues such as liver, heart and blood. Brain is the most important part of our body that controls everything such as learning, hearing, flexibility, sight, thinking, touch and emotions in our everyday life. The brain has a more complex structure than other parts of our body. So the protein structure in brain tissues is very different than other soft tissues, which leads to different mechanical characteristics.

5. CONCLUSIONS

The overall goal of this line of work is to use the ultrasound technology in the detection of brain injury especially because it is less expensive and portable compared with other modalities such as MRI and CT scans. In this work we examined the ultrasonic scattering and attenuation properties of ovine brain tissues focusing on three parameters, apparent backscatter transfer function (ABTF), attenuation coefficient and backscatter coefficient (BSC). We found that the apparent backscatter transfer function was a monotonically decreasing function of frequency and the other two parameters generally were increasing functions of frequency, results consistent with other soft tissues such as liver, blood, kidney and heart**.** The results obtained from this study may serve as reference measurements for undamaged tissues in the detection of brain injury. As the next step of this project, compressed and/or distressed brain tissues can be characterized using the same method, and the ultrasonic properties of normal and damaged tissues can be compared. Even though we are in a good agreement with earlier work with the characterization of soft tissues, further experimentation is necessary for a credible conclusion. In this study we were restricted to observing the ultrasonic properties of mixed matter due to the small size of ovine brain. In future work large brain samples can be used and the ultrasonic properties of white, grey and mixed matter can be characterized separately. Further we can observe the ultrasonic properties using different types of transducers such as unfocused transducers and transducers with different frequencies.

6. BIBLIOGRAPHY

1. Finnie, J. W.; Blumbergs, P. C. *Veterinary Pathology Online* 2002, *39*, 679.

2. Jiang, Q.; Zhang, Z. G.; Chopp, M. *Stroke* 2010, *41*, S112.

3. Mobley, J.; Mathur, A. N.; Vo-Dinh, T.; 1 ed.; Vo-Dinh, T., Grundfest, W. S., Benaron, D. A., Eds.; SPIE: San Jose, CA, USA, 2001; Vol. 4254, p 7.

4. Reed, G.M.; Sheppard, V.F. Basic Structures of the Head and Neck. W. B. Saunders Company, 1976.

5. Fredberg, L. Discovering Biological Psychology. Second edition. USA: Wadsworth, Cengage learning, 2009.

6. Kremkau, F. W.; Barnes, R. W.; McGraw, C. P. *The Journal of the Acoustical Society of America* 1981, *70*, 29.

7. Levi, S. *Ultrasound in Medicine and Biology* 1997, *23*, 481.

8. Donald, I.; Macvicar, J.; Brown, T. G. *Lancet* 1958, *1*, 1188.

9. Nicholas, D. *Ultrasound in Medicine and Biology* 1982, *8*, 17.

10. Fei, D. Y.; Shung, K. K. *The Journal of the Acoustical Society of America* 1985, *78*, 871.

11. Culjat, M. O.; Goldenberg, D.; Tewari, P.; Singh, R. S. *Ultrasound in Medicine and Biology* 2010, *36*, 861.

12. Ishimaru, A. Wave Propagation and Scattering in Random Media. USA: Institute of Electrical and Electronics Engineers Press, 1997.

13. Hill, C.R.; Bamber, J.C.; ter Haar, G.R. Physical Principles of Medical Ultrasonics. Second edition. England: John Willey and Sons,Ltd.2004.

14. Ginzel, E.A. Ultrasonic inspection 2 - training for nondestructive testing. Canada: Prometheus Press.

15. Hall, C. S.; Marsh, J. N.; Hughes, M. S.; Mobley, J.; Wallace, K. D.; Miller, J. G.; Brandenburger, G. H. *The Journal of the Acoustical Society of America* 1997, *101*, 1162.

16. Lide, D.R. CRC Handbook of Chemistry and Physics. Seventieth edition. Boca Raton (FL): CRC Press, 1990.

17. Francis, A. D. Physical Properties of Tissue. Academic Press, 1990.

18. Cutnell, J. D.; Kenneth W.J. Physics. New York: Wiley, 1997.

19. Strother, J. “Ultrasonic Properties of Brain Tissue as a Means of Quantifying Brain Injury ", The University of Mississippi, 2012.

20. Wear, K. A.; Garra, B. S.; Hall, T. J. *The Journal of the Acoustical Society of America* 1995, *98*, 1852.

21. Hoffmeister, B. K. *Physics in Medicine and Biology* 2011, *56*, 667.

7. LIST OF APPENDICES

APPENDIX A: MATLAB PROGRAM TO DOWNLOAD THE DATA FROM LECROY OSCILLOSCOPE TO DELL COMPUTER, WRITTEN BY PROF. JOEL MOBLEY, THE DEPARTMENT OF PHYSICS AND ASTRONOMY

```
%% Wavesurfer 432

dsoWS432 = actxcontrol('LeCroy.ActiveDSOCtrl.1');
invoke(dsoWS432,'MakeConnection','IP:130.74.33.96');
haxc = gcf;
 % set number of averages
number_to_average = 100;
% set number to acquire, must be <1000
waveforms2acquire = 30;
% set up root name for rf
rootname = 'backscatter data';
do_manual_acquisition_FLAG = 1;
dsoWS432.invoke('WriteString','COMM_HEADER OFF',1);
figure;
%   set up the scope for averaging
%   this is for summed:  the channel stops after averaging
cmdstr = ['F1:DEF EQN,"AVG(C1)",AVERAGETYPE,SUMMED,SWEEPS,',num2str(
number_to_average ),' SWEEP'];
dsoWS432.invoke('WriteString',cmdstr,1);
for k=1:waveforms2acquire
% clear traces
dsoWS432.invoke('WriteString','CLEAR_SWEEPS',1);
% wait for completion
fprintf('Averaging, %g s delay\n',(number_to_average*0.12 + 2));
pause( number_to_average*0.12 + 2);
% download waveforms
dsoWS432.invoke('WriteString','BUZZ BEEP',1);
aa=dsoWS432.invoke('GetScaledWaveform','F1',500000,0);
aa=double(aa);
fprintf('Waveform %d of %d acquired\n',k,waveforms2acquire );
% write waveforms to workspace
if k<10
namestr = [ rootname,'_00',num2str(k) ];
elseif k<100
namestr = [ rootname,'_0',num2str(k) ];
else
namestr = [ rootname,'_',num2str(k) ];
end
if k == 1
% get the time per division
dsoWS432.invoke('WriteString','TIME_DIV?',1);
timeperdiv=str2num( dsoWS432.invoke('ReadString',100) );
% get the trigger position
dsoWS432.invoke('WriteString','TRIG_DELAY?',1);
trigpos=str2num( dsoWS432.invoke('ReadString',100) );
numberofpts = length( aa );
timepersample = 1e6*10*timeperdiv/(10*floor(numberofpts/10));  % in microseconds
```

```
tax=((1:numberofpts)-1)*timepersample;% in microseconds
trigoffset = trigpos*1e6;
tax=tax-trigoffset-round(mean(tax));
fprintf('TDIV = %d, TOFFSET = %g, NUMPTS = %g, TPERSAMP = %g\n\n', ...
timeperdiv, trigoffset, numberofpts, timepersample );
end
assignin( 'base', namestr, aa );
plot(tax, eval(namestr) );title(['Acquisition ',num2str(k),' of ',num2str( waveforms2acquire )]);
if do_manual_acquisition_FLAG == 1 && k< waveforms2acquire
fprintf('\nPress the spacebar to continue...');
pause;
fprintf('ok\n\n');
end
end
dsoWS432.invoke('Disconnect');
close(haxc);
close gcf;
clear dsoWS432 haxc;
clear aa namestr cmdstr rootname;
```

APPENDIX B: MATLAB CODE FOR GATING THE BACKSCATTER DATA USING A SLIDING WINDOW, WRITTEN BY PROF. JOEL MOBLEY, DEPARTMENT OF PHYSICS AND ASTRONOMY

```
function [ linear_avg, log_avg, steps ] = CalcSpectralAverageWithSlidingWindow( data,
start_index, stop_index, gate_width, step_size, show_waveforms_FLAG )%[ linear_avg,
log_average, steps ] = CalcSpectralAverageWithSlidingWindow( data,...

% start_index, stop_idx, gate_width, step_size, show_waveforms_FLAG )
% detailed explanation goes here
steps = floor( (stop_index - start_index + 1 - gate_width)/step_size );
len = length( data );
idx = start_index + floor( gate_width/2 );
linear_avg=zeros(1,len);
log_avg=zeros(1,len);
data = data - mean( data );
for k=1:steps
[gated_data, junk, gate] = Calc_RemoveDC_andHanningGate( data, gate_width, idx, 0 );
ft_data = fft( gated_data );
linear_avg = linear_avg + abs( ft_data );
log_avg = log_avg + 20*log10( abs( ft_data ) );
idx = idx + step_size;
if show_waveforms_FLAG == 1
plot( 0.2*data/max(abs(data(start_index:stop_index))) );
hold on;
plot(gated_data/max(abs(gated_data)),'r');
plot(gate/max(gate),'k');
xlim([start_index stop_index]);
hold off;
drawnow;
end
end
linear_avg = linear_avg/steps;
log_avg = log_avg/steps;
```

APPENDIX C: MATLAB CODE FOR GATING THE REFLECTION DATA USING A ONE WINDOW. WRITTEN BY PROF. JOEL MOBLEY, DEPARTMENT OF PHYSICS AND ASTRONOMY

```
function [GatedData, CenterPoint, gate] = Calc_RemoveDC_andHanningGate( the_data,
window_length, center_point, autoset_centerpointFLAG );

size_array=size( the_data );
array_length = max( size_array );
xx=fft( the_data );
the_data = the_data - mean(the_data);
if autoset_centerpointFLAG==1
[mx, mxi] = max( the_data );
[mn, mni] = min( the_data );
if abs(mx) > abs(mn)
CenterPoint = mxi;
else
CenterPoint = mni;
end
else
CenterPoint = center_point;
end
gate = HanningWindow( window_length, CenterPoint, array_length );
if array_length ~= size_array(1)
gate = gate.';
end
GatedData = gate.*the_data;
```

APPENDIX D: DETERMINING THE TEMPORAL POSITION OF THE WINDOW AFTER THE FRONT REFLECTION OF SAMPLE (*X*), IN CALCUATING THE BACKSCATTER COEFFICIENT

In order to calculate the backscatter coefficient using equations 1.4.5.1 and 1.4.5.2 we need to determine the value x that is the position of the window after the front reflection of sample. For this we used the sample rate of our measurements, which is 1Gs/s.

x is given by,

$x = c\Delta t$

Where, Δt is the time difference between front wall reflection and the starting point of the hanning window and c is the speed of sound through the tissue sample.

Δt can be calculated using the sample rate and the number of points in that time interval.

Δt= number of points × time difference between two points

$\frac{1}{sample\ rate}$ Gives the time difference between two points, therefore

$$\frac{1}{sample\ rate} = \frac{1}{\frac{1Gs}{s}} = \frac{1}{10^9}s = 10^{-9}s$$

Now we need to determine the number of points in that time interval as shown in Figure 8.1.In Figure 8.1 I have identified the starting point for backscatter data as 240600 points and the front reflection starts at 236800 points. Figure 8.2 shows the backscatter data with time axis after applying the hanning window at 240600 points.

Now,

Δt = number of points × time difference between two points
= (240600-236800) × $10^{-9}s$
= 3.8×10^{-6} s

Therefore,

x =1560 m/s × 3.8×10^{-6} s
= 0.006m

This calculation is for one measurement site.

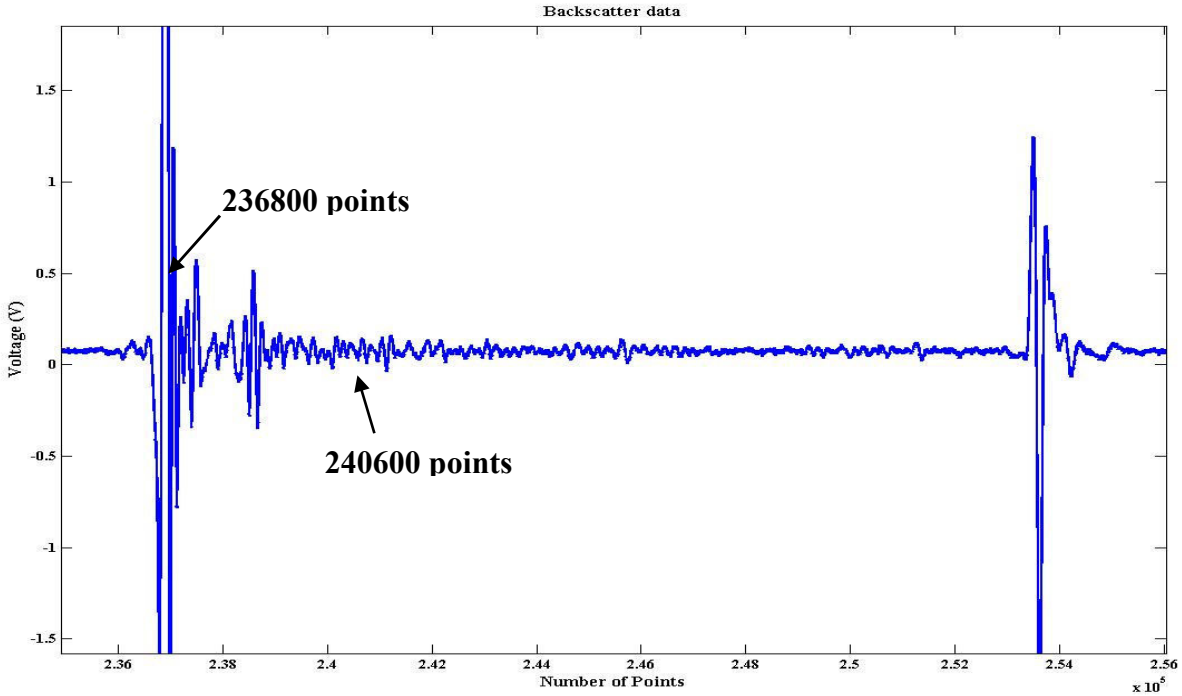

Figure 7.1: Position of the Hanning window after the front reflection from sample.

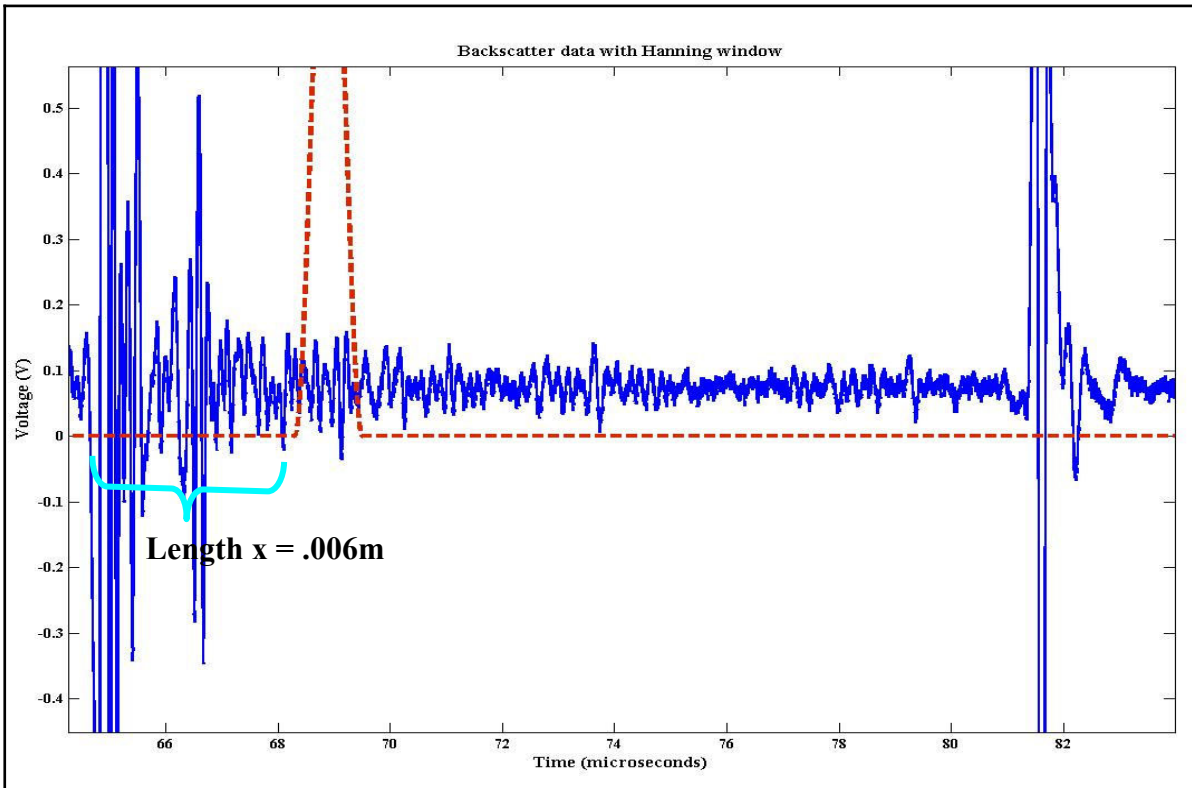

Figure 7.2: Backscatter data with Hanning window.

APPENDIX E: OLYMPUS PANAMETRICS - NDT MODEL 5800 PULSER/RECEIVER UNIT SETTINGS

- General setup for each measurement

  Mode: P/E
  PRF: 100 Hz
  Energy: 100 μJ
  Damping: 17 Ω
  HP Filter: 300 KHz
  LP Filter: 35 MHz

  Settings for the damping were changed for few measurements.

- Gain settings for the backscatter measurements were 60.0 dB for each and every measurement and it was reduced to 40.0dB or 20.0dB value for the reflection signals.

- Input attenuation and output attenuation settings of the Pulser/Receiver were changed on both backscatter and attenuation measurements.

APPENDIX F: TRANSDUCER SPECIFICATIONS

During this study we used an immersion pulse echo transducer of center frequency 5 MHz and focal length 2" FPF of model Panametrics NDT V 309,549587.

8. VITA

PUSHPANI VIHARA WIJEKULARATNE

1731 Anderson rd • Oxford, MS 38655 • (662) 701 2599 • pvwijeku@go.olemiss.edu

EDUCATION

MSc., Physics, University of Mississippi, May 2013
Concentrations: Scattering, Attenuation
Thesis: Backscatter and attenuation properties of mammalian brain tissues

BSc., Physics, University of Peradeniya, Sri Lanka, May 2005

TEACHING EXPERIENCE

Teaching Assistant, 2009 - present
University of Mississippi
Courses: General Physics Lab

Teaching Assistant, 2005 - 2007
University of Peradeniya, Sri Lanka
Courses: General Physics Lab